A Validation Study for the Computation of Nonlinear Modal Frequency using a Hamiltonian Reduced Order Model

K. Sinha

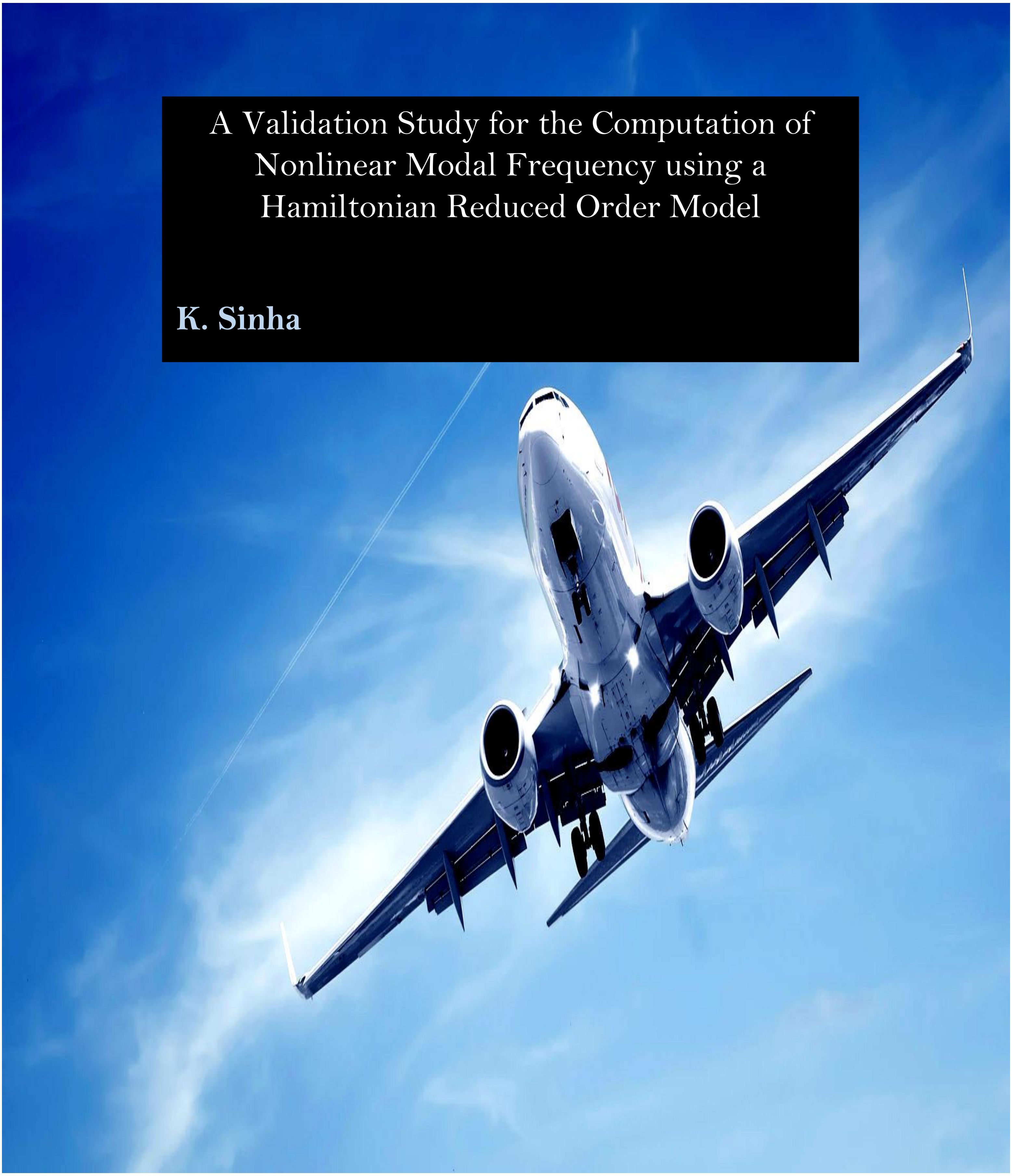

Faculty of Aerospace Engineering . Delft University of Technology

A Validation Study for the Computation of Nonlinear Modal Frequency using a Hamiltonian Reduced Order Model

MASTER OF SCIENCE THESIS

For obtaining the degree of Master of Science in Aerospace Engineering at
Delft University of Technology

Kautuk Sinha

Date: 29.08.2017

Faculty of Aerospace Engineering · Delft University of Technology

DELFT UNIVERSITY OF TECHNOLOGY
FACULTY OF AEROSPACE ENGINEERING
DEPARTMENT OF AEROSPACE STRUCTURES AND MATERIALS

GRADUATION COMMITTEE

Dated: 29th August 2017

Chair Holder:

Dr. Roeland De Breuker

Committee Members:

Dr. Farbod Alijani

Dr. Boyang Chen

Acknowledgements

The beauty of being an academic researcher lies in exploring the limitless expanse of knowledge, in the joys of reaching a goal after seemingly endless hours of frustration and the bond one develops with fellow researchers in sharing that experience. The report presented here is the outcome of my journey as a Master thesis student at the Aerospace engineering faculty at TU Delft. Numerous people have been a part of this enriching experience and I would like to take this opportunity to express my appreciation to them for their contribution.

I would like to thank Dr. Mostafa Abdalla who introduced me to the field of nonlinear structural dynamics and patiently guided me through the first half of the thesis. His ideas have been instrumental in the successful achievement of the project goals. I would like to thank Dr. Farbod Alijani who supervised my experimental work in this project. His advice was extremely helpful in conducting the experiments smoothly. I would like to thank Dr. Roeland De Breuker who agreed to take over the supervision from Dr. Mostafa Abdalla. He has always found time for an open discussion about the project, regardless of his busy schedule and I highly appreciate that. I would like to thank Dr. Boyang Chen for agreeing to be in the committee member for my assessment. I would like to thank Niels Singh who allowed me to use the model reduction code written by him. I would like to thank Bas Hemming for a short introduction to the Polytec Laser Doppler Vibrometer and PAK MK-II measurement systems.

All work and no play makes Kautuk a dull boy. The journey would not have been easy without the presence of friends in my life. I would like to thank my girlfriend Priyanka and all my friends across the globe for the moments of happiness we have shared and the animated discussions we have had. These moments have been truly precious.

Lastly and most importantly, I would like to thank my parents and my sisters. I would like to express my gratitude to my mother and father for inculcating in me the discipline and the will necessary to pursue one’s dreams and for their love, encouragement and support. I would like to thank my sisters Surabhi and Neha who have been epitomes of excellence and my childhood heroes. You always inspire me to be a better person.

Delft University of Technology
29th August 2017

Kautuk Sinha

Abstract

Modern-day design procedures are focused on obtaining optimized structural models. In the field of Aerospace engineering, where the weight reduction is quite significant for improved flight performance and cost, design optimization is of greater importance. A common design verification is to conduct modal analysis and to ensure that the vibration modes of the structure do not get harmonically excited during operation. Since the modal frequencies are dependent on the mass and stiffness properties of the structure, they are an influencing factor in the design optimization. Modal frequencies are obtainable using eigenvalue analysis after linearization approximations in the restoring force terms of the governing equation of motion. While this approximation is valid for lower loads, it is not acceptable for strong nonlinear vibrations. A measurable shift in the modal frequency is observable when the amplitude of vibrations is in the order of the dimensions of the vibrating structure. This phenomenon is more pronounced in thin walled and flexible structures where the vibration amplitudes can exceed the linear threshold relatively more easily.

The phenomenon of frequency–amplitude dependency for large amplitude vibrations has been previously studied extensively for plates and shells. The use of continuation scheme for computation of nonlinear modes has gained credibility through the work of various researchers. However, the use of continuation method with full scale models remains a computationally expensive procedure and therefore necessitate the use of reduced order models. A model reduction method for dynamics termed as Hamiltonian reduced order model, recently developed at Delft University of Technology, has been found to be extremely accurate and efficient in computing time domain response of structures in comparison to commercial finite element programs. The work done in this thesis validates the reduced order model (ROM) experimentally by computing the frequency domain response of a stiffened plate undergoing nonlinear vibrations. The reduced order model for computations is derived from an initial full-scale finite element model. The equations of motion are formulated using the ROM in a Hamiltonian framework. The nonlinear frequency response is obtained using a continuation scheme. The experiments are conducted using laser doppler vibrometer which is a non-contact form of measurement system. A comparison between the dynamics of a stiffened plate and a plate without stiffener is presented to demonstrate the effect of presence of the stiffener.

Table of Contents

List of Figures

List of Tables

List of Symbols

δ	Variational operator
H	Hamiltonian of a system
p	Momentum
q	State variable
$\boldsymbol{\xi}$	State variable in the reduced system
$\boldsymbol{\pi}$	Momentum in the reduced system
$\mathbf{f_{ex}}$	External force vector
F	Load matrix consisting of external force and perturbation loads
$\boldsymbol{\phi}$	Load amplitudes
$\boldsymbol{\mathcal{L}}$, ***Q***, ***C***	Linear, quadratic and cubic stiffness operator
$\bar{\boldsymbol{\mathcal{L}}}, \bar{\boldsymbol{Q}}, \bar{\boldsymbol{C}}$	Linear, quadratic and cubic stiffness in the reduced system
P	Momentum basis for reduced order model in dynamics
M	Mass matrix
$\boldsymbol{\Phi_n}$	Eigenvector for the n^{th} mode
T	Kinetic energy
V	Potential energy
$\bar{\mathbf{M}}$	Reduced mass matrix
D	Dissipative energy
$\mathbb{C}$	Damping coefficient
θ, φ	Variables of the nonlinear oscillator
ω	Frequency of forcing function in harmonic load
DFDQ	Jacobian of the equations of motion with respect to state variable
DFDP	Jacobian of the equations of motion with respect to continuation parameters
$\boldsymbol{\eta}$	State variable in modal coordinates
α, β, γ	Scale factors

Chapter 1

Introduction

1.1 Background and Motivation

Dynamic analysis of structures forms an essential part of the modern-day design procedures in the fields of Aerospace, Mechanical and Civil engineering. One of the primary design criterions is to ensure that the first mode of vibration occurs at a frequency higher than the expected maximum frequency of harmonic loads on the structure. If this design criterion is satisfied, resonant conditions are preventable throughout the operating cycle of the structure in consideration. A common industrial practice, therefore, is to conduct a modal analysis on the structure to estimate the modal frequencies which gives an idea of the structural safety against harmonic loads. The evolution of computing systems and the advancements in the field of finite element analysis have simplified the analysis procedures and improved the accuracy in the analysis. Most commercial finite element programs incorporate the linear eigenvalue analysis procedure for predicting the modal frequencies (Siller [3]). While this method is sufficiently accurate for small amplitude vibrations, a measurable deviation in the resonant frequencies is observable in the presence of geometrically induced nonlinearity or large amplitude vibrations (Kerschen *et al.* [1]). Vibrations are categorized as geometrically nonlinear when the amplitude is in the order of thickness / dimensions of the structure. Some real-life examples of large amplitude vibrations are aeroelastic flutter in aircraft wings or helicopter rotor blades, wind induced vibrations in power transmission towers, vibrations in unbalanced rotating shafts, etc.

The change in the resonant frequency arises due to the hardening or softening type nonlinearity present in the structure, the effect of which grows more prominent as the vibration amplitude increases (Peeters et al. [2]). The hardening or softening nonlinearities cause a corresponding increase or reduction in the modal frequency with increasing amplitudes. The dependency of the modal frequency on the vibration amplitude necessitate development of dedicated methods for its prediction to obtain better accuracies in structural design. The amplitude - frequency dependence can be optimally studied by developing methods to obtain the backbone curve of a system.

Backbone curves define the natural frequencies as a function of vibration amplitudes in free and undamped vibration (Londoño et al. [5]). An alternative approach is to generate an approximation of backbone curve from a damped and forced system by varying the load amplitude in the nonlinear regime of vibrations. For analysing large scale structural models, analytical methods are less preferred since they often lead to complex mathematical problems which, otherwise, can be more easily solved using numerical computations. However, the drawback in using numerical methods for large models is the high computation time and effort required. This gives motivation for the development of model reduction methods with the aim of reducing the computation time and effort while maintaining accuracy in the solutions. A recent development in the reduced order modelling for nonlinear structural analysis was instigated at Delft University of Technology. The resultant approach is based on perturbation method and use of truncated Taylor series expansion for the solution (Liang et. al. [4]). The reduced order model (ROM) was subsequently adapted for application in nonlinear dynamic analysis by N. Singh [30] and was termed as Hamiltonian ROM. The ROM is based on considerations of geometric nonlinearity only and the material behaviour is assumed to be within the elastic limit. The model reduction was found to be extremely successful with a large reduction in analysis time, when tested for beams, plates and shells, in comparison to commercial finite element software Abaqus. The ROM is utilized in this thesis for numerical analysis with the emphasis on validating the numerical approach experimentally and demonstrating the effectiveness of the ROM.

The chapter is organized in the following manner: In Section 1.2, a concise literature review on nonlinear dynamic analysis of plates and stiffened plate is presented. Section 1.3 defines the project objectives, the research questions to be answered and the methodology adapted to answer the research questions. The layout of the thesis report is presented in Section 1.4.

1.2 Literature Review

Extensive research has been conducted by various authors on development of optimal numerical methods for computation of nonlinear modes. Consequently, several methods for model reduction in nonlinear analysis have been developed. The literature review presented here comprises of two sections: Nonlinear forced vibration in thin walled structures in Section 1.2.1 which covers the progress in this field historically, and model reduction methods for nonlinear vibration analysis in Section 1.2.2.

1.2.1. Nonlinear forced vibration in thin walled structures

Thin walled structures find a wide application in Aerospace engineering. As the focus is shifted on improving flight performance, cost and energy efficiency, more flexible and light weight structures are being designed. A consequence of higher flexibility is larger deformations under load which necessitate considerations of geometric nonlinearity in structural design. Considerations for geometric nonlinearity in the dynamics analysis of thin walled structures have been recognized since the pioneering work of Chu and Herrmann [6] who obtained the backbone curve of a simply supported rectangular plate using perturbation method on second order differential equation of motion. The rotary inertia and in-plane inertia were neglected in the formulation of the equations. The same formulation was used by Yamaki [7] and the analytical solution was obtained by using a double harmonic series as an initial assumption. The backbone curve and the forced response of a simply supported square plate was obtained through the analysis.

Eisley [8] derived the amplitude–frequency correlation of a plate using von Kármán plate theory and first order approximation in the Ritz method. Sathyamoorthy [9] extended the work to anisotropic and skewed plate where the frequency ratios were obtained using first order Galerkin approximation and Runge-Kutta method.

The work considered so far have used a single mode approximation or first order perturbation method for the analysis. Yamaki and Chiba [10] proposed a method using third order Galerkin approximation and Harmonic balance approach to obtain a more accurate solution. The harmonic balance transforms the problem to a set of algebraic equations where only the coefficients of the functions are unknown (Nayfeh and Balachandran [12]). To validate the approach, Yamaki *et. al.* [11] conducted experiments on a square plate with clamped boundary conditions. The authors concluded that some discrepancies were observable for large amplitude vibrations due to the approximations used in the analytical approach. D. Hui [13] studied the effect of geometry imperfection in a laminated rectangular plate. The author used von Kármán plate theory and obtained the solution using first order Galerkin approximation. The imperfection was induced into the structure in the form of the first mode shape. It was concluded that the imperfection causes a softening effect in the laminated plate and considerably shifts the modal frequency. Leung and Mao [41] used Galerkin discretization to obtain a Hamiltonian formulation of governing equation and solved the system using symplectic integration. Symplectic integration is a numerical integration scheme for Hamiltonian systems which ensures that the change from any initial state q_0, p_0 of the system to q_1, p_1 at time τ is a canonical transformation (Yoshida [14]). The authors compared their method with Runge-Kutta method and concluded that while Runge-Kutta method decreases the energy of an undamped system, symplectic integration almost preserves the total energy. The analysis was used to produce nonlinear frequency response for simply supported rectangular plates with different aspect ratios.

The advent of finite element methods offered the potential of obtaining more accuracy in solutions albeit with the drawback of high computation times. Han and Petyt [15 - 16] studied the nonlinear vibrations of isotropic and laminated plates using Hierarchical finite element method (HFEM). The authors concluded that the use of HFEM yields accurate results with lesser number of elements as compared to conventional finite element models. Comparison of mathematical models were made with and without considerations of in-plane displacements. The studies showed that in-plane displacement consideration in the model has a strong effect on the nonlinear dynamic properties and therefore, should not be neglected in the analysis. HFEM was later used by Ribeiro and Petyt [17-18] in combination with Harmonic balance approach to formulate the frequency domain equations of the system. The analysis was conducted for clamped rectangular isotropic and laminated plates by using continuation methods. A continuation scheme is an iterative predictor–corrector approach used to generate solution families from an initially known solution (Doedel [28]). The use of continuation scheme is advantageous for nonlinear analysis as stability of the solutions and bifurcations can be easily captured in the forced vibration analysis.

The continuation scheme was further adopted by Amabili [40] for analysing the nonlinear dynamics of rectangular plates with various boundary conditions. The analysis results were compared to several literature and experiments were also conducted to validate the results. The author used von-Kármán plate theory for dynamics to formulate the Lagrangian equations of motion. The in-plane and out-of-plane displacements were assumed to be a double Fourier sine series in the formulation.

The resulting set of differential equations were solved using the continuation scheme in the software AUTO. By varying the number of terms in the series, the author concluded that a 9 degree of freedom model is sufficiently accurate for nonlinear analysis of simple rectangular plate with movable simple support. However, the analysis with immovable simple support was shown to have accuracy with a 16 degree of freedom model. The software AUTO is based on a parametric continuation scheme called the pseudo-arclength method. A periodic solution is computed using a method called Orthogonal collocation using piecewise polynomials. A detailed theoretical discussion of AUTO can be found in the work of (Doedel [28]). An alternate approach using the iterative shooting algorithm and Newton method was adopted by Ribeiro [19] to study dynamic behaviour of isotropic plates. The author used HFEM to formulate the discretized equations of motion. Shooting algorithm is another variation of the predictor–corrector approach and offers the same advantage as the continuation schemes by providing the stability of the solution. Alijani and Amabili [20] studied the large amplitude vibrations of laminated and sandwich plates with free boundary conditions. The authors formulated the governing equations using classical and higher order shear deformation theories. An assumption for the displacements and rotations was chosen comprising of a product of a spatial and a temporal component. The spatial term was expanded as Chebyshev polynomials for the discretization of the problem. A linear eigenvalue analysis was first conducted to evaluate the linear mode shapes. The appropriate mode shapes were then chosen as the shape function for the nonlinear analysis. The choice of specific mode shapes greatly reduced the number of terms required in the expansion for the analysis and was the basis for a reduced order model. The final governing equations were solved using a continuation scheme. The authors concluded that the retention of in-plane degrees of freedom in their reduced order model was an important factor in achieving convergence. Up to 78 degree of freedom model was required to achieve converged results for the laminated plates. In an interesting study, Amabili and Carra [21] investigated the effect of geometric imperfections and ambient temperature on the nonlinear dynamics of a clamped rectangular plate. The authors conducted experiments on clamped stainless steel plate and concluded that the temperature changes in the order of 1^{o} Celsius and / or presence of imperfections in the plate can affect the hardening behaviour of the plate. Thinner plates were found to be more sensitive to imperfections and temperature changes.

The nonlinear forced vibration behaviour of rectangular plates has been extensively researched as evident from the variety of literature listed. However, literature on nonlinear analysis of stiffened plates is relatively much lesser. One of the early investigations on nonlinear vibrations of stiffened plates was done by Prathap and Varadan [22] who used single mode Galerkin method for the formulation of the problem and solved it analytically. Simply supported movable and immovable boundary conditions were compared and the authors concluded that the hardening nonlinearity is more prominent for the immovable case as compared to the movable case. Kolli and Chandrashekhara [23] used a finite element formulation for the analysing laminated stiffened plates. The transient response was obtained using Newmark integration scheme. Although, the frequency-amplitude response curves were not obtained in this analysis. Mitra et al. [24] conducted free vibration analysis of isotropic stiffened plates and obtained the backbone curves for different boundary conditions. An energy based formulation was used to derive the governing equations. The nonlinear dynamic response was coupled to a preliminary static analysis. A nonlinear static analysis was conducted in which the stiffness matrix is reformulated at each load step. The deflection of the plate in each load step was assumed as an initial approximation of spatial functions chosen for the analysis.

The modal frequency was obtained using an eigenvalue analysis and considering the new stiffness matrix for each load step. Ma et al. [25] studied the dynamic response of a stiffened plate with clamped boundary conditions using method of multiple scales. The authors observed a 3:1 internal resonance in the analysis. Internal resonance is the energy transfer between two different modes such that when one of the modes is excited, an intermittent switch to the other mode occurs during the vibrations.

1.2.2. Model Order Reduction in Nonlinear Dynamic Analysis

The reduced order models are developed with the objective of improving computational efficiency of numerical methods while maintaining the ability to capture the dynamics of the system with accuracy in the solutions. In this section, some of the reduced order models used in nonlinear vibration analysis are presented.

1. Mode-Superposition Method

This method is based on the principle of local mode superposition which states that the nonlinear vibration response of a system may be obtained by superimposing small harmonic motion on a large static deflection and small forced vibrations are representable by tangential stiffness. The principle gives rise to an incremental iterative procedure for obtaining temporal response. The modes are computed using the conventional eigenvalue analysis, however, tangential stiffness matrix is used for the analysis.

$$(\boldsymbol{K}(\mathbf{u_n}) - \omega_i{}^2 \, \boldsymbol{M}\,)\boldsymbol{\phi_i} = \mathbf{0} \tag{1. 1}$$

In the above equation, $\boldsymbol{K}(\mathrm{u_n})$ is the tangential stiffness matrix when a displacement $\mathrm{u_n}$ has been achieved. The tangential stiffness matrix is recomputed frequently during the iterative approach wherein the load is given small increments in each step. The model order is reduced by using the following transformation:

$$\boldsymbol{\Delta}\mathbf{u_{n,n+1}} = \boldsymbol{\phi}\,\boldsymbol{\Delta}\mathbf{X} \tag{1. 2}$$

In the above equation, $\boldsymbol{\Delta}\mathrm{u_{n,n+1}}$ is the increment in the static deflection, ϕ is the modal matrix consisting of ‘M’ eigenvectors and $\boldsymbol{\Delta}\mathbf{X}$ is the incremental modal displacement for the reduced system. In the analysis presented by Nickell [43], the lower modes are assumed to be most influential in determining the incremental modal displacement. The reduced order model is designed for obtaining temporal response and has no direct impact on the eigenvalue analysis. The analysis is time consuming since it requires an update in the tangential stiffness matrix frequently for the principle of local mode superposition to hold validity. Furthermore, the number of modes in the reduced order model required for convergent and accurate results in each incremental step of the nonlinear analysis is not predictable prior to the analysis.

2. Galerkin Method

From Section 1.2.1 it is evident that the Galerkin approximation has been utilized by several authors in their analysis. The main element of this method is to define a trial function of the displacement terms by using reduced number of terms.

The generic form of such an approximation is,

$$u(x,t) = \sum_{\mathrm{j}=1}^{\mathrm{N}} \mathrm{A_j(t)}\ \phi_{\mathrm{j}}(x) \tag{1. 3}$$

where u is the displacement field, $\mathrm{A_j}$ defines the time dependency in the variable separable form and ϕ_{j} is an admissible function; for example, defined by Fourier series, Legendre polynomials, Chebyshev polynomials etc.; appropriately chosen to define the displacements while also satisfying the geometric boundary conditions. The unknown functions $\mathrm{A_j}$ are computed using the weighted residual method where an orthogonality condition is imposed between the residual and the weight functions. The residual function is obtained by substituting the trial function into the original differential equation. The weight functions are usually derived from the subspace of the original trial function and can be chosen to be the trial function itself. The approximation discretizes a continuous system and provides a finite set of equations defining the motion of the object. The convergence rate as a function of the number of terms in the approximate solution depends on the choice of the trial function.

3. Proper Orthogonal Decomposition

An alternative to the conventional Galerkin approximation is the proper orthogonal decomposition (POD) method. In this approach, empirical mode shapes called the proper orthogonal modes are computed and used as a basis in the formulation of the reduced order model. A comparison has been made by Amabili *et al*. [44] between the performance of the conventional Galerkin method and proper orthogonal decomposition for the nonlinear vibration analysis of a cylindrical shell structure. It was observed that accurate results could be obtained using a 3-degree of freedom model using POD in comparison to a 16–degree of freedom model using Galerkin method. The POD is used to extract useful spatial information from snapshots of time domain response of the structure (Amabili *et. al*. [44]) which is obtained either from experiments or numerical simulations. The solution in the reduced system can be expressed using the proper orthogonal modes $\psi(\xi)$ as,

$$w(\xi,t) = \sum_{\mathrm{j}=1}^{\mathrm{N}} \mathrm{A_j(t)}\ \psi_{\mathrm{j}}(\xi) \tag{1. 4}$$

where ξ is the spatial variable, t is the time variable, N is the number of degrees of freedom. The POM's $\psi(\xi)$ are derived by maximization of the objective function with respect to $\psi(\xi)$,

$$\lambda = \frac{\int \left(\psi(\xi)\ \overline{w}(\xi,t)\right)^2 \mathrm{d}\xi}{\int \psi^2(\xi)\ \mathrm{d}\xi} \tag{1.5}$$

where $\overline{w}(\xi,t) = w(\xi,t) - \overline{w}(\xi)$, $\overline{w}(\xi)$ is the time average of temporal response obtained from simulation or experiments. A Galerkin projection of the POM's $\psi(\xi)$ on the eigenmodes $\phi(\xi)$ of the structure is used in the maximization problem,

$$\psi(\xi,t) = \sum_{\mathrm{j}=1}^{\mathrm{N}} \alpha_{\mathrm{j}}\ \phi_{\mathrm{j}}(\xi) \tag{1.6}$$

where α_j is an unknown. The maximization results in an eigenvalue problem which provides the unknown α_j as the eigenvector. The proper orthogonal modes are subsequently used as the basis in formulating the reduced order model using Galerkin approach. The method is quite useful in creating reduced order models, however, the requirement of a preliminary time domain data in the formulation extends the overall computation time.

4. Reduced Order Model for Asymptotic Numerical Method

The Asymptotic numerical method (ANM) is an alternate class of continuation method utilized for nonlinear dynamics. The formulation of the governing equations of the nonlinear problem is done using Harmonic balance approach. The number of harmonics used in the formulation greatly affects the size of the problem and therefore the computation time. To reduce the size of the matrices, Boumediene et al. [45] proposed a model reduction method suitable for the ANM. In the ANM, a power series expansion with respect to a path parameter is used to define the unknown quantities. The path parameter is computed as a projection of displacement vector increment in each step and frequency increment onto the tangent vector of the curve. Substituting the power series expansion into the governing equations and comparing the coefficients of terms with the same power, the nonlinear problem is transformed to a set of linear equations which are then solved using the finite element method. It is notable that comparison of the zero power terms give an additional single nonlinear equation which must be solved by classical iterative techniques like Newton- Raphson.

The basic idea of the reduced order model is to transform the displacement space into a smaller subspace using a reduction matrix with the transformation,

$$\boldsymbol{U} = \boldsymbol{\phi u} \tag{1.7}$$

where **u** is the reduced displacement vector. Two different methods are used to determine the reduction matrix. In the first method, eigenvectors from a linear eigenvalue analysis are used as the basis of the reduced order model. In concurrence to past work, lowest out-of-plane and in-plane modes are chosen to formulate the basis matrix for the reduction model. In a second approach, the basis matrix is obtained from a nonlinear analysis. The first step of the ANM model is solved without using a reduction method. The displacement vectors obtained from the initial iteration are used to formulate the reduction matrix. The total number of vectors available depends on the truncation order of the asymptotic expansion. A few vectors can be selected from the available ones to formulate the ROM. The methods were implemented to analyse simply supported and clamped plate models and the results were found to require 15 to 20 degrees of freedom models for good accuracy. In conclusion, the authors propose the use of proper orthogonal decomposition to select only the most significant vectors in the formulation of the ROM.

5. Reduced order model based on Nonlinear normal modes

Normal mode motion is defined as a synchronous oscillation where each point on the structure is oscillating in phase and reach their extrema at the same time. This property allows correlating the motion of every point to a single point on the structure. The whole normal mode motion is then definable in a two-dimensional subspace of the state space.

For a dynamical system of the form,

$$\dot{x}_i = y_i \tag{1.8a}$$

$$\dot{y}_i = \mathrm{f}_i\,(x_1, x_2, \dots, x_N, y_1, y_2 \dots, y_N) \tag{1.8b}$$

to compute the 'k th' nonlinear normal mode the motion of all points on the structure is correlated to the displacement u_k and velocity v_k of the 'k th' point.

$$x_i = X_i\,(u_k\,, v_k)\ ,\ y_i = Y_i\,(u_k\,, v_k) \tag{1.9}$$

Substituting Equation 1.9 into the governing equations, a set of constraint equations describing the geometry of nonlinear invariant manifold is obtained.

$$\frac{\partial X_i}{\partial u_k}\,v_k + \frac{\partial X_i}{\partial v_k}\,f_k = Y_i \tag{1.10a}$$

$$\frac{\partial Y_i}{\partial u_k}\,v_k + \frac{\partial Y_i}{\partial v_k}\,f_k = f_i \tag{1.10b}$$

In general, it is difficult to find an exact solution to the above equations, therefore, an asymptotic polynomial function in $u_k\,, v_k$ is assumed as an approximation for X_i and Y_i **.** Substituting the expansion into the constraint equations and equating coefficients of same powers of u_k and v_k **,** the unknown terms in the asymptotic expansion are computed. The known X_i and Y_i can be now substituted in the Equation 1.8. A single ordinary differential equation needs to be solved to obtain the 'k th' normal mode motion. The above method is a summary for undamped and free vibration described by Pesheck *et al.* [46]. The method has been utilized by Touzé and Amabili [47] and Amabili and Touzé [48] in analysing harmonically forced and damped structures in which the authors observe that the method is accurate only up to moderately high value of vibrations amplitudes. At larger amplitudes, the response deviates from other reference solutions.

6. Reduced Order Model from the Koiter–Newton analysis

The perturbation based reduced order model developed for the Koiter–Newton post buckling analysis (Liang [31]) is the foundation of the Hamiltonian reduced order model utilized in this thesis. The method has been developed in a finite element framework using the von Kármán plate theory. The method is extensively reviewed in the next chapter and therefore would not be summarized here.

The literature search highlights some notable points which are taken into consideration in the present analysis. First, the von Kármán plate theory has been used frequently in many of the previous works and the formulations have been found to have a good level of accuracy in predicting the nonlinear modal frequencies. Second, continuation schemes are advantageous over conventional numerical methods as they provide fast convergent solutions and provide information about the stability of the solution. Third, the ambient temperature can have a significant effect on the experimental results if clamped boundary conditions are used. Therefore, free boundary condition is more suitable for the analysis to eliminate the temperature effect. Finally, imperfections in the test structure can affect the hardening behaviour of the plate. Therefore, the plate should be manufactured as flat as possible.

1.3 Research Objective & Methodology

The primary objective of the research is to design a test structure, generate a ROM using the Hamiltonian model reduction technique, numerically compute the nonlinear modal frequencies for several load cases, validate the results through experimental procedures and thus, demonstrate the feasibility of the numerical approach for real life structural problems while utilizing minimal number of degrees of freedom for the analysis. Furthermore, the experimental results add to the body of knowledge on the nonlinear dynamic analysis of stiffened plates and can be used for future validation studies.

The main research questions to be answered through this thesis are:

What is the effectiveness of the model reduction method in computing nonlinear modes?

a. What is the percentage deviation of the numerically computed fundamental modal frequency in comparison to the experimental modal frequency?
b. What is the model size sufficient to achieve the desired accurate results?

A secondary field of interest in this research is:

How does the dynamics of the stiffened plate compare to the dynamics of a plate without stiffeners for large amplitude vibrations?

The model reduction algorithm is adapted from the work of N. Singh [30] who developed a Matlab based program for nonlinear vibration analysis of simple rectangular plates. The formulation was done in a finite element framework where the strains are defined by a modified form of von- Kármán kinematic model. In this model, in-plane rotation degrees of freedom are also accounted for. The finite element model for plates was created using high performance triangular shell elements, the equations for which were extracted from Militello and Felippa [26], Alvin et al. [27]. The governing equations for the dynamics of forced and damped vibrations of a stiffened plate will be developed using the Hamiltonian formulation. The continuation scheme in the software AUTO will be used to solve the differential equations and predict the first nonlinear modal frequency. Numerical results showing frequency vs amplitude curves for harmonic load with different magnitudes would be generated.

A convergence study is planned to find the minimum number of degrees of freedom required in the ROM to achieve accurate results. Experiments have been planned using Polytec Laser Doppler Vibrometer (LDV) and PAK MK-II measurement systems. The LDV is a non-contact form of measurement system which has the capability of scanning across the test structure to take measurements at multiple points in a single run. The LDV is based on the commonly known Doppler effect which describes the frequency shift in a wave when there is relative motion between the source and an observer. PAK MK-II system is used for nonlinear vibration measurements. All edge free boundary condition would be used for the experimental setup to avoid any effect of temperature changes. The experimental results would be compared to the results from the numerical model to find the accuracy of the model. The second research question would be answered using a comparison between the numerical results from plates with and without stiffener. An approximation of backbone curves would be generated using the peaks of frequency response for forced and damped vibrations. The general hardening or softening behaviour of the two structures would be compared.

1.4 Thesis Layout

The thesis report is organized in the following manner: The validation of the Hamiltonian ROM is of primary importance in this thesis. Therefore, a detailed review of the model reduction method is described in Chapter 2, which also leads to the formulation of the governing equations of the dynamics of the plate in a Hamiltonian framework. In Chapter 3, the methodology adopted to develop the final numerical model for the stiffened plate is discussed in detail. This chapter includes description of modifications done in the model reduction code to incorporate the stiffener. It also includes description of normalization procedures included in the formulation of ROM to optimize the analysis procedure. The experimental setup and measurement procedure for linear and nonlinear vibration test are described in Chapter 4. The results obtained from the numerical analysis and experiments are compared and presented in Chapter 5. Some results are also compared to results from commercial finite element software Nastran for preliminary validation of the numerical model. Furthermore, results comparing the dynamic behaviour of the plate with and without stiffener is presented. The thesis results and findings are summarized in the Chapter 6, followed by recommendations for extension of the work in Chapter 7.

Chapter 2

Review of Hamiltonian Model Reduction Method for Nonlinear Dynamics

Numerical models for full scale structures are usually extremely large and therefore its solution requires a high computation time. Consequently, development and implementation of model reduction methods for numerical analysis is a necessity for reduction in the analysis time. For nonlinear dynamic analysis, a Hamiltonian model reduction method has been adopted in this thesis. The method is an extension of a reduction method for static problems called the Koiter-Newton method (K. Liang [31]). The main idea behind this reduction method is to use truncated asymptotic expansion to replace the original governing equations by the reduced system. This model reduction method, although developed for static problems, has been proven to be also directly applicable to dynamics problem and is highly effective for linear and nonlinear dynamic analysis in comparison to the conventional Finite element codes (N. Singh [30]). In this chapter, the theoretical basis of the model reduction method has been reviewed, which is then used to formulate the reduced order governing differential equations used for computing the nonlinear modes.

This chapter is organized in the following manner: in Section 2.1 the conditions for canonical transformations are derived which ensure that the Hamiltonian form is retained after transformation to the reduced system. It is followed by an elaborate discussion of the model reduction method for the statics case in Section 2.2, and finally the extension of the static model reduction to the dynamics case is discussed in Section 2.3. The chapter is completed with some concluding comments in Section 2.4.

2.1. Canonical Transformations

Formulation of the reduced order model (ROM) involves the transformation of the original system to a system containing reduced number of degrees of freedom. This transformation, however, should be done in a manner that the properties of the system, such as energy and momentum, are conserved and the system is still representative of the original model. In the ROM developed for dynamics, this is ensured by maintaining the form of the Hamiltonian equations of motion through Canonical Transformations. The requirement of Canonical transformation is that the Hamiltonian equation of motion is satisfied with a new Hamiltonian defined with the new variables (W. Greiner [33]).

The Hamilton's principle derives the equation of motion of a system using the variational principle on the Lagrangian of the system integrated over time. A modified form of the Hamilton's principle (H. Goldstein et. al. [32]) is given in Equation 2.1.

$$\int_{t_1}^{t_2} (\delta \mathrm{H} + \dot{\mathrm{p}}_{\mathrm{i}} \,.\, \delta \mathrm{q}_i - \dot{\mathrm{q}}_{\mathrm{i}} \,.\, \delta \mathrm{p}_i)\, \mathrm{d}t = 0 \tag{2.1}$$

In the above equation $\mathbf{q}$ refers to the displacement and $\mathbf{p}$ refers to the momentum. Canonical transformation ensures that the form of the terms inside bracket in Equation 2.1 is conserved. For the ROM derivation, transformation to a reduced system with displacement $\boldsymbol{\xi}$ and momentum $\boldsymbol{\pi}$ is considered.

$$\mathbf{q} = \mathbf{q}\,(\boldsymbol{\xi}, \boldsymbol{\pi}) \tag{2.2}$$

$$\mathbf{p} = \mathbf{p}\,(\boldsymbol{\xi}, \boldsymbol{\pi}) \tag{2.3}$$

Substituting Equations 2.2 and Equation 2.3 into $\dot{\mathbf{p}}^t\, \delta\mathbf{q} - \dot{\mathbf{q}}^t\, \delta\mathbf{p}$ gives the conditions required for a Canonical transformation of variables.

$$\begin{aligned}\dot{\mathbf{p}}^t\, \delta\mathbf{q} - \dot{\mathbf{q}}^t\, \delta\mathbf{p} = {} & \left[\left(\frac{\partial \mathbf{p}}{\partial \boldsymbol{\xi}}\right)^{\mathbf{t}} . \left(\frac{\partial \mathbf{q}}{\partial \boldsymbol{\xi}}\right) - \left(\frac{\partial \mathbf{q}}{\partial \boldsymbol{\xi}}\right)^{\mathbf{t}} . \left(\frac{\partial \mathbf{p}}{\partial \boldsymbol{\xi}}\right)\right] . \, \dot{\boldsymbol{\xi}}^{\mathbf{t}}\, \delta\boldsymbol{\xi} + \\ & \left[\left(\frac{\partial \mathbf{p}}{\partial \boldsymbol{\pi}}\right)^{t} . \left(\frac{\partial \mathbf{q}}{\partial \boldsymbol{\pi}}\right) - \left(\frac{\partial \mathbf{q}}{\partial \boldsymbol{\pi}}\right)^{t} . \left(\frac{\partial \mathbf{p}}{\partial \boldsymbol{\pi}}\right)\right] . \, \dot{\boldsymbol{\pi}}^{\mathbf{t}}\, \delta\boldsymbol{\pi} + \\ & \left[\left(\frac{\partial \mathbf{q}}{\partial \boldsymbol{\xi}}\right)^{t} . \left(\frac{\partial \mathbf{p}}{\partial \boldsymbol{\pi}}\right) - \left(\frac{\partial \mathbf{p}}{\partial \boldsymbol{\xi}}\right)^{t} . \left(\frac{\partial \mathbf{q}}{\partial \boldsymbol{\pi}}\right)\right] . \, (\dot{\boldsymbol{\pi}}^{\mathbf{t}}\, \delta\boldsymbol{\xi} - \dot{\boldsymbol{\xi}}^{\mathbf{t}}\, \delta\boldsymbol{\pi})\end{aligned} \tag{2.4}$$

From the above equation, it is clear that to retain the form of the equation the following conditions given by Equations 2.5-2.7 must be satisfied.

$$\left[\left(\frac{\partial \mathbf{p}}{\partial \boldsymbol{\xi}}\right)^{t} \cdot \left(\frac{\partial \mathbf{q}}{\partial \boldsymbol{\xi}}\right) - \left(\frac{\partial \mathbf{q}}{\partial \boldsymbol{\xi}}\right)^{t} \cdot \left(\frac{\partial \mathbf{p}}{\partial \boldsymbol{\xi}}\right)\right] = \mathbf{0} \tag{2.5}$$

$$\left[\left(\frac{\partial \mathbf{p}}{\partial \boldsymbol{\pi}}\right)^{t} \cdot \left(\frac{\partial \mathbf{q}}{\partial \boldsymbol{\pi}}\right) - \left(\frac{\partial \mathbf{q}}{\partial \boldsymbol{\pi}}\right)^{t} \cdot \left(\frac{\partial \mathbf{p}}{\partial \boldsymbol{\pi}}\right)\right] = \mathbf{0} \tag{2.6}$$

$$\left[\left(\frac{\partial \mathbf{q}}{\partial \boldsymbol{\xi}}\right)^{t} \cdot \left(\frac{\partial \mathbf{p}}{\partial \boldsymbol{\pi}}\right) - \left(\frac{\partial \mathbf{p}}{\partial \boldsymbol{\xi}}\right)^{t} \cdot \left(\frac{\partial \mathbf{q}}{\partial \boldsymbol{\pi}}\right)\right] = \mathbf{I} \tag{2.7}$$

If these conditions are satisfied it implies that the form of the Hamiltonian equation of motion is maintained, as evident from Equation 2.8. Further, it shows that the Hamiltonian equation of motion remains valid in the transformed system.

$$\dot{\mathbf{p}}^{t}\, \delta\mathbf{q} - \dot{\mathbf{q}}^{t}\, \delta\mathbf{p} = \dot{\boldsymbol{\pi}}^{\mathrm{t}}\, \delta\boldsymbol{\xi} - \dot{\boldsymbol{\xi}}^{t}\, \delta\boldsymbol{\pi} \tag{2.8}$$

This characteristic of the canonical transformations is used in development of the reduced order model in the Hamiltonian framework. The Hamiltonian principle is applied on the reduced system to derive the governing equations of motion as shown in the later sections.

2.2. Reduced Order Model for Statics

In this section, the model reduction method used in Koiter-Newton approach (K. Liang [31]) is discussed. The method is developed using truncated asymptotic expansion as an approximation for the displacements. The expansions are truncated at third order terms to reduce the complexity and computational effort required to solve the problem.

To derive the ROM a governing equation of the form given in Equation 2.9 is considered.

$$\mathbf{f}(\mathbf{q}) = \lambda \mathbf{f}_{\mathbf{ex}} \tag{2.9}$$

Here $\mathbf{f}(\mathbf{q})$ is a function representing the internal restoring forces of the system, $\mathbf{f}_{\mathbf{ex}}$ is the external force and λ is a load parameter.

If the initial equilibrium position for the system is at $\boldsymbol{q}_0$ and the relative displacements/ rotations at increasing load steps are represented by $\mathbf{u}$, then the absolute deformed shape is obtainable using a vector composition.

$$\mathbf{q} = \mathbf{q}_{\mathbf{0}} \circ \mathbf{u} \tag{2.10}$$

The vector is not composed by direct addition since it also contains rotations of each degree of freedom. The absolute rotations may not necessarily be simple additions with respect to reference position.

The Koiter-Newton method was originally developed for buckling sensitive structures which contain bifurcating equilibrium branches from the main equilibrium path. These bifurcating branches are a result of instabilities on the primary equilibrium path. To include the bifurcations, secondary perturbation loads are included in the external force matrix of the system.

$$\lambda\, \mathbf{f_{ex}} = \mathbf{F}\ \boldsymbol{\phi} \tag{2.11}$$

In the above equation $\mathbf{F}$ is the load matrix which is composed of the external force vector and additional perturbation load vectors to excite bifurcating branches, $\boldsymbol{\phi}$ is a vector containing load amplitudes.

By substituting Equation 2.10 into Equation 2.9, using a Taylor series expansion upto third order and using Equation 2.11, the nonlinear governing equation is obtained for the full model.

$$\boldsymbol{\mathcal{L}}\,(\boldsymbol{u}) + \boldsymbol{Q}\,(\boldsymbol{u},\boldsymbol{u}) + \boldsymbol{C}(\boldsymbol{u},\boldsymbol{u},\boldsymbol{u}) = \mathbf{F}\boldsymbol{\phi} \tag{2.12}$$

$\boldsymbol{\mathcal{L}}$, $\boldsymbol{Q}$, $\boldsymbol{C}$ are the functions representing the stiffness coefficients for the linear, quadratic and cubic displacement terms while **L, Q, C** represent their matrix form.

To obtain a reduced order model the displacement vector $\mathbf{u}$ is parameterized using generalized displacements $\boldsymbol{\xi}$ so that $\boldsymbol{u} = \boldsymbol{u}(\boldsymbol{\xi})$**.** The expansion is again performed upto third order terms.

$$\mathbf{u} = \mathbf{u}_{\boldsymbol{\alpha}}\, \xi_\alpha + \mathbf{u}_{\boldsymbol{\alpha\beta}}\, \xi_\alpha \xi_\beta + \mathbf{u}_{\boldsymbol{\alpha\beta\gamma}} \xi_\alpha \xi_\beta \xi_\gamma \tag{2.13}$$

In the above equation, the Einstein notation has been used and subscripts vary from 1 to m+1 where m is the number of perturbation loads chosen, $\boldsymbol{u}_{\boldsymbol{\alpha}}$ is a vector which represents the first order displacement field, $\boldsymbol{u}_{\boldsymbol{\alpha\beta}}$ and $\boldsymbol{u}_{\boldsymbol{\alpha\beta\gamma}}$ describe the higher order displacement fields.

The choice of $\boldsymbol{\xi}$ for parameterizing the displacement field is fixed by considering it to be a work conjugate of the load amplitudes. This ensures that the work done in the reduced system is equal to the work done in the actual system.

$$(\mathbf{F}\boldsymbol{\phi})^t\, \delta\mathbf{u} = \boldsymbol{\phi}^t\, \delta\boldsymbol{\xi} \tag{2.14}$$

Substituting the Equation 2.13 into Equation 2.14, constraint equations for the system are obtained. These constraint equations would be used at a later stage to show that the form of the equations for dynamics is equivalent to the static one.

$$\begin{aligned}
(\mathbf{F}\boldsymbol{\phi})^t\, \delta\boldsymbol{u} &= \boldsymbol{\phi}^t \mathbf{F}^t\, (\mathbf{u}_{\boldsymbol{\alpha}}\, \delta\xi_\alpha + \mathbf{u}_{\boldsymbol{\alpha\beta}}\, \delta\xi_\alpha\xi_\beta + \mathbf{u}_{\boldsymbol{\alpha\beta}}\, \xi_\alpha\delta\xi_\beta + \cdots) \\
&= \phi_p \mathbf{f_p}^t\, (\mathbf{u}_{\boldsymbol{\alpha}}\, \delta\xi_\alpha + \mathbf{u}_{\boldsymbol{\alpha\beta}}\, \delta\xi_\alpha\xi_\beta + \mathbf{u}_{\boldsymbol{\alpha\beta}}\, \xi_\alpha\delta\xi_\beta + \cdots) \\
&= (\mathbf{f_p}^t\mathbf{u}_{\boldsymbol{\alpha}})\, \phi_p\delta\xi_\alpha + (\mathbf{f_p}^t\mathbf{u}_{\boldsymbol{\alpha\beta}})\phi_p\, \delta\xi_\alpha\xi_\beta + (\mathbf{f_p}^t\mathbf{u}_{\boldsymbol{\alpha\beta}})\phi_p\xi_\alpha\delta\xi_\beta + \cdots \\
&\equiv \boldsymbol{\phi}^t\, \boldsymbol{\delta\xi}
\end{aligned} \tag{2.15}$$

Comparing this equation with the RHS of the Equation 2.14 , the conditions for the validity of the equation or the constraint equations are obtained.

$$\mathbf{f_\alpha}^{\mathbf{t}}\mathbf{u_\beta} = \delta_{\alpha\beta} \tag{2.16a}$$

$$\mathbf{f_\alpha}^{\mathbf{t}}\mathbf{u_{\beta\gamma}} = 0 \tag{2.16b}$$

$$\mathbf{f_\alpha}^{\mathbf{t}}\mathbf{u_{\beta\gamma\delta}} = 0 \tag{2.16c}$$

where $\delta_{\alpha\beta}$ is the Kronecker Delta and the vectors $\mathbf{f_\alpha}^{\mathrm{t}}$ are the perturbation load vectors.

In similarity to the third order expansion of the original equation of motion, the load amplitudes of the reduced system can also be expressed in terms of the displacement $\boldsymbol{\xi}$.

$$\boldsymbol{\phi} = \overline{\boldsymbol{\mathcal{L}}}\,(\xi) + \overline{\boldsymbol{Q}}\,(\xi,\xi) + \overline{\boldsymbol{C}}\,(\xi,\xi,\xi) \tag{2.17}$$

where $\overline{\boldsymbol{\mathcal{L}}}$, $\overline{\boldsymbol{Q}}$, $\overline{\boldsymbol{C}}$ are linear, quadratic and cubic functions in the equation while $\overline{\mathbf{L}}$, $\overline{\mathbf{Q}}$, $\overline{\mathbf{C}}$ are representative of their matrix forms.

The ROM equations are obtained by substituting Equation 2.17 and Equation 2.13 into Equation 2.12 and solving for the coefficient of the $\boldsymbol{\xi}$ variable. These equations are combined with the constraint Equations 2.16 a-c and solved to obtain the reduced order model.

$$\begin{bmatrix} \mathbf{L} & -\mathbf{F} \\ -\mathbf{F}^{\mathbf{t}} & \mathbf{0} \end{bmatrix} \begin{Bmatrix} \mathbf{u}_\alpha \\ \overline{\mathbf{L}}_\alpha \end{Bmatrix} = \begin{Bmatrix} \mathbf{0} \\ -\mathbf{E}_\alpha \end{Bmatrix} \tag{2.18}$$

$$\begin{bmatrix} \mathbf{L} & -\mathbf{F} \\ -\mathbf{F}^{\mathbf{t}} & \mathbf{0} \end{bmatrix} \begin{Bmatrix} \mathbf{u}_{\alpha\beta} \\ \overline{\mathbf{Q}}_{\alpha\beta} \end{Bmatrix} = \begin{Bmatrix} -\boldsymbol{Q}(\boldsymbol{u}_\alpha, \boldsymbol{u}_\beta) \\ \mathbf{0} \end{Bmatrix} \tag{2.19}$$

The linear, quadratic and cubic operators can be alternately computed using the following simplified form of the ROM equations:

$$\bar{L}_{\alpha\beta} = \mathbf{u_\alpha}^{\mathbf{t}}\,\boldsymbol{\mathcal{L}}(\mathbf{u_\beta}) \tag{2.20}$$

$$\bar{Q}_{\alpha\beta\gamma} = \mathbf{u_\alpha}^{\mathbf{t}}\,\boldsymbol{Q}(\mathbf{u_\beta}, \mathbf{u_\gamma}) \tag{2.21}$$

$$\bar{C}_{\alpha\beta\gamma\delta} = \boldsymbol{C}(\mathbf{u_\alpha}, \mathbf{u_\beta}, \mathbf{u_\gamma}, \mathbf{u_\delta}) - \frac{2}{3}\left[\mathbf{u_{\alpha\beta}}^{\mathbf{t}}\,\boldsymbol{\mathcal{L}}(\mathbf{u_{\delta\gamma}}) + \mathbf{u_{\beta\gamma}}^{\mathbf{t}}\,\boldsymbol{\mathcal{L}}(\mathbf{u_{\delta\alpha}}) + \mathbf{u_{\gamma\alpha}}^{\mathbf{t}}\,\boldsymbol{\mathcal{L}}(\mathbf{u_{\delta\beta}})\right] \tag{2.22}$$

The derivation of the ROM equations is found in Appendix B

The reduced system is solved using a path following technique for the displacement variable ξ to obtain a load-displacement history. It is notable that the third order displacement terms are used only for the derivation of the reduced model and it is not required to be computed in the actual solution. The model reduction method used for static problems has been extended successfully to a dynamics problem (N. Singh [30]). The implementation of the model reduction method for dynamics is discussed in the next section.

2.3. Extension of Model Reduction to Dynamics

In this section, the validity of the reduced order model for application to dynamics is discussed. The dynamics problem is formulated using Hamiltonian mechanics. The governing equations are formulated considering geometric nonlinearity only i.e. large displacements induce small but finite strains in the system while material behaviour is assumed to lie within the linear elastic regime.

The Hamiltonian equation of motions for an N-dimensional discrete system (Greiner [33]) is defined by Equation 2.23.

$$\dot{q}_i = \frac{\partial \mathrm{H}}{\partial p_i} \tag{2.23a}$$

$$\dot{p}_i = -\frac{\partial \mathrm{H}}{\partial q_i} \tag{2.23b}$$

where H is the Hamiltonian of the system and represents the sum of the total kinetic energy and total potential energy of a conservative system, q_i and p_i represent the displacement and momentum variables each of which are elements of N-dimensional vectors. These equations are later used to determine the governing equation of the reduced order model.

To derive a comparable formulation of the reduced order model in dynamics an assumption is made for the momentum of the system. The momentum basis is chosen as an alternative to the load matrix used in Equation 2.12 of the static method. Since the initial formulation of the governing equations in the reduced system is done for a conservative system, external forces are not directly introduced into the formulation. Therefore, a momentum basis is used to derive the ROM equations.

$$\mathbf{p} = \mathbf{P}\,\boldsymbol{\pi} \tag{2.24}$$

where $\mathbf{p}$ is the momentum vector of the full model, $\mathbf{P}$ is the basis matrix consisting of reduced number of degrees of freedom and π is a vector of unknown momentum amplitudes. The choice of the basis matrix $\mathbf{P}$ has been pre-determined based on the work done by N. Singh [30]. For the computations done in this thesis, a modal basis, i.e. product of the mass matrix and the modal matrix is chosen as the basis, which is described by Equation 2.25.

$$\mathbf{P} = \mathbf{M}\,[\boldsymbol{\Phi}_1\ \boldsymbol{\Phi}_2\ \boldsymbol{\Phi}_3 \dots \boldsymbol{\Phi}_n\,] \tag{2.25}$$

In the Equation 2.25, $\boldsymbol{\Phi}_n$ represents the eigen vector for the $\mathrm{n^{th}}$ mode. The modal matrix contains only the modes chosen for the analysis and not necessarily all the modes computed. The number of modes determine the size of the reduced order model.

The transformation to the reduced system in the Hamiltonian formulation are achieved from the following equations:

$$\mathbf{u} = \mathbf{u}(\boldsymbol{\xi}) = \mathbf{u}_{\boldsymbol{\alpha}}\, \xi_\alpha + \mathbf{u}_{\boldsymbol{\alpha\beta}}\, \xi_\alpha \xi_\beta + \mathbf{u}_{\boldsymbol{\alpha\beta\gamma}} \xi_\alpha \xi_\beta \xi_\gamma \tag{2.26a}$$

$$\mathbf{p} = \mathbf{p}(\boldsymbol{\pi}) = \mathbf{P}_{\boldsymbol{\delta}}\, \pi_\delta \tag{2.26b}$$

It is recalled from Section 2.1 that the transformed system retains its Hamiltonian form only if the transformation is canonical. Therefore, the Equation 2.5 to Equation 2.7 must be satisfied for the chosen transformation.

Since the Equation 2.26a is independent of $\boldsymbol{\pi}$ and Equation 2.26b is independent of $\boldsymbol{\xi}$, the first two conditions for canonical transformations are automatically satisfied. The third condition reduces to:

$$\left(\frac{\partial \mathbf{u}}{\partial \xi_a}\right)^{t} \cdot \left(\frac{\partial \mathbf{p}}{\partial \pi_b}\right) = \delta_{ab} \tag{2.27}$$

Substituting the expressions for $\mathbf{u}$ and $\mathbf{p}$ from Equation 2.24 in the above equation and differentiating yields:

$$\left(\mathbf{u}_{\mathbf{a}} + 2\mathbf{u}_{\mathbf{a\beta}}\, \xi_\beta + \mathbf{u}_{\mathbf{a\beta\gamma}} \xi_\beta \xi_\gamma\right). \mathbf{P}_{\boldsymbol{b}} = \delta_{ab} \tag{2.28}$$

The equation is valid if the following constraint conditions hold:

$$\mathbf{P}_{\boldsymbol{\delta}}{}^{\mathbf{t}} \mathbf{u}_{\boldsymbol{\alpha}} = \delta_{\alpha\delta} \tag{2.29a}$$

$$\mathbf{P}_{\boldsymbol{\delta}}{}^{\mathbf{t}} \mathbf{u}_{\boldsymbol{\alpha\beta}} = 0 \tag{2.29b}$$

$$\mathbf{P}_{\boldsymbol{\delta}}{}^{\mathbf{t}} \mathbf{u}_{\boldsymbol{\alpha\beta\gamma}} = 0 \tag{2.29c}$$

The constraint equations derived here are analogous to the Equation 2.16 stated for statics. The difference here is that a momentum vector $\mathbf{P}_{\boldsymbol{\delta}}$ is present instead of a load vector. The analogy between the constraint equations shows that the reduced order model for statics can be directly implemented for the dynamics problem with a variation from the load subspace to the momentum subspace.

The governing equations of motion for the reduced model is derived using Equation 2.23. The Hamiltonian of the system is computed as the sum of the total kinetic energy T $(\mathbf{u}, \mathbf{p})$ and the total potential energy V$(\mathbf{u})$.

$$\mathrm{H}(\boldsymbol{u}, \boldsymbol{p}) = \mathrm{T}(\boldsymbol{u}, \boldsymbol{p}) + \mathrm{V}(\boldsymbol{u}) \tag{2.30}$$

$$\mathrm{T}(\boldsymbol{u}, \boldsymbol{p}) = \frac{1}{2}\, \mathbf{p}^{\mathbf{t}}\, \mathbf{M}^{-\mathbf{1}} \mathbf{p} = \frac{1}{2}\, \boldsymbol{\pi}^{\mathbf{t}}\; (\mathbf{P}^{\mathbf{t}}\, \mathbf{M}^{-\mathbf{1}}\, \mathbf{P})\, \boldsymbol{\pi} \tag{2.31}$$

The equivalent kinetic energy $\overline{\mathrm{T}}$ in the reduced system is:

$$\overline{\mathrm{T}}\,(\boldsymbol{\xi}, \boldsymbol{\pi}) = \frac{1}{2}\, \boldsymbol{\pi}^{\mathbf{t}}\; \overline{\mathbf{M}}^{-\mathbf{1}}\, \boldsymbol{\pi} \tag{2.32}$$

where the reduced mass matrix is computed from $\overline{\mathbf{M}} = (\mathbf{P}^{\mathbf{t}}\, \mathbf{M}^{-\mathbf{1}}\, \mathbf{P})^{-1}$

The total potential energy of the reduced system (in Einstein's notation) is:

$$\overline{\mathrm{V}}(\boldsymbol{\xi}) = \frac{1}{2}\, \overline{\mathrm{L}}_{\alpha\beta}\, \xi_\alpha \xi_\beta + \frac{1}{3}\, \overline{\mathrm{Q}}_{\alpha\beta\gamma}\, \xi_\alpha \xi_\beta \xi_\gamma + \frac{1}{4}\, \overline{\mathrm{C}}_{\alpha\beta\gamma\delta}\, \xi_\alpha \xi_\beta \xi_\gamma \xi_\delta \tag{2.33}$$

Using the Hamiltonian formulation, the equations of motion of a conservative free vibration is derived to be:

$$\dot{\boldsymbol{\xi}} = \overline{\mathbf{M}}^{-\mathbf{1}}\, \boldsymbol{\pi} \tag{2.34a}$$

$$\dot{\boldsymbol{\pi}} = -(\overline{\boldsymbol{\mathcal{L}}}\,(\boldsymbol{\xi}) + \overline{\boldsymbol{Q}}\,(\boldsymbol{\xi}, \boldsymbol{\xi}) + \overline{\boldsymbol{C}}\,(\boldsymbol{\xi}, \boldsymbol{\xi}, \boldsymbol{\xi})) \tag{2.34b}$$

For a forced response, the external force for the reduced system is computed by using the following equation,

$$\overline{\boldsymbol{\phi}}(\mathrm{t}) = \mathbf{u}_{\boldsymbol{\alpha}}{}^{\boldsymbol{t}}\, \mathbf{f}_{\mathbf{ext}} \tag{2.35}$$

where $\mathbf{u}_{\boldsymbol{\alpha}}$ is a vector of first order derivatives of true displacements with respect to the displacements in the reduced system $\boldsymbol{\xi}$.

Structures designed for real-life applications often work in a dissipative environment i.e. in the presence of external damping. When the dissipative effect is considered, a damping model is required to formulate the governing equation. For the damping formulation described by Singh [30], a quadratic damping model is used. The dissipative energy in such a model is given by:

$$\mathrm{D} = \frac{1}{2}\, \dot{\mathbf{u}}^{\mathbf{t}}\, \mathbb{C}\, \dot{\mathbf{u}} \tag{2.36}$$

The damping coefficient is derived from a two parameter Rayleigh damping model (M. Liu et al. [34]).

$$\mathbb{C} = \alpha \mathbf{M} + \beta \mathbf{K} \tag{2.37}$$

The damping coefficient for the reduced order model is defined by Equation 2.38 and the derivation of the reduced damping matrix is described in the Appendix C.

$$\bar{\mathbb{C}} = \bar{\mathbf{M}} \left(\mathbf{P}^{t} \, \mathbf{M}^{-t} \, \mathbb{C} \, \mathbf{M}^{-1} \, \mathbf{P}\right) \overline{\mathbf{M}} \tag{2.38}$$

Considering the external temporal load and the damping model, the system of equations is transformed to:

$$\dot{\boldsymbol{\xi}} = \bar{\mathbf{M}}^{-1} \boldsymbol{\pi} \tag{2.39a}$$

$$\dot{\boldsymbol{\pi}} = -\left(\bar{\boldsymbol{\mathcal{L}}}\,(\boldsymbol{\xi}) + \bar{\boldsymbol{Q}}\,(\boldsymbol{\xi},\boldsymbol{\xi}) + \bar{\boldsymbol{C}}\,(\boldsymbol{\xi},\boldsymbol{\xi},\boldsymbol{\xi})\right) - \bar{\mathbb{C}}\,\bar{\mathbf{M}}^{-1}\boldsymbol{\pi} + \bar{\boldsymbol{\phi}}\,(t) \tag{2.39b}$$

The Equation 2.39 a-b are the governing equations of motion of a structure in terms of variables of the reduced order model. These equations are later utilized to compile and generate an executable AUTO file for the nonlinear analysis of the structure.

2.4. Conclusion

In this chapter, the formulation of the reduced order model used for the nonlinear analysis in this thesis has been reviewed. In the first section, Canonical transformations have been discussed and the conditions for the canonical transformations are derived. These conditions ensure that the reduced order model retains the Hamiltonian form. In the following section, the Koiter-Newton model reduction method developed for statics problems is reviewed. The static reduction method forms the basis of the model reduction in dynamics. The computation steps for the stiffness coefficients in the ROM have been described. In the final section, the extension of the reduced order model to a dynamics problem has been discussed. It has been proven that the method described for statics can be directly adopted for the dynamics problem. Furthermore, the governing equation of motion for dynamics has been derived in a Hamiltonian framework for conservative systems. The equations of motion have been readjusted for consideration of external loading and damping to formulate the final equations used for forced and damped systems. In the next chapter, the application of the reduced order model in the AUTO analysis is discussed.

Chapter 3

Methodology for Numerical Computations

In the previous chapters, an introduction to research topic has been given and the procedure for the development of the reduced order model has been discussed. The algorithm for the model reduction is used in combination with the continuation approach in AUTO to generate nonlinear frequency response curves for large scale structures. To minimize the overall computation time in the combined algorithms and to generalize the method, certain normalization procedures have been included. In this chapter, the application of the reduced order model in combination with AUTO, is discussed. The implementation of the governing equations in AUTO is described and adaptation of the model reduction code for the stiffened plate is discussed.

The chapter is organized in the following manner: In Section 3.1 the elaboration on implementation of Hamiltonian equations of motion in AUTO is given. Section 3.2 describes the adaptation of the model reduction code for the present analysis. The chapter is concluded through a summary in Section 3.3.

3.1. Implementation in AUTO

The continuation and bifurcation program AUTO is written in the programming language Fortran. To successfully run the analysis, the user needs to define the equation file in Fortran language containing the governing equation of the system and initial conditions for system. The governing equations need to be defined under a fixed subroutine name “FUNC” while the initial conditions are defined under the fixed subroutine “STPNT”. AUTO also offers the option to provide equations for user defined derivatives for a problem, instead of using the in-built finite difference method to obtain the derivatives. Finite difference method is based on a truncated Taylor series expansion and therefore contains truncation errors. In the present implementation, equations for analytical derivatives are also provided in the equation file for greater accuracy in the solution. Furthermore, AUTO has a pre-defined format for inducing forced oscillations into a system the details of which is discussed in the next section.

3.1.1. Periodically Forced systems

In this thesis, the analyses have been conducted for forced and damped vibrations and therefore the methodology adopted in AUTO for solving such systems is discussed in this section. The full mathematical procedure followed in the continuation scheme is described in detail in the Appendix A. The solution to a periodically forced system in AUTO, is computed by adding a nonlinear oscillator to the system of equations (Doedel et. al. [35]). The nonlinear oscillator is defined in such a way that one of its solution components is equal to the desired periodic forcing for the original nonlinear system. Furthermore, the utilization of a nonlinear oscillator for inducing the external force ensures that the system of equations remain autonomous i.e. there is no explicit time dependence in the equations. If the dynamic behaviour is modelled in a non-autonomous form, the time variable appears as an additional parameter in the system of equations. The form of the equation then deviates from the Equation A.6 stated for the pseudo-arclength continuation implemented in AUTO. Therefore, it is necessary to transform the governing equation to an autonomous form.

The equations of nonlinear oscillator used for the computations in this validation study are defined by:

$$\dot{\theta} = \omega\,\varphi + \omega\;\theta(1-\theta^2 - \varphi^2) \tag{3. 1a}$$

$$\dot{\varphi} = -\omega\,\theta + \omega\;\varphi(1-\theta^2 - \varphi^2) \tag{3. 1b}$$

This system of equation gives the asymptotically stable solutions (Doedel [28]):

$$\theta = \sin(\omega t) \tag{3. 2a}$$

$$\varphi = \cos(\omega t) \tag{3. 2b}$$

It means that the response of the system converges to the stable solution, defined by the above equations, if the initial conditions are sufficiently close to the stable solution. This characteristic of the nonlinear oscillator ensures that the induced periodic forcing function always has a known unit amplitude. It can be easily demonstrated by integrating the system of equations over time and plotting a phase portrait diagram of the variables θ and φ. Some of the phase portrait diagrams for the nonlinear oscillator defined by Equations 3.1 a-b are shown in Figure 3.1. Different initial conditions are chosen and the differential equations are solved by the in-built ode45 solver of MATLAB. It is clearly observed that the solution converges to a stable unit circle for any initial conditions chosen. Furthermore, the multiplication of the frequency parameter ω to the nonlinear term in Equation 3.1 a-b ensures that the time required for convergence to the stable solution, during a time integration, is independent of the applied frequency.

Considering the Hamiltonian formulation of equation of forced and damped system in Section 2.3 along with the equations of nonlinear oscillator, the equations implemented in the input file of AUTO (denoted in Einstein's notation) are:

$$\dot{\xi}_i = \pi_i \tag{3. 3a}$$

$$\dot{\pi}_i = -\left(\bar{\mathrm{L}}_{\mathrm{ij}}\xi_{\mathrm{j}} + \bar{\mathrm{Q}}_{\mathrm{ijk}}\xi_j\xi_k + \bar{\mathrm{C}}_{\mathrm{ijkl}}\,\xi_j\xi_k\xi_l\right) + \bar{\Phi}_i f\theta - \bar{\mathbb{C}}_{\mathrm{ij}}\pi_{\mathrm{j}} \tag{3. 3b}$$

$$\dot{\theta} = \omega \, \varphi + \omega \;\; \theta(1 - \theta^2 - \varphi^2) \tag{3. 3c}$$

$$\dot{\varphi} = -\omega \, \theta + \omega \;\; \varphi(1 - \theta^2 - \varphi^2) \tag{3. 3d}$$

$\bar{\phi}_i$ is an element of the reduced load vector, *f* is the constant load parameter, ω is the frequency continuation parameter. In the above equations, it is assumed that the mass matrix is normalized and is an identity matrix. This assumption always holds true when the orthonormalized modal basis matrix is chosen, as can be deduced from the reduced mass matrix in Equation 2.32 .The adaptation of the model reduction method for the present nonlinear frequency analysis is discussed in the next section.

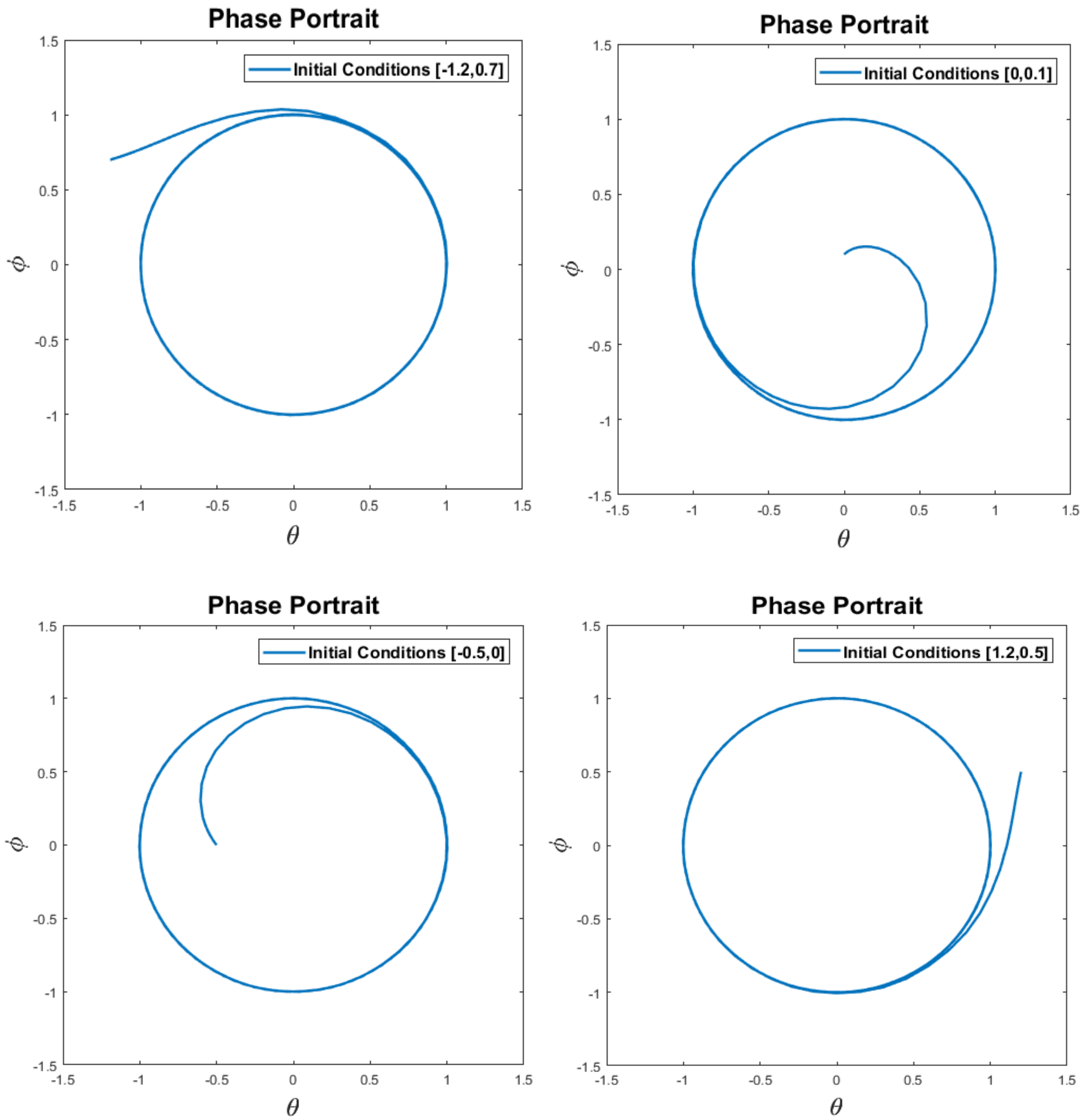

Figure 3. 1 *: Phase portrait diagrams for the nonlinear oscillator considering different initial conditions*

3.1.2. Analytical Derivatives

The requirement of derivatives of input equations arises due to the continuation procedure used in AUTO. It is evident from the computation steps described in Section A.2 that the derivatives with respect to the state variable and the continuation parameters are utilized in the corrector step of the pseudo-arclength continuation. As stated earlier, the user-defined analytical derivatives are used for the computations in this thesis, for greater accuracy. The derivatives are evaluated with respect to the state variable vector comprising of displacement variable $\boldsymbol{\xi}$, momentum variable $\boldsymbol{\pi}$, variables of the nonlinear oscillator θ and φ. Another set of derivatives are evaluated with respect to the continuation parameters. The continuation parameters used are: the load parameter *f* and the frequency parameter ω. The derivatives computed are essentially Jacobians of the Equations 3.3 a-d.

Assuming that there are 'N' degrees of freedom in the reduced order model, the total number of governing equations are $\mathrm{k} = 2\times\mathrm{N} + 2$. For the RHS of each equation a denotation $\mathrm{F_i}$ is used where i = 1 → $2\times\mathrm{N} + 2$. The Jacobian of the system of equations with respect to the state variable vectors, denoted here as DFDQ, is then defined as:

$$\mathbf{DFDQ} = \begin{bmatrix} \frac{\partial \mathrm{F_1}}{\partial \xi_1} & \frac{\partial \mathrm{F_1}}{\partial \xi_2} & \cdots & \frac{\partial \mathrm{F_1}}{\partial \xi_\mathrm{N}} & \frac{\partial \mathrm{F_1}}{\partial \pi_1} & \frac{\partial \mathrm{F_1}}{\partial \pi_2} & \cdots & \frac{\partial \mathrm{F_1}}{\partial \theta} & \frac{\partial \mathrm{F_1}}{\partial \varphi} \\ \frac{\partial \mathrm{F_2}}{\partial \xi_1} & \frac{\partial \mathrm{F_2}}{\partial \xi_2} & & \frac{\partial \mathrm{F_2}}{\partial \xi_\mathrm{N}} & \frac{\partial \mathrm{F_2}}{\partial \pi_1} & \frac{\partial \mathrm{F_2}}{\partial \pi_2} & \cdots & \frac{\partial \mathrm{F_2}}{\partial \theta} & \frac{\partial \mathrm{F_2}}{\partial \varphi} \\ \vdots & & \ddots & & & \vdots & & & \\ \frac{\partial \mathrm{F_k}}{\partial \xi_1} & \frac{\partial \mathrm{F_k}}{\partial \xi_2} & \cdots & \frac{\partial \mathrm{F_k}}{\partial \xi_\mathrm{N}} & \frac{\partial \mathrm{F_k}}{\partial \pi_1} & \frac{\partial \mathrm{F_k}}{\partial \pi_2} & \cdots & \frac{\partial \mathrm{F_k}}{\partial \theta} & \frac{\partial \mathrm{F_k}}{\partial \varphi} \end{bmatrix} \tag{3. 4}$$

For i = 1 → N,

$$\frac{\partial \mathrm{F_i}}{\partial \xi_i} = 0 \tag{3. 5}$$

$$\frac{\partial \mathrm{F_i}}{\partial \pi_i} = 1 \tag{3. 6}$$

$$\frac{\partial \mathrm{F_i}}{\partial \theta} = 0 \tag{3. 7}$$

$$\frac{\partial \mathrm{F_i}}{\partial \varphi} = 0 \tag{3. 8}$$

For i = N+1 → 2N,

$$\frac{\partial \mathrm{F_i}}{\partial \xi_i} = -\left(\overline{\mathrm{L}}_{\mathrm{ij}} + 2\,\overline{\mathrm{Q}}_{\mathrm{ijk}}\xi_\mathrm{k} + 3\,\overline{\mathrm{C}}_{\mathrm{ijkl}}\,\xi_\mathrm{k}\xi_l\right) \tag{3.9}$$

$$\frac{\partial \mathrm{F_i}}{\partial \pi_i} = -\bar{\mathbb{C}}_{\mathbf{ij}} \tag{3.10}$$

$$\frac{\partial \mathrm{F_i}}{\partial \theta} = \bar{\Phi}_i f \tag{3. 11}$$

$$\frac{\partial \mathrm{F_i}}{\partial \varphi} = \quad 0 \tag{3. 12}$$

For i = 2N+1,

$$\frac{\partial \mathrm{F_i}}{\partial \xi_i} = 0 \tag{3. 13}$$

$$\frac{\partial \mathrm{F_i}}{\partial \pi_i} = 0 \tag{3. 14}$$

$$\frac{\partial \mathrm{F_i}}{\partial \theta} = \ \omega(1 - 3\theta^2 - \ \varphi^2) \tag{3. 15}$$

$$\frac{\partial \mathrm{F_i}}{\partial \varphi} = \omega \ (1 - 2\theta\varphi) \tag{3. 16}$$

For i = 2N+2,

$$\frac{\partial \mathrm{F_i}}{\partial \xi_i} = 0 \tag{3. 17}$$

$$\frac{\partial \mathrm{F_i}}{\partial \pi_i} = 0 \tag{3. 18}$$

$$\frac{\partial \mathrm{F_i}}{\partial \theta} = \ -\omega(1 + 2\theta\varphi) \tag{3. 19}$$

$$\frac{\partial \mathrm{F_i}}{\partial \varphi} = \omega \ (1 - \theta^2 - 3\varphi^2) \tag{3. 20}$$

Similarly, the derivatives with respect to the continuation parameters, denoted here as DFDP, are derived analytically as:

$$\mathbf{DFDP} = \begin{bmatrix} \frac{\partial \mathrm{F_1}}{\partial \omega} & \frac{\partial \mathrm{F_1}}{\partial \mathrm{f}} \\ \frac{\partial \mathrm{F_2}}{\partial \omega} & \frac{\partial \mathrm{F_2}}{\partial \mathrm{f}} \\ \vdots & \vdots \\ \frac{\partial \mathrm{F_k}}{\partial \omega} & \frac{\partial \mathrm{F_k}}{\partial \mathrm{f}} \end{bmatrix} \tag{3. 21}$$

For i = 1 → N

$$\frac{\partial \mathrm{F_i}}{\partial \omega} = 0 \tag{3.22}$$

$$\frac{\partial \mathrm{F_i}}{\partial \mathrm{f}} = 0 \tag{3.23}$$

For i = N+1 → 2N

$$\frac{\partial \mathrm{F_i}}{\partial \omega} = 0 \tag{3.24}$$

$$\frac{\partial \mathrm{F_i}}{\partial \mathrm{f}} = \bar{\phi}_i \theta \tag{3.25}$$

For i = 2N+1,

$$\frac{\partial \mathrm{F_i}}{\partial \omega} = \varphi + \theta\,(1 - \theta^2 - \varphi^2) \tag{3.26}$$

$$\frac{\partial \mathrm{F_i}}{\partial \mathrm{f}} = 0 \tag{3.27}$$

For i = 2N+2,

$$\frac{\partial \mathrm{F_i}}{\partial \omega} = \varphi\,(1 - \theta^2 - \varphi^2) - \theta \tag{3.28}$$

$$\frac{\partial \mathrm{F_i}}{\partial \mathrm{f}} = 0 \tag{3.29}$$

These derivatives are arranged into a matrix form to provide an input to the continuation algorithm in AUTO. Using analytical derivatives is not a necessity for simple problems, however, it is highly recommended for sensitive problems where convergence issues exist or a high number of bifurcating branches are obtained in the solution (Doedel et. al. [35]).

In addition to the equation file, a module has been created in Fortran to read the reduced order model as an input. The code for this module is presented in the Appendix D. This file, in combination with the equation file and the already existing AUTO library files are combined to form an executable file. The executable file is used for all subsequent analyses done to generate the nonlinear frequency response curves. The next step is to adapt the existing model reduction code in Matlab for a simple rectangular plate, developed by N. Singh [30], such that it can be effectively used for the AUTO analysis.

3.2. Adaptation of the Model reduction code

The model reduction code originally consisted of a finite element model of a simple rectangular plate created using three node high performance triangular shell elements. The code has capabilities of conducting modal analysis, linear static analysis, time domain linear dynamic and nonlinear dynamic analyses. The dynamic analyses are conducted in the reduced system i.e. after the generation of the reduced order model. For the computation of nonlinear modes in this thesis project, the following features of this code is utilized: modal analysis, algorithm for generation of the reduced order model, and conversion of the response of the reduced system to the real system. However, certain modifications were incorporated into the code to make it more suitable for the present analysis. Firstly, the system is transformed to modal coordinates. Secondly, a scaling factor is introduced to normalize the stiffness terms and the applied frequency of forcing function. The utility of this scaling factor is discussed later. Finally, the geometric modelling and adaptation of the code to incorporate a stiffener for the plate is done. The following subsections discuss in detail the methodology adopted to include the aforementioned modifications.

3.2.1. Modal Coordinates

The transformation to modal coordinates is done to decouple the mass and linear stiffness matrices such that the diagonal terms are representative of the modal mass and the modal stiffness respectively. The decoupled system is utilized later for computing the scale factors introduced to non-dimensionalize the system of equations. The transformation is done using the sequence of steps described below.

An eigenvalue analysis is done using the linear stiffness matrix and the mass matrix of the reduced order model. This computation produces eigenvectors $\boldsymbol{\mathcal{V}}$ corresponding to the modes chosen in the basis matrix. The eigenvectors are mass orthonormalized to reduce the mass matrix to an identity matrix. The modal mass for the j^{th} mode is computed using:

$$\mathrm{m_{jj}} = \boldsymbol{\mathcal{V}_{\mathrm{j}}}^{\boldsymbol{t}}\, \bar{\mathbf{M}}\, \boldsymbol{\mathcal{V}_{j}} \tag{3. 30}$$

Each eigenvector is normalized by its modal mass.

$$\mathcal{V}_{\mathrm{jk}} = \frac{\mathcal{V}_{\mathrm{jk}}}{\mathrm{m_{jj}}} \tag{3. 31}$$

The normalized eigenvectors are used for the transformation to modal coordinates.

$$\xi_i = \mathcal{V}_{i\alpha}\, \eta_\alpha \tag{3. 32}$$

If the above transformation is used, the total kinetic energy (in Einstein's notation) is given by Equation 3.33.

$$T = \frac{1}{2}\,\overline{\mathrm{M}}_{\mathrm{ij}}\,\mathcal{V}_{i\alpha}\,\mathcal{V}_{j\beta}\,\dot{\eta}_{\alpha}\,\dot{\eta}_{\beta} \tag{3. 33}$$

The total potential energy is:

$$\begin{aligned} V = \frac{1}{2}\,\overline{\mathrm{L}}_{\mathrm{ij}}\,\mathcal{V}_{i\alpha}\,\mathcal{V}_{j\beta}\,\eta_{\alpha}\,\eta_{\beta} + \frac{1}{3}\,\overline{\mathrm{Q}}_{\mathrm{ijk}}\,\mathcal{V}_{i\alpha}\,\mathcal{V}_{j\beta}\,\mathcal{V}_{k\gamma}\,\eta_{\alpha}\,\eta_{\beta}\,\eta_{\gamma} \\ + \frac{1}{4}\,\overline{\mathrm{C}}_{\mathrm{ijkl}}\,\mathcal{V}_{i\alpha}\,\mathcal{V}_{j\beta}\,\mathcal{V}_{k\gamma}\,\mathcal{V}_{l\delta}\,\eta_{\alpha}\,\eta_{\beta}\,\eta_{\gamma}\,\eta_{\delta} \end{aligned} \tag{3.34}$$

From Equation 3.33 and Equation 3.34, reduced mass and stiffness matrices in the transformed coordinates are:

$$\overline{\mathrm{M}}_{\alpha\beta} = \overline{\mathrm{M}}_{\mathrm{ij}}\,\mathcal{V}_{i\alpha}\,\mathcal{V}_{j\beta} \tag{3. 35}$$

$$\overline{\mathrm{L}}_{\alpha\beta} = \overline{\mathrm{L}}_{\mathrm{ij}}\,\mathcal{V}_{i\alpha}\,\mathcal{V}_{j\beta} \tag{3.36}$$

$$\overline{\mathrm{Q}}_{\alpha\beta\gamma} = \overline{\mathrm{Q}}_{\mathrm{ijk}}\,\mathcal{V}_{i\alpha}\,\mathcal{V}_{j\beta}\,\mathcal{V}_{k\gamma} \tag{3.37}$$

$$\overline{\mathrm{C}}_{\alpha\beta\gamma\delta} = \overline{\mathrm{C}}_{\mathrm{ijkl}}\,\mathcal{V}_{i\alpha}\,\mathcal{V}_{j\beta}\,\mathcal{V}_{k\gamma}\,\mathcal{V}_{l\delta} \tag{3. 38}$$

To obtain the reduced damping matrix in transformed coordinates, the total dissipative energy is considered.

$$D = \frac{1}{2}\,\overline{\mathbb{C}}_{\mathbf{ij}}\,\mathcal{V}_{i\alpha}\,\mathcal{V}_{j\beta}\,\dot{\eta}_{\alpha}\,\dot{\eta}_{\beta} \tag{3.39}$$

$$\overline{\mathbb{C}}_{\alpha\beta} = \overline{\mathbb{C}}_{\mathrm{ij}}\,\mathcal{V}_{i\alpha}\,\mathcal{V}_{j\beta} \tag{3.40}$$

The load vector is transformed by considering the equivalent work done.

$$\bar{\phi}_{\alpha}\,\delta\xi_{\alpha} = \bar{\phi}_{i}\,\mathcal{V}_{i\alpha}\,\delta\eta_{\alpha} \tag{3. 41}$$

$$\bar{\phi}_{\alpha} = \bar{\phi}_{i}\,\mathcal{V}_{i\alpha} \tag{3.42}$$

The transformation to modal coordinates ensures that the reduced mass matrix is always an identity matrix since the eigenvectors used in its formulation are orthonormalized with respect to mass. The ROM matrices are now used to derive scale factors for non-dimensionalization of the variables in the governing equations.

3.2.2. Scale Factors

Scale factors are introduced to non-dimensionalize the system parameters: time, force and the state variable. The method used to derive the scale factors is illustrated using the Lagrange form of equation of motion. With the assumption of an identity mass matrix, the nonlinear differential equation of motion is:

$$\ddot{\boldsymbol{\eta}} + \bar{\mathbb{C}}\,\dot{\boldsymbol{\eta}} + \overline{\boldsymbol{\mathcal{L}}}(\boldsymbol{\eta}) + \overline{\boldsymbol{Q}}(\boldsymbol{\eta},\boldsymbol{\eta}) + \overline{\boldsymbol{C}}(\boldsymbol{\eta},\boldsymbol{\eta},\boldsymbol{\eta}) = \overline{\boldsymbol{\phi}}\ \sin(\omega t) \tag{3.43}$$

The scale factors introduced are:

$$\overset{\frown}{\boldsymbol{\eta}} = \boldsymbol{\eta}/\alpha \tag{3. 44a}$$

$$\overset{\frown}{\mathrm{t}} = \mathrm{t}/\beta \tag{3. 44b}$$

$$\overset{\frown}{\overline{\boldsymbol{\phi}}} = \overline{\boldsymbol{\phi}}/\gamma \tag{3. 44c}$$

By substituting the scale factors into Equation 3.43, it is transformed to:

$$\frac{\alpha}{\beta^2}\ddot{\overset{\frown}{\boldsymbol{\eta}}} + \frac{\alpha}{\beta}\bar{\mathbb{C}}\,\dot{\overset{\frown}{\boldsymbol{\eta}}} + \alpha\,\overline{\boldsymbol{\mathcal{L}}}(\overset{\frown}{\boldsymbol{\eta}}) + \alpha^2\,\overline{\boldsymbol{Q}}(\overset{\frown}{\boldsymbol{\eta}},\overset{\frown}{\boldsymbol{\eta}}) + \alpha^3\,\overline{\boldsymbol{C}}(\overset{\frown}{\boldsymbol{\eta}},\overset{\frown}{\boldsymbol{\eta}},\overset{\frown}{\boldsymbol{\eta}}) = \gamma\overset{\frown}{\overline{\boldsymbol{\phi}}}\ \sin(\omega\,\overset{\frown}{\mathrm{t}}\ \beta) \tag{3.45}$$

The form of the equation is rearranged by multiplying all terms with $\frac{\beta^2}{\alpha}$.

$$\ddot{\overset{\frown}{\boldsymbol{\eta}}} + \beta\,\bar{\mathbb{C}}\,\dot{\overset{\frown}{\boldsymbol{\eta}}} + \beta^2\,\overline{\boldsymbol{\mathcal{L}}}(\overset{\frown}{\boldsymbol{\eta}}) + \alpha\,\beta^2\,\overline{\boldsymbol{Q}}(\overset{\frown}{\boldsymbol{\eta}},\overset{\frown}{\boldsymbol{\eta}}) + \alpha^2\beta^2\,\overline{\boldsymbol{C}}(\overset{\frown}{\boldsymbol{\eta}},\overset{\frown}{\boldsymbol{\eta}},\overset{\frown}{\boldsymbol{\eta}}) = \frac{\beta^2}{\alpha}\gamma\overset{\frown}{\overline{\boldsymbol{\phi}}}\ \sin(\omega\,\overset{\frown}{\mathrm{t}}\ \beta) \tag{3.46}$$

The scale factors are now computed by equating the coefficients in the above equation. This ensures that the large linear, quadratic and cubic stiffness terms are normalized and scaled down to a similar order of magnitude. The scaling minimizes any existing error percentage in the stiffness terms. It also reduces the possibility of numerical instabilities which may occur due to the presence of errors.

The scale factor α_i for the i^{th} mode is determined using the diagonal elements of the stiffness matrices.

$$\alpha_i = \sqrt{\frac{L_{ii}}{C_{iiii}}} \tag{3.47}$$

Alternately, α_i can also be computed from:

$$\alpha_i = \frac{L_{ii}}{Q_{iii}} \tag{3.48}$$

The maximum of these two values is chosen as the scale factor α for the mode under consideration in AUTO analysis.

The scale factor β_i is obtained from the linear stiffness and identity mass matrix.

$$\beta_i = \sqrt{\frac{1}{L_{ii}}} = \frac{1}{\omega_{ni}} \tag{3.49}$$

ω_{ni} is the modal frequency for the i^{th} mode.

Since, the system of equations has been transformed to modal coordinates with an identity mass matrix, the diagonal terms of the linear stiffness matrix are representative of the linear modal frequency. By substituting this scale factor in Equation 3.46 it is observed that the applied frequency of forcing function is normalized by the linear modal frequency. This is extremely useful in computations in AUTO since the frequency sweep range is reduced to the vicinity of unity. The sweep range, otherwise, has a rather large margin depending on the magnitude of the linear modal frequency resulting in a large computation time.

The scale factor γ_i is computed using:

$$\gamma_i = L_{ii}\,\alpha_i \tag{3.50}$$

The scale factors are then used to scale the load vector, stiffness and damping matrices.

$$\acute{\mathbf{L}} = \beta^2 \bar{\mathbf{L}} \tag{3.51a}$$

$$\acute{\mathbf{Q}} = \alpha\,\beta^2\,\bar{\mathbf{Q}} \tag{3.51b}$$

$$\acute{\mathbf{C}} = \alpha^2\beta^2\,\bar{\mathbf{C}} \tag{3.51c}$$

$$\acute{\mathbb{C}} = \beta\bar{\mathbb{C}} \tag{3.51d}$$

The load vector is transformed according to Equation 3.44c.

The ROM parameters derived from Equations 3.51(a-d) are the final input to AUTO for the nonlinear frequency analysis.

3.2.3. Geometric Model of Stiffened Plate

The model reduction algorithm was initially written for a simple rectangular plate. The present analysis is conducted on a stiffened plate keeping in consideration its broad application on Aerospace structures. Therefore, modification of the Matlab code for inclusion of the stiffener geometry is necessary. The primary task in this procedure is to define a connectivity table for the nodes in the stiffener and eliminate the common nodes between the stiffener and plate. The connectivity table defines the triangular elements used in the Finite element model. An example of the meshed structure generated from the Matlab code is depicted below in Figure 3.2.

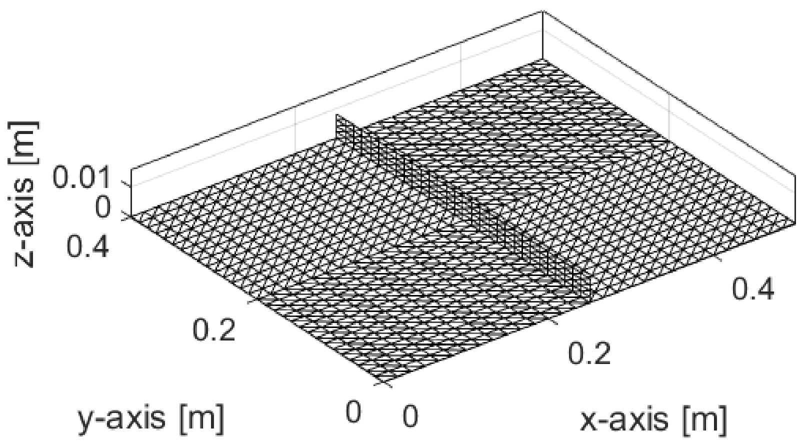

Figure 3. 2 : *Stiffened plate model used for the dynamic analysis*

3.3. Conclusion

In this chapter, the methodology adopted to obtain the nonlinear frequency response of the stiffened plate is discussed. In the first section, the details of the implementation done in AUTO to generate the executable file is discussed. The equations used for periodically forced oscillation along with the governing equations of motion have been described. The analytical derivatives with respect to state variables and continuation parameters have been derived. These analytical derivatives are used to improve accuracy of the computations in AUTO. In the second section adaptation of the model reduction code has been discussed. The system of equations has been transformed to modal coordinates. Scale factors, used in the analysis to simplify the computations and reduce the errors, have been derived. Finally, the geometry of the finite element model of the stiffened plate has been displayed. The development of the numerical model has been fully described and the vibration experiments conducted for the validation study are described in the next chapter.

Chapter 4

Experimental Setup and Procedure

In the previous chapters, the complete numerical model of the stiffened plate has been developed. Foundation has been laid to formulate the reduced order model of the stiffened plate and obtain the nonlinear frequency response using AUTO. The next step is to conduct the dynamic experiments to validate the numerical model developed. First, a linear vibration test is conducted to validate the linear modal analysis and to estimate the linear damping ratio. Subsequently, the damping ratio is used in the nonlinear analysis which is validated using nonlinear dynamics experiments. The experiments are conducted using Polytec Scanning Vibrometer (PSV) setup in the Mechanical, Maritime and Materials engineering faculty. The PSV offers a fast and accurate means of measuring linear vibration response on multiple points on the structure. The nonlinear vibration response is generated using a combination of PSV and PAK-MK II measurement system which is developed by Müller-BBM Vibroakustik Systeme. In this chapter, the experimental setup and procedure is described.

The chapter is organized in the following way: In Section 4.1, the test structure designed for the validation study is described. In Section 4.2, a description of the experimental setup used in the study is given. Section 4.3 describes the measurement procedure and settings used. The chapter is concluded with a summary in Section 4.4.

4.1. Description of the Test structure

The validation study is conducted using a stiffened plate. The material of the test structure was chosen to be Aluminium 5083 as per the availability at the manufacturing facility. The dimensions of the plate have been decided, keeping in consideration dimensional limitation of the test frame and manufacturing aspects of the plate. The final dimensions of the test structure manufactured are defined in Table 4.1. The plate was manufactured at the Demo Workshop at the faculty of Aerospace Engineering. CNC Milling was used to create the integrally stiffened plate from an Aluminium block. Tool forces in the machining process can often imbibe residual stresses into the structure which results in a spring-back action, thus, resulting in plate bending. Manufacturing imperfections have a tendency to change the dynamic response of the structure (F. Alijani et. al. [39]).

The modelling of manufacturing imperfections is not included in the present analysis and therefore, a greater plate thickness was chosen to minimize the plate bending during manufacturing. Furthermore, the choice of an integrally stiffened plate, instead of mechanically fastened or bonded stiffeners, is also justified by the modelling limitations of the current model reduction code. Modifications would be necessary in the finite element model for accurate modelling of the structure if adhesive bonding or mechanical fasteners are used.

Parameter	Dimension in (m)
Length of the plate	0.5
Width of the plate	0.4
Thickness of the plate	0.002
Height of stiffener	0.008
Thickness of stiffener	0.005
Length of stiffener	0.4

Table 4. 1 *: Dimensions of the Stiffened plate*

The material properties of Aluminium 5083 is described in Table 4.2.

Property	Value	Unit
Modulus of elasticity	71e9	Pascal
Density	2660	kg/m^3
Poisson's ratio	0.33	-

Table 4. 2 *: Material properties for Aluminium 5083*

The CAD model of the stiffened plate created in Catia v5 is depicted in Figure 4.1.

4.2. Experimental Setup

The PSV is an optical sensing device based on the principles of Doppler effect. It is a non-contact form of measurement device which uses laser signals to measure velocity, displacement and acceleration at the user-defined points on a structure (Castellini et. al. [36] and P. Sriram et. al. [37]) . The Doppler effect is an apparent shift in the frequency of a wave due to relative motion between a source and an observer (H. Tabatabai et. al. [38]). The frequency shift is measured by comparing the frequencies of the laser beam incident on the test structure to an internal reference beam. This frequency shift is then correlated to the velocity at the point through an internal algorithm in the system. PSV has certain advantages compared to using accelerometers for vibration measurement. Firstly, the effect of the added mass on the dynamics of the structure due to accelerometers is completely eliminated. Secondly, measurement points can be defined with a high spatial resolution which gives an accurate prediction of the mode shape.

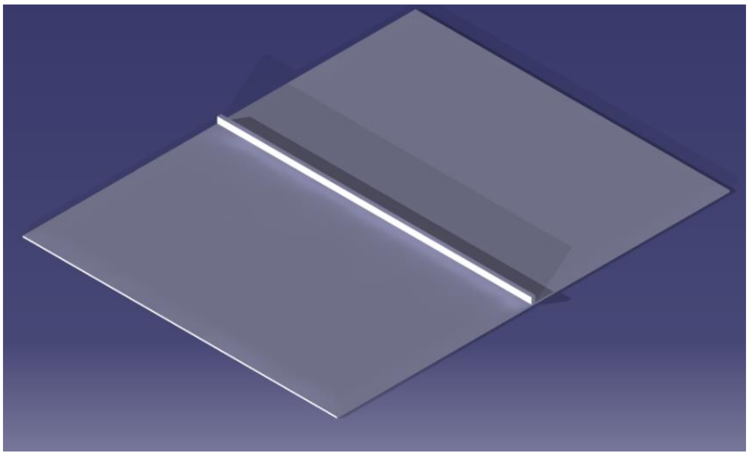

Figure 4. 1 *: CAD model of the stiffened plate used to generate part drawing for the manufacturing process*

The primary components used in the setup are: PSV controller, Junction Box, PSV laser scanning head, PSV data management system, PAK hardware device (nonlinear dynamics), excitation source (shaker), force sensor and stinger. The functionalities of the different components are described below.

Figure 4. 2 *: Assembly of Polytec controller, junction box, and the connected computer for real time monitoring of data*

Vibrometer Controller – The controller consists of velocity and displacement decoders which transform the measured optical data to the vibration velocity and displacement respectively. Different decoders with varying sensitivities are available for choice. The decoder can be chosen from the PSV software depending on the peak vibration amplitudes.

Junction Box - It receives the measurement data from the controller and transfers it to the data management system (DMS). The velocity output, force measurement and the drive signal are received as an input to the Junction box. It also has the functionality of generating the drive signal which is delivered to the shaker using cables.

Data Management System – It stores and processes the measurement data. The PSV software is also installed in the DMS. Real time monitoring of the measurement data can be done through the DMS.

Laser Scanning Head - The scanning head emits the laser beam which is used to measure the velocity at any point on the structure. It contains internal reflective mirrors which are used to change the position of the laser beam on the structure. The intensity of the signal received in the scanning head is a major factor determining the accuracy of the measurement. If the laser intensity is too low due to poor reflectivity of the surface of the test structure, then the measurements are likely to be erroneous.

Shaker - The modal exciter B&K4809 is used in this measurement setup. The exciter has a force rating of 45 N and 10 kHz frequency bandwidth for excitation. The force is transmitted to the test structure using a thin stinger. The choice of a thin stinger ensures that test structure is decoupled from the dynamics of the shaker.

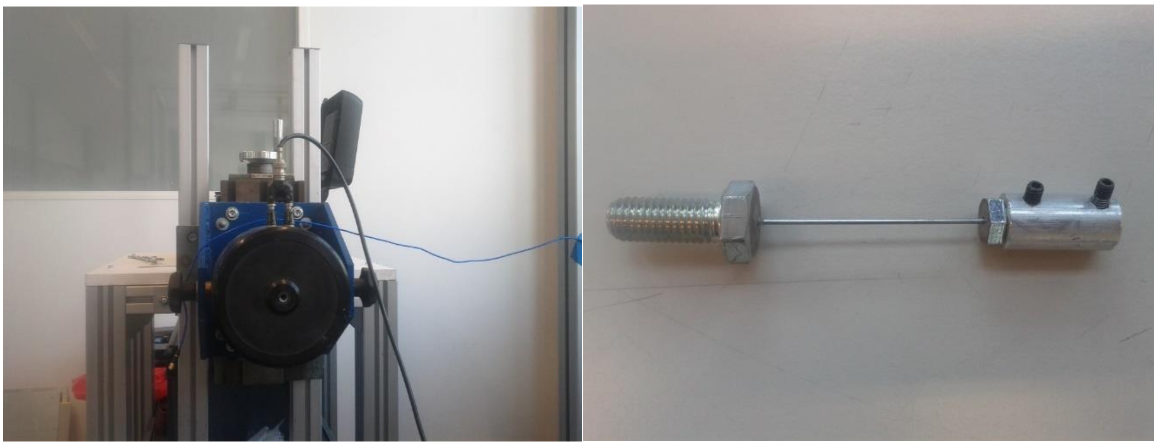

Figure 4. 3 a-b*: B&K Modal exciter mounted on its supporting rails (left) and the stinger assembly connecting the exciter and structure (right)*

Force Sensor - It is attached at the excitation point to get a measure of the actual load acting on the structure. The response of the force sensor is used as the input to compute the transfer function or the Frequency response function (FRF) for the test structure in linear vibrations.

The sensitivity of the force sensor used is 0.021834 V / N. The force sensor used is depicted in Figure 4.4.

Figure 4. 4 : *Force sensor attached at excitation point*

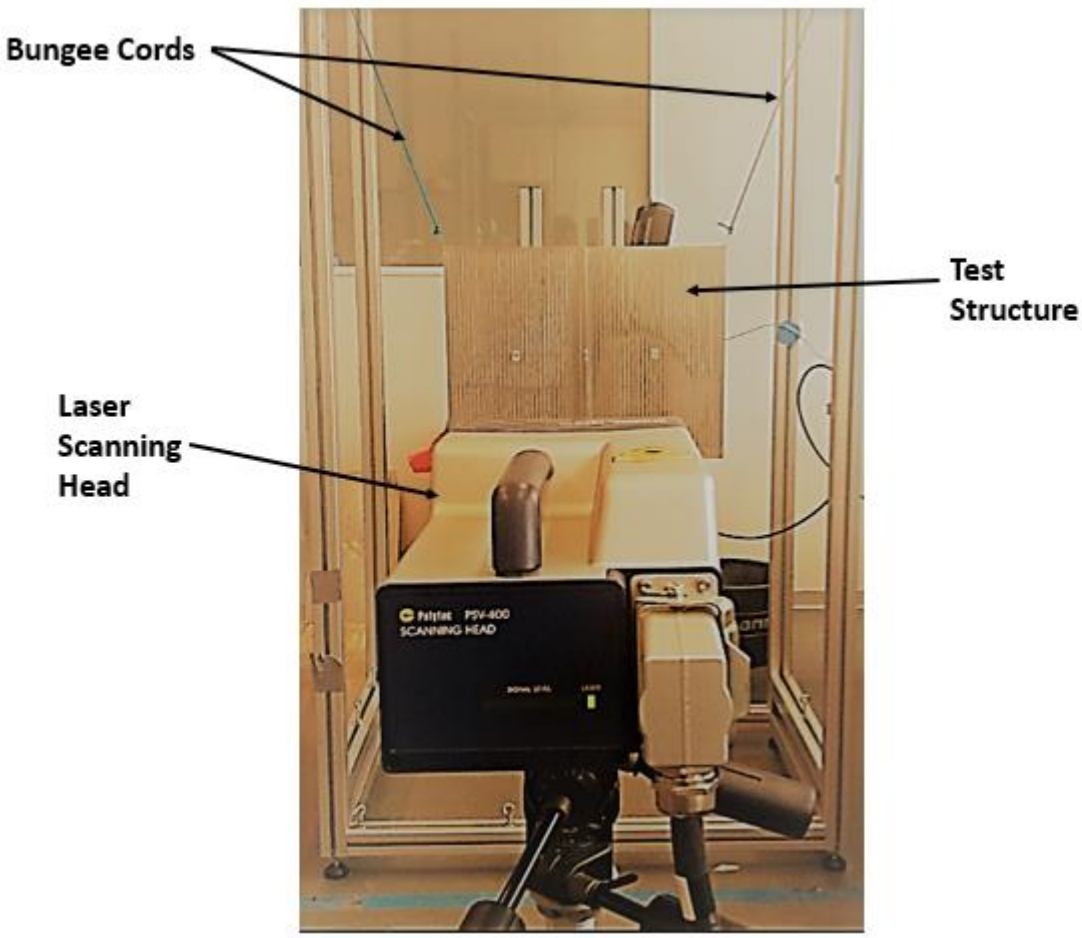

Figure 4. 5 *: Assembly of the test structure with free boundary conditions and laser scanning head*

The experiments are conducted by simulating free boundary conditions for the stiffened plate. This is achieved by suspending the stiffened plate using bungee cords from two points near the top edge. The high elasticity in the cord ensures that the degrees of freedom at the points of suspension are not rigidly constrained and instead is a close approximation of the free boundary condition. All other edges of the plate are completely free. A pictorial depiction of the experimental setup is given in Figure 4.5.

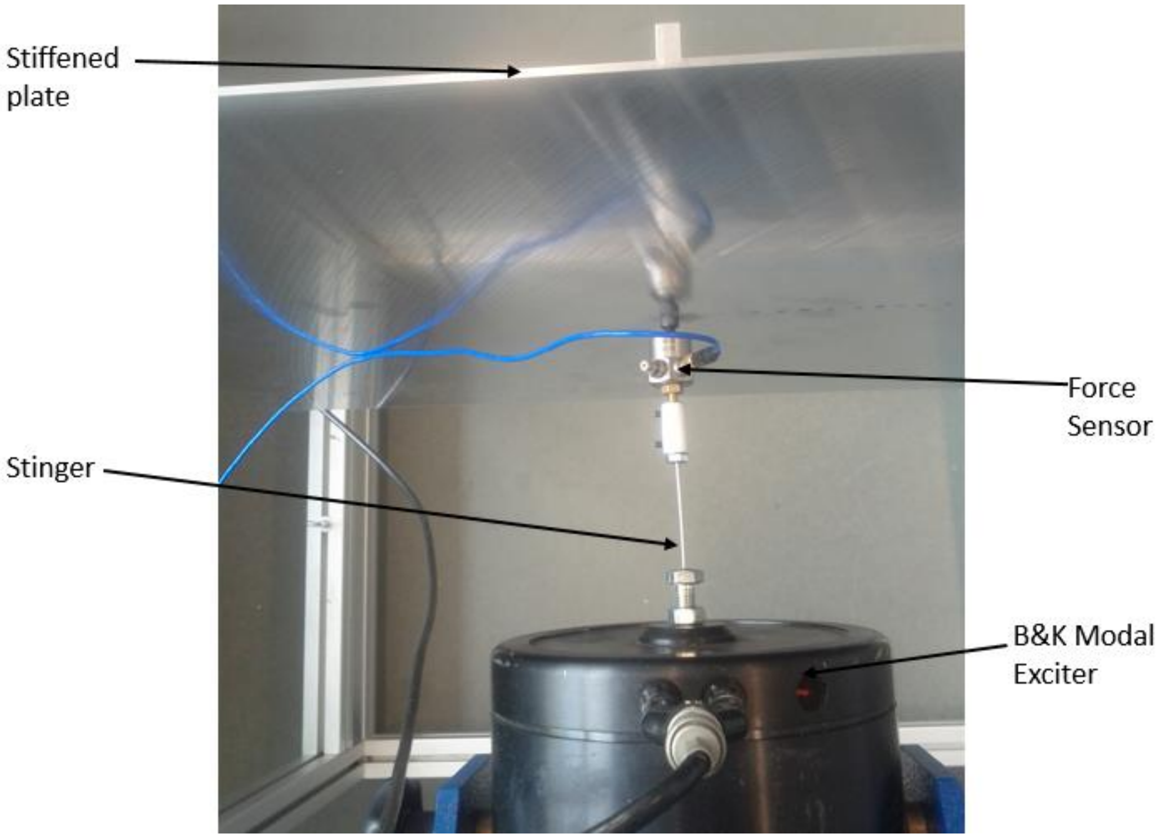

Figure 4. 6 *: Assembly of the modal exciter, stinger and force sensor connecting to the test structure*

The experimental setup has now been completely described. The same setup is used for both linear and nonlinear experiments. For the nonlinear dynamic experiments, the PAK hardware is included in the setup and it replaces the functionality of the Junction Box used in the Polytec Scanning Vibrometer. In the following sections, the measurement procedure and settings for the linear and nonlinear vibration tests is described.

4.3. Measurement Procedure and Settings

This section is used to describe the procedure followed during the measurements and the settings chosen for the measurements. Separate measurement setting and procedure is used for the linear and nonlinear vibration test.

4.3.1. Linear Vibration Test

The primary objective of the linear vibration test is to obtain a preliminary validation for the finite element model. The mode shapes and the linear modal frequencies are compared with the analysis results for the initial validation. Furthermore, the frequency response curves are also used to determine the damping ratios which are used in the subsequent nonlinear analysis using AUTO.

The linear vibration test is conducted using the PSV and the measurement data is processed in real-time using the PSV analysing software. PSV offers the user the ability to define multiple scan points for a measurement. The measurement data is obtained by the automated scanning of the laser on the user-defined points. To start the measurement certain parameters are defined in the PSV software. The sequence of steps followed to obtain the final experiment results are defined in this section.

Step 1: Checking the laser intensity before the start of measurement is essential to obtain useful data. The laser intensity is checked at the back of the laser scanning head. If the intensity is close to zero, the measurement data is likely to have random errors and outliers. To improve reflectivity of the surface of test structure, a reflective tape is used at the point of measurement.

Step 2: 2D alignment is done to define points for an interpolation function of the internal scanning algorithm of the PSV software. The alignment points are chosen at the four corners of the rectangular plate which covers the complete measurement area. A correct alignment ensures that the laser pointer is positioned at the correct measurement point during scanning.

Step 3: The scan points are now defined on the test structure. For the final measurements conducted a grid consisting of ninety-nine points is created. Large number of scan points are chosen for greater accuracy in the mode shape. The scan point definition is depicted in Figure 4.7. The light coloured dots represent the measured points and the dark dots represent the points yet to be measured.

Step 4: Next, the data acquisition settings are defined. The mode of measurement is chosen to be ‘Frequency’. This measurement mode generates the frequency domain response of the structure along with the time domain response. The internal averaging option is used such that measurement at each point is done for eight cycles and the frequency response is averaged over the eight cycles. Averaging reduces the errors in the frequency response.

This is followed by the channel setting definition. In the channel settings, the sensitivities and the measurement quantities are defined for each channel. For the linear vibration test conducted, only two channels are used. The first channel reads the measured velocity and the second channel reads the measured force at the excitation point. The sensitivities of the sensors used in the measurement are given in Table 4.3.

The excitation signal is selected to be a random excitation with a 1V amplitude of the drive signal. Random excitation is chosen to simultaneously excite multiple modes of the structure.

The sampling frequency is chosen to be 0.5 kHz in consideration of the Nyquist sampling theorem. The sampling frequency ensures that frequency domain analysis has useful data for at least up to 200 Hz frequency.

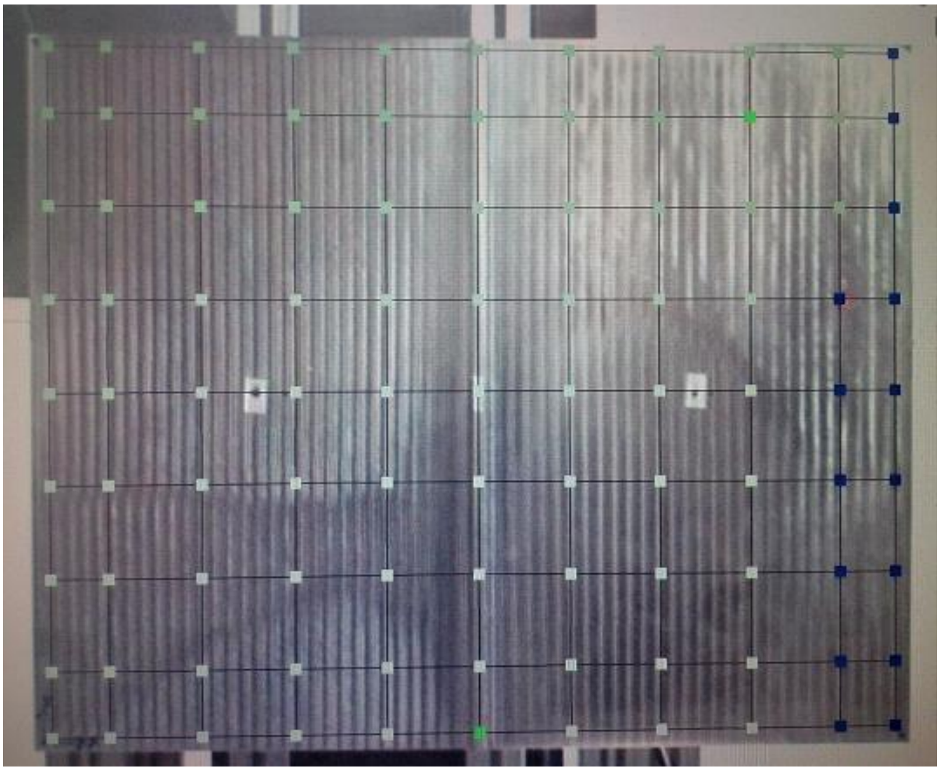

Figure 4. 7 *: Grid which defines the scan points on the test structure*

Measured Quantity	Sensitivity	Unit
Velocity	50	(mm/s) / V
Force	0.021834	V / N

Table 4. 3 *: Sensitivity definition for measurement channels*

Step 5: The measurement is now started from the PSV software. While the measurement is running, the frequency response generated can be observed in real-time. After the completion of the measurement the mode shapes are plotted in the 'Presentation Mode' of the PSV software. The frequency response data is downloadable in the universal file format and is used for further data processing. The results obtained through the linear vibration test is discussed in Chapter 5.

4.3.2. Nonlinear Vibration Test

The objective of conducting the nonlinear vibration test is to validate the frequency vs amplitude response generated using the reduced order model and AUTO. To achieve this goal, a harmonic load is applied and a frequency sweep is done within a range near the linear fundamental mode of the test structure. The load amplitude is chosen high enough to induce geometrically nonlinear vibrations. The experiment is repeated with increasing load amplitudes. The nonlinear vibration test is conducted using PAK measurement system in combination with Polytec laser scanning head. The vibrometer laser is used to measure the velocity response from the test structure. The measured data is transferred to the PAK hardware, instead of the Junction box of the PSV, which establishes the connection between PSV laser scanning head and the processing software of PAK MK-II system. The measurement procedure followed is described in this section.

Step 1: The laser pointer of the PSV is positioned manually on the point of measurement on the test structure. Definition of a scanning grid is not required since the measurement is done at the point of maximum deflection. The type of boundary condition used and the mode under consideration determines this point of measurement, which in the case of free boundary condition and first mode of the plate is the corner point.

Step 2: A velocity decoder with the appropriate sensitivity is chosen for the measurement. The choice of the velocity decoder is influenced by the maximum velocity amplitudes at the resonant frequency. This is a limitation of the measurement system which allows a maximum of 10 V for the measured signal. Therefore, the sensitivity is chosen in a way that the voltage does not cross this limit. For the final nonlinear vibration measurements, a sensitivity of 125 (mm/s / V) for the velocity decoder is used. All remaining settings are chosen in the PAK software.

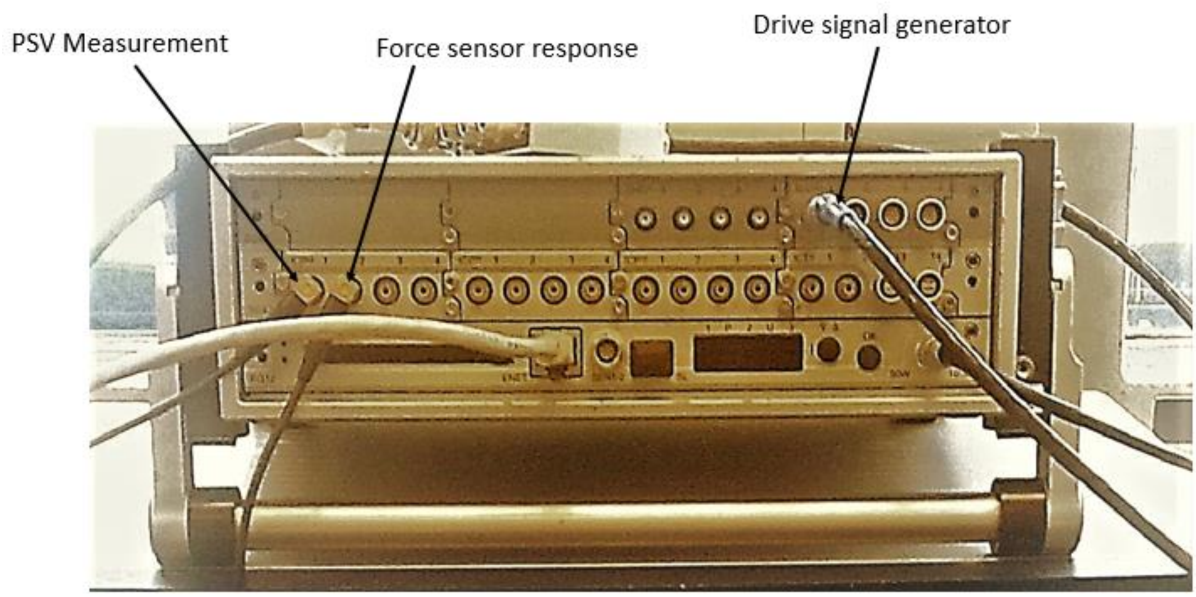

Figure 4. 8: *PAK Hardware used to read the measurement data.*

Step 3: The channel settings are defined in the PAK software which describes the measurement quantities and the sensitivities of measuring devices. In similarity to the linear vibration test, two measurement channels are used. The notable difference is the higher sensitivity value for the vibrometer velocity decoder. The parameters for Fast Fourier Transform (FFT), to obtain frequency domain response, are defined. A sampling frequency of 1.024 kHz is used as that is the minimum sampling frequency allowed in the software.

Step 4: A sinusoidal excitation signal is chosen to drive the modal exciter. A frequency range is defined for the sweep. The frequency range is increased as the load amplitude is increased to ensure that the frequency shift due to geometric nonlinearity is captured. A frequency increment step of 0.3125 Hz is allocated for the sweep.

The load amplitude level is set along with an apt tolerance level. As the frequency is incremented step wise in the frequency sweep and approaches the resonant frequency, the vibration amplitude increases correspondingly. The increment in the inertial load due to the vibration amplitude amplifies the reaction force at the excitation point. PAK uses an active control loop for monitoring the reaction force at the excitation point. The control loop ensures that the effective load level is brought to the pre-defined magnitude by reducing the input drive signal amplitude. The structural response is measured only after the load levels are within an acceptable limit defined by the pre-set tolerance. The tolerances were set in the order of 1 % in the experiments conducted for the present study.

Step 5: The measurements can now be started. The measured data is observable in real-time on the PAK analysing software. Both, time and frequency domain data, are available for visual inspection during the measurement. The in-built plot functions directly generate the frequency vs peak amplitude response. The system has an internal integrator/ differentiator for the measured variable such that the velocity can be transformed to displacement and vice versa. Therefore, the measured velocity from PSV is transformed and plotted as the displacement. The measured response and the comparison with numerical results is discussed in the next chapter.

4.4. Conclusion

In this chapter, the experimental setup has been described, the design of the test structure used in the experiments is discussed. The geometric and material properties of the test structure is defined. The components used to conduct the linear and nonlinear vibration tests have been explained. A brief description of the PSV components along with their functionalities is given and working principle of the vibrometer is summarized. The measurement procedure and settings of both linear and nonlinear vibration tests are described. The chapter gives an overview of the experimental setup and procedure followed for the validation study. The results of the validation study are discussed in detail in the next chapter.

Chapter 5

Results

In the previous chapters, the methodologies adopted for the numerical analysis and the experiments have been established. This chapter is dedicated to the results discussion. A broad set of results have been obtained from preliminary comparisons with literature, comparisons with commercial Finite element software Nastran and the main comparisons from linear and nonlinear vibration tests. The results are used to demonstrate the validity and accuracy of the procedure established in the previous chapters.

The chapter is divided into the following sections: In Section 5.1, results for the numerical analysis of a simple rectangular plate is compared to literature. Results for comparisons with Nastran are presented in Section 5.2. Modal frequencies, mode shapes and damping ratio predicted from linear vibration experiments are presented in Section 5.3. The comparison between nonlinear numerical analysis of stiffened plate and nonlinear vibration experiment is presented in Section 5.4. The chapter is concluded with brief summary in Section 5.5.

5.1. Comparison to Literature

The initial comparison is done to check the correctness of the AUTO executable file generated using the reduced order Hamiltonian equations of motion. The use of analytical derivatives is also validated through this comparison. The analysed geometry is chosen from the work of M. Amabili [40]. A simple rectangular plate (without stiffeners) is modelled for the analysis. The geometrical dimensions of the plate are: length = 0.3 m, width = 0.3 m, thickness = 0.001 m. The material properties are: Modulus of elasticity E = 70e9 Pa, density ρ = 2778 kg / m^3 and Poisson's ratio $\nu = 0.3$. The fundamental mode for this geometry is found to be at frequency 53.02 Hz in linear vibrations. Two different boundary conditions are analysed for this geometry. In the first Case (a), simple support with immovable edges is used. A harmonic load of F= 1.74 N is applied with a modal damping ratio $\zeta = 0.065$. In the second Case (b), simple support with movable edges is used. A harmonic load of F= 0.49 N is applied with a modal damping ratio of $\zeta = 0.015$.

In the Case (a), the displacement constrain is defined by $\mathrm{u} = \mathrm{v} = \mathrm{w} = 0$ for all edges of the plate, where 'u' represents the in-plane displacement along x-direction, 'v' represents in-plane displacement along y-direction and 'w' represents the out-of-plane displacement. In Case (b), the displacement constrain is defined by: $\mathrm{v} = \mathrm{w} = 0$ along the edges x= 0 and x= 0.3, $\mathrm{u} = \mathrm{w} = 0$ along the edges y= 0 and y= 0.3.

The response is simultaneously compared to the tabulated data of backbone curve provided by Leung and Mao [41]. The backbone curve ideally should pass approximately through the peak of the forced and damped frequency response. A plot of maximum vibration amplitude normalized by the thickness of the plate vs the applied frequency of the forcing function normalized by the first modal frequency is created for comparisons. The result of the comparison is depicted in Figure 5.1a-b, and is found to be in good agreement with the literature in both cases. Only a single mode used to formulate the ROM is found to be sufficient for accurate results whereas 16-degree of freedom model is required in the method used by M. Amabili for Case (a). Two-degree of freedom model was required to obtain good results for the Case (b) in comparison to the 27-degree of freedom model presented by M. Amabili. The method used by Leung and Mao is based on a single mode Galerkin approximation for both the cases. In both cases it was observed that inclusion of certain modes in the ROM basis introduces greater inaccuracies in the response. Since the continuation scheme is sensitive to errors in the input parameters, this could purely be a consequence of minor numerical errors in the ROM formulation.

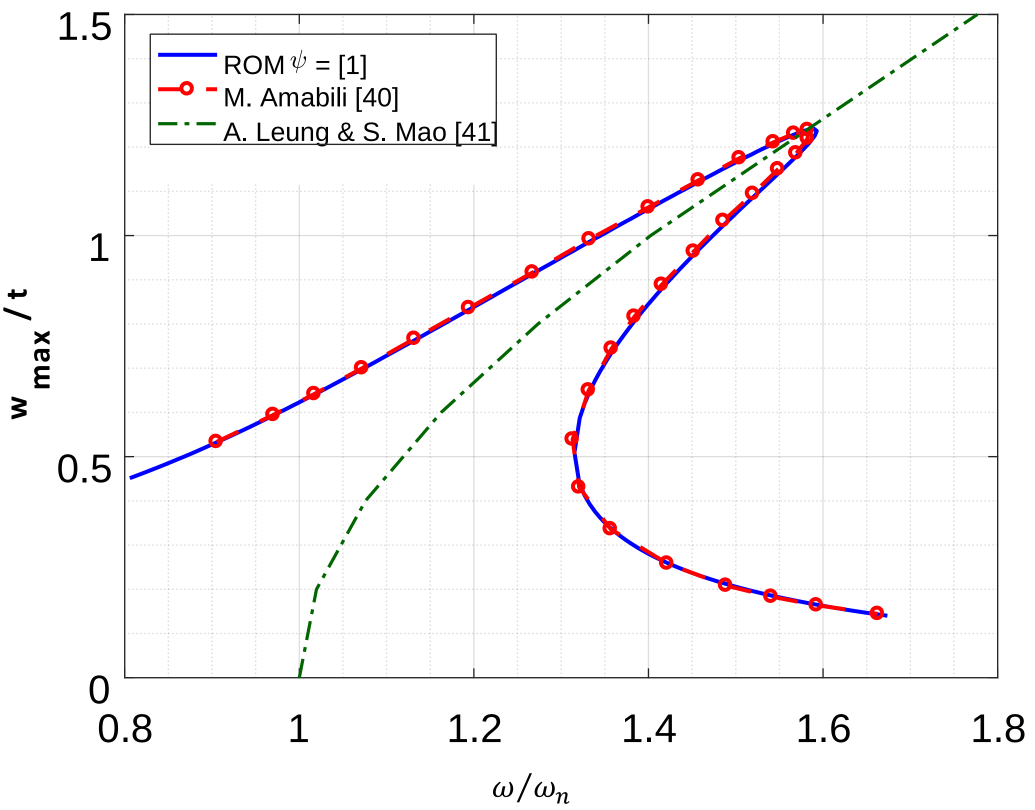

Figure 5. 1 a: *Comparison of Frequency ratio vs amplitude ratio for simply supported rectangular plate with immovable edges. (references M. Amabili [40], Leung & Mao [41])*

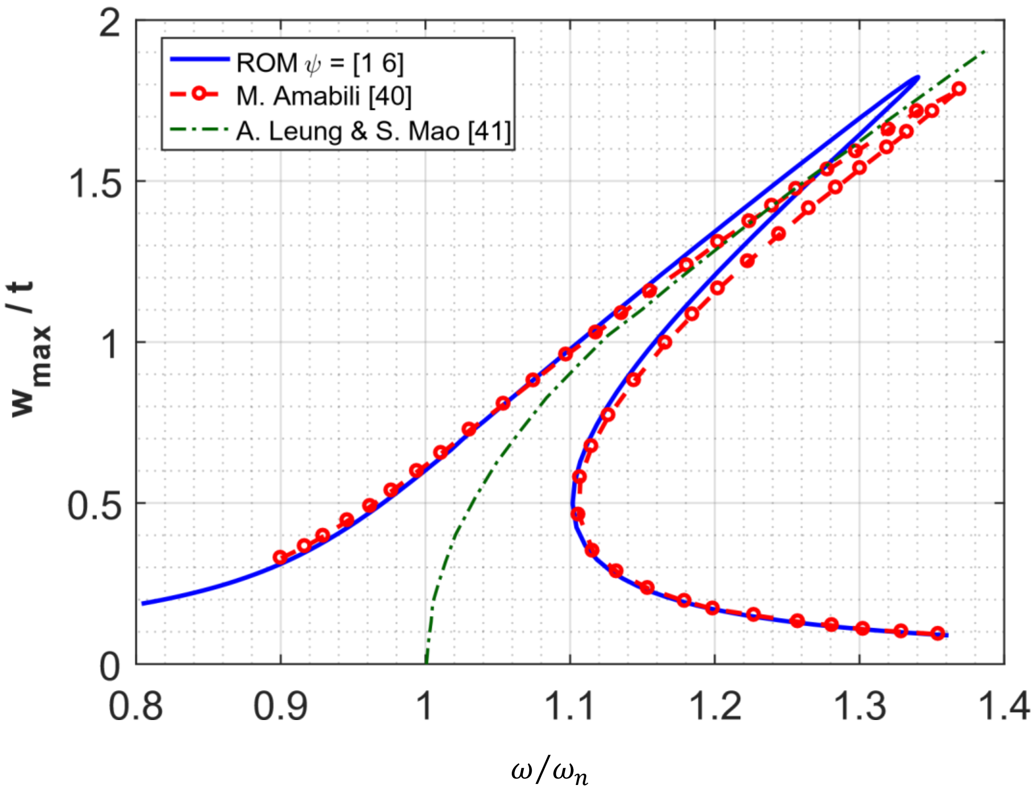

Figure 5. 1 b: *Comparison of Frequency ratio vs amplitude ratio for simply supported rectangular plate with movable edges. (references M. Amabili* [40], *Leung & Mao* [41])

5.2. Comparison to Nastran

The second comparative study is done after the geometric modelling of the stiffened plate in the Matlab code. The idea is to validate the finite element model before proceeding to the experimental work since new variables and modifications were introduced into certain sections of the code. A modal analysis is done initially which validates the correctness of the linear stiffness and mass matrix. The nonlinear stiffness matrices are checked by comparing the transient response of the structure from a nonlinear vibration analysis in Nastran.

5.2.1. Modal Analysis

The geometrical and material properties chosen are the same as defined in Table 4.1 and Table 4.2 respectively. A highly refined mesh model is used for Nastran for convergent results. Since the original model reduction code in Matlab is formulated with triangular shell elements, the same choice is made for the Nastran analysis. Free boundary conditions are used for the modal analysis to keep it consistent with the experiments. A comparison of the predicted modal frequencies can be seen in Table 5.1. The comparison shows a good agreement between the predicted modal frequencies in Nastran and the Finite element formulation in Matlab. The rigid body modes are excluded in this comparison. The mode shapes are compared directly with the results of the linear vibration test and are shown in the next section. The next step is to validate the higher order stiffness matrices by conducting a nonlinear vibration analysis.

Mode No.	Frequency (Hz) Nastran	Frequency (Hz) Matlab	% deviation
1	35.75	36.78	2.88
2	42.84	42.81	-0.07
3	77.74	77.78	0.051
4	94.81	94.38	-0.45
5	97.32	97.97	0.66
6	123.96	123.59	-0.29
7	160.89	162.4	0.93

Table 5. 1: *Comparison of the predicted modal frequencies*

5.2.2. Nonlinear Transient Analysis

The nonlinear transient analysis is conducted using SOL 129 in Nastran. To obtain the transient response, a harmonic load of magnitude 5 N is applied at the centre of the stiffened plate. Simply supported boundary conditions are used to constrain all four edges of the plate. A Rayleigh damping is introduced with a damping ratio of 0.0407 for the fundamental mode. The applied harmonic frequency is 490 rad/s which is very close to the first modal frequency for the simply supported boundary condition. The time response from Matlab is generated using the in-built ode45 solver. The results are found to be in good agreement and gives assurance about the reduced order model formulated for nonlinear dynamics. The comparison is depicted in Figure 5.2. It is observed that sufficiently accurate results are obtained just by using two modes (mode one and mode three) in the basis matrix of the ROM.

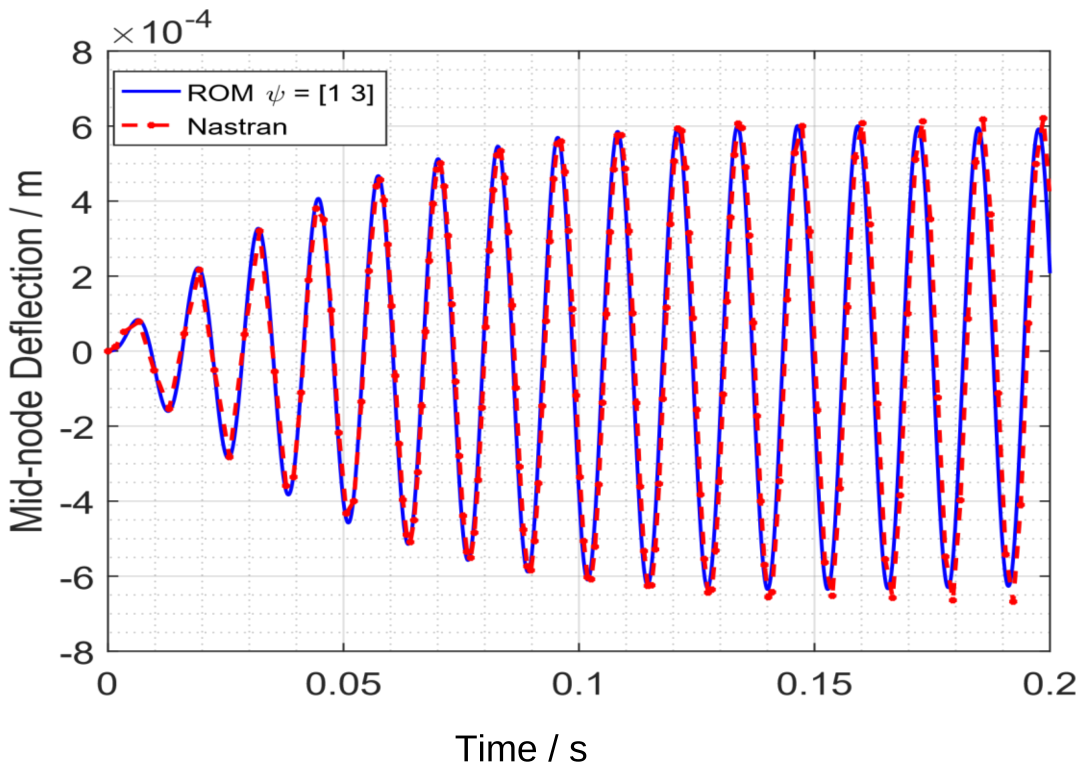

Figure 5. 2 : *Comparison between Nastran and ROM for a nonlinear transient response to harmonic load*

The nonlinear response in this case is an example of a stable limit cycle oscillation where the trajectory approaches a stable periodic cycle as $t \rightarrow \infty$. A phase portrait diagram for the system under the previously defined load and boundary condition would be similar to the diagrams depicted in Figure 3.1.

5.3. Linear Vibration Experiments

The linear vibration tests are conducted to primarily estimate the modal damping ratios. The damping ratio is later used as an initial guess for the numerical analysis of nonlinear vibrations. Furthermore, the predicted linear modal frequencies and mode shapes are validated using the experimental results. Six experimental modes and modal frequencies are compared with the numerical model developed in Matlab. The structure is excited using a random load at the location x = 0.2 m and y = 0.16 m in the coordinate frame depicted by Figure 3.2. The mode shapes and frequencies are found to be in excellent agreement with the numerical model. The comparison of modal frequencies and damping ratios are listed in Table 5.2. The mode shapes are compared in Figures 5.4a -f. The damping ratios are computed using the 'modalfit' function in Matlab 2017 which uses the experimental frequency response functions as an input.

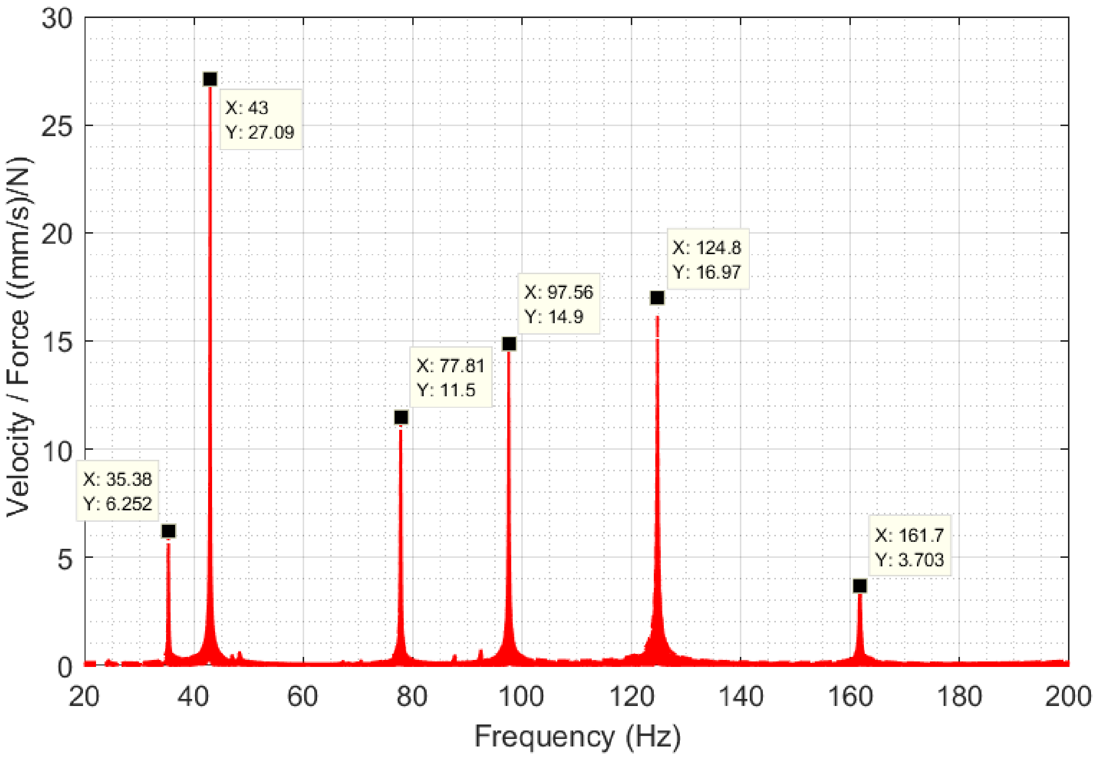

Figure 5. 3 *: Frequency response for all measurement points in the linear vibration test*

Mode Number	Experimental Modal Frequencies (Hz)	Matlab prediction (Hz)	% deviation	Damping Ratio
1	35.39	36.78	3.9	0.0012
2	42.97	42.72	-0.58	0.0011
3	77.8	77.59	-0.27	0.00062
4	97.57	94.84	-2.79	0.00068
5	-	97.97	-	-
6	124.7	123.62	-0.86	0.00087
7	161.7	162.4	0.43	0.00067

Table 5. 2 : *Comparison of the experimental modal frequencies with the Matlab numerical model along with the modal damping ratios*

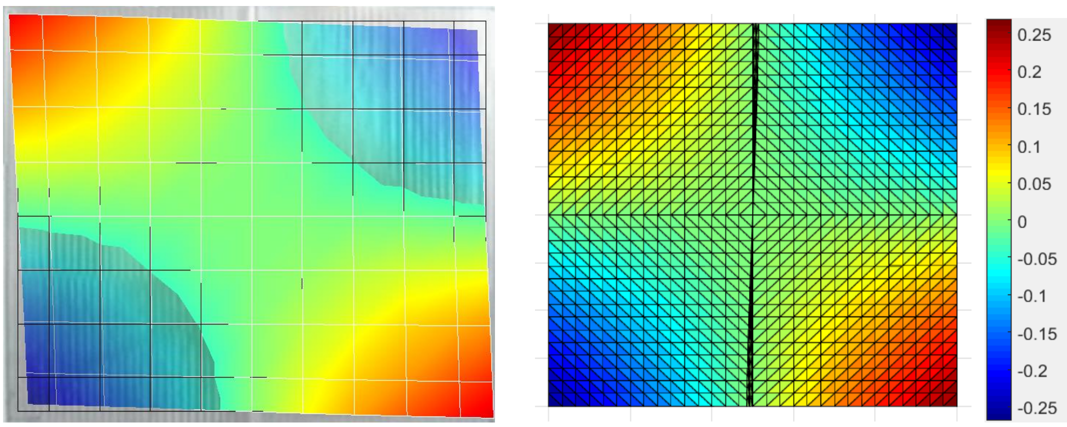

Figure 5. 4 a: *Comparison of first mode shape, experiment (left) and numerical (right)*

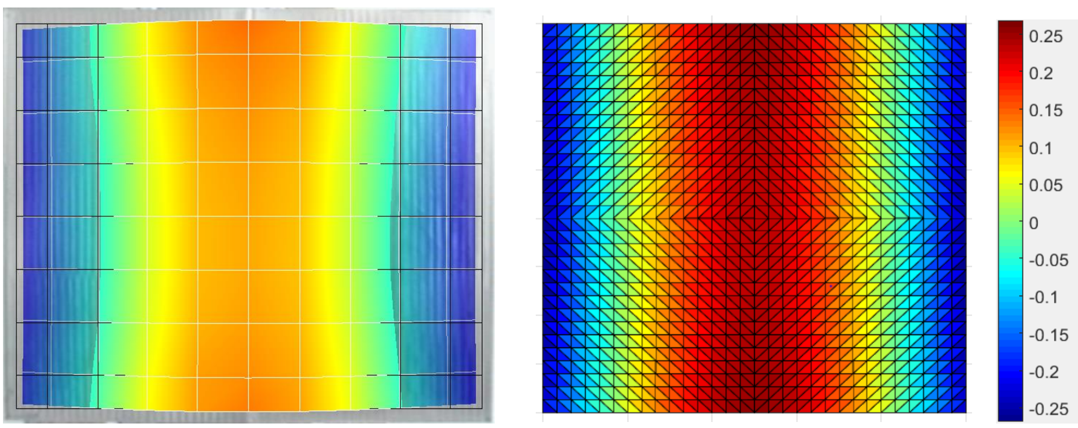

Figure 5. 4 b: *Comparison of second mode shape, experiment (left) and numerical (right)*

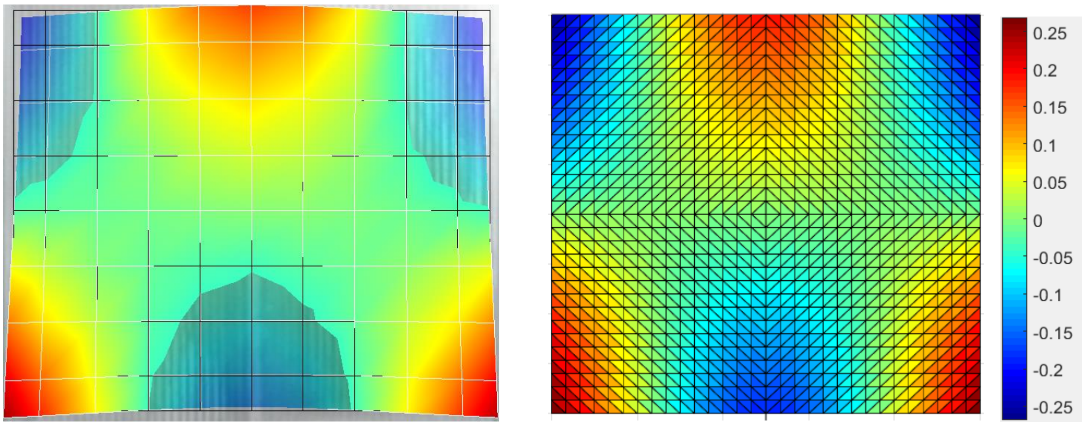

Figure 5. 4 c: *Comparison of third mode shape, experimental (left) and numerical (right)*

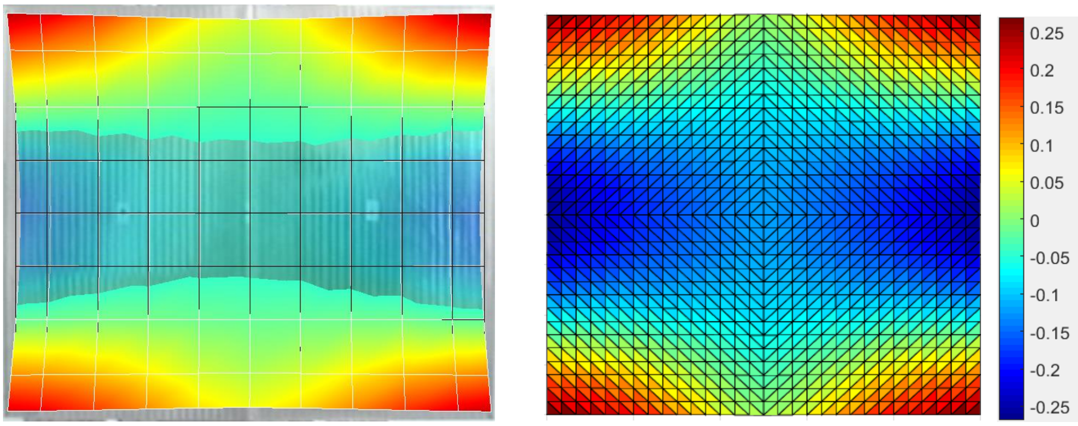

Figure 5. 4 d: *Comparison of fourth mode shape, experimental (left) and numerical (right)*

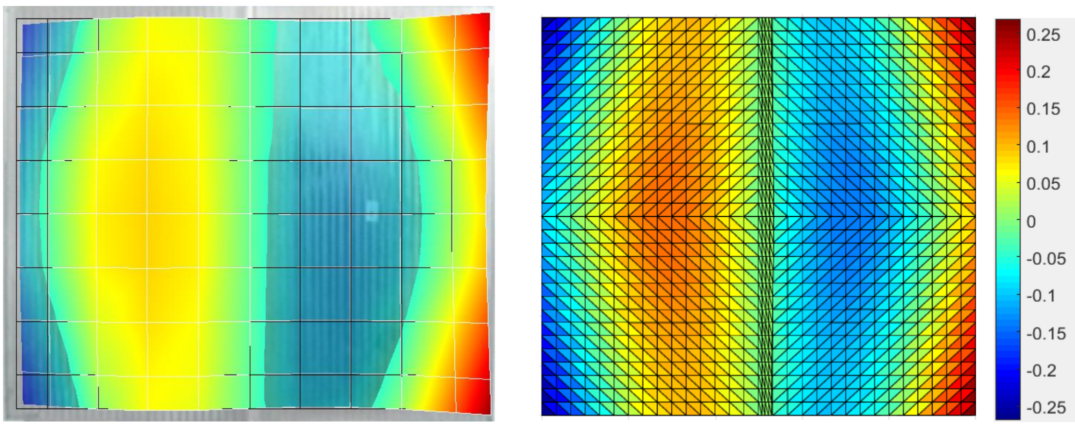

Figure 5. 4 e: *Comparison of sixth mode shape, experimental (left) and numerical (right)*

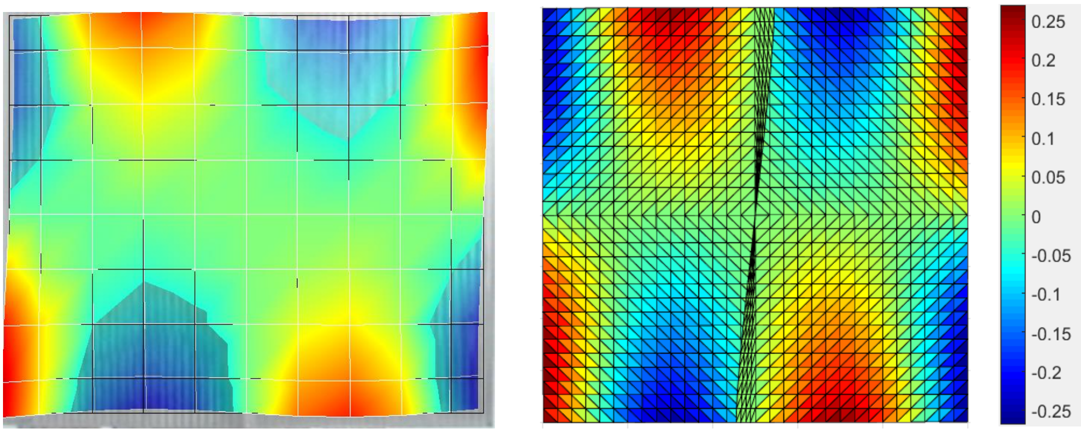

Figure 5. 4 f: *Comparison of seventh mode shape, experimental (left) and numerical (right)*

It is noted that the fifth mode from the numerical model is not captured in the experimental response. This is a result of the choice of the excitation point. Since the excitation point is close to the nodal region of the fifth mode of vibration, sufficient energy transfer does not occur to excite the mode visibly. For visualization, the fifth numerical mode shape is depicted in Figure 5.4g , where the excitation point is also marked. The primary focus for the nonlinear analysis is on the fundamental mode of vibration, therefore, the exclusion of fifth experimental mode does not have any consequence on the study.

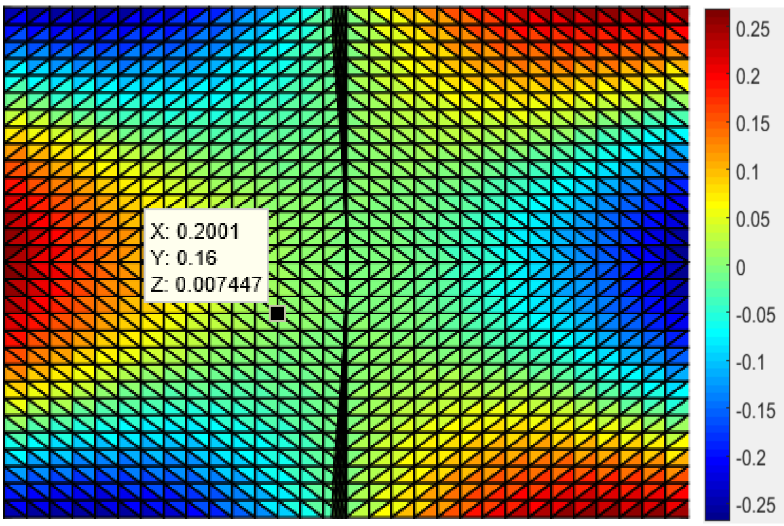

Figure 5. 4 g: *Fifth numerical mode shape*

Furthermore, the first mode shape shows that the maximum deflection with free boundary conditions occurs in the corner region of the plate. The point of measurement for the nonlinear experiments is, therefore, determined to be on the top left plate corner to obtain the maximum vibration amplitude. The results of the nonlinear measurements are presented in the next section.

5.4. Nonlinear Vibration Experiments

Experiments are conducted for large amplitude vibrations using a combination of Polytec laser scanner for the measurement and the PAK analyser for data monitoring and processing. The objective here is to generate a plot of normalized peak vibration amplitude vs normalized applied frequencies. The plot gives a close approximation of the resonant frequency for forced and damped nonlinear vibration. The plot is then compared to similar response curves generated using the ROM and the continuation scheme in AUTO. To induce geometric nonlinearity, vibration amplitudes in the order of the thickness of the plate is targeted. Therefore, load levels are selected to reach a peak vibration amplitude in the neighbourhood of 2 mm. Five experiments are conducted with load levels 0.2 N, 0.5 N, 0.8 N, 1.0 N and 1.2 N. The active control loop, discussed in step 4 of Section 4.3.2, ensures that the load level remains approximately constant at the defined value during the measurement. The focus of measurements is on the first mode which is usually the main reference criteria for design considerations. A frequency sweep is done in a range between 32 Hz to 40 Hz for different load levels. A step size of 0.3125 Hz is used for the increment of frequency during the sweep.

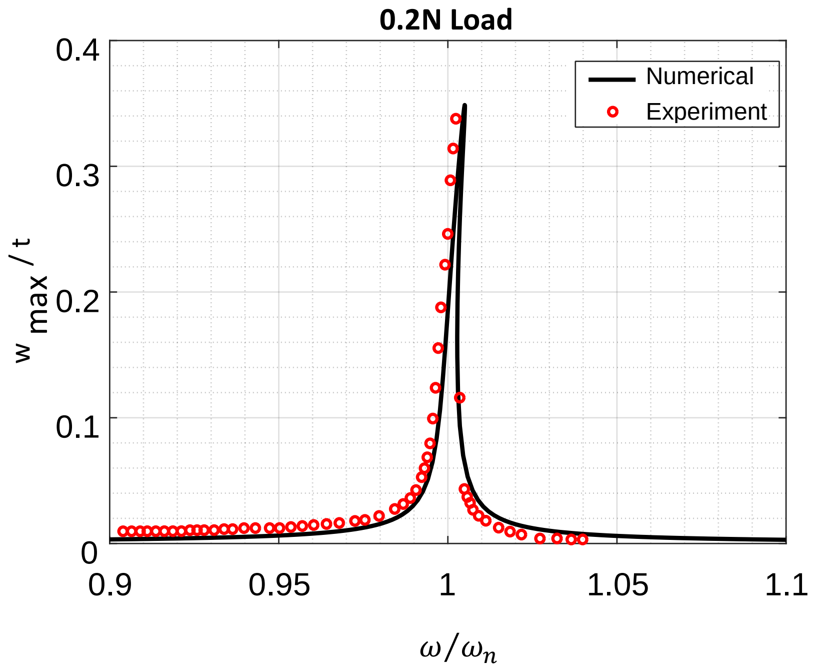

Figure 5.5: *Comparison for ROM and experiments (0.2 N load and damping ratio 0.000917)*

The results of the numerical analysis are found to be in good agreement with the experimental data. The results are achievable just by using a single mode in the basis matrix for the formulation of the ROM. This effectively reduces the structure to a single degree of freedom model and enables fast computations. On an average, when a single mode was used in the basis matrix for ROM formulation, the total time required for obtaining the response was less than 300 seconds. The plots comparing the numerical and experimental results are depicted in Figures 5.5 – 5.9.

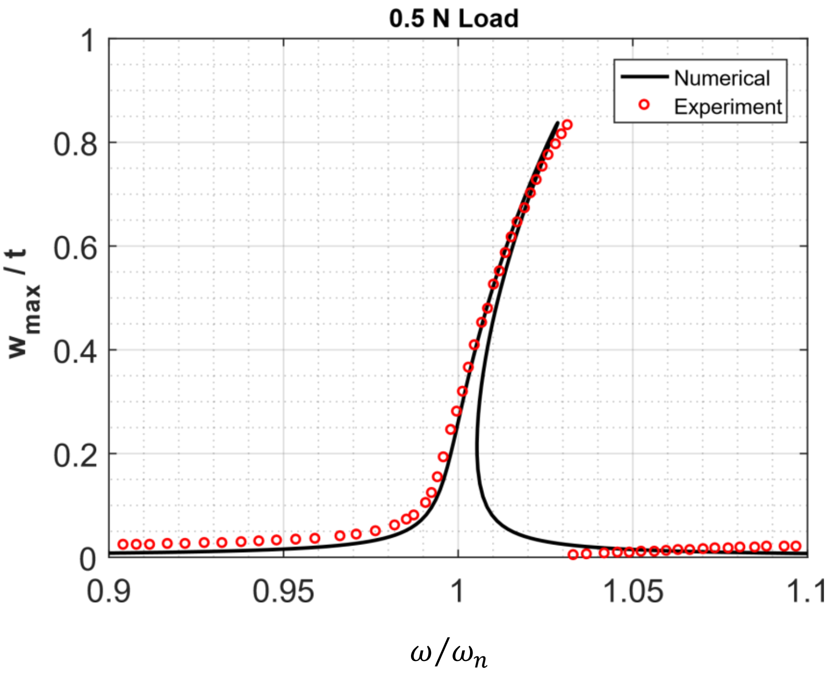

Figure 5.6: *Comparison for ROM and experiments (0.5 N load and damping ratio 0.000944)*

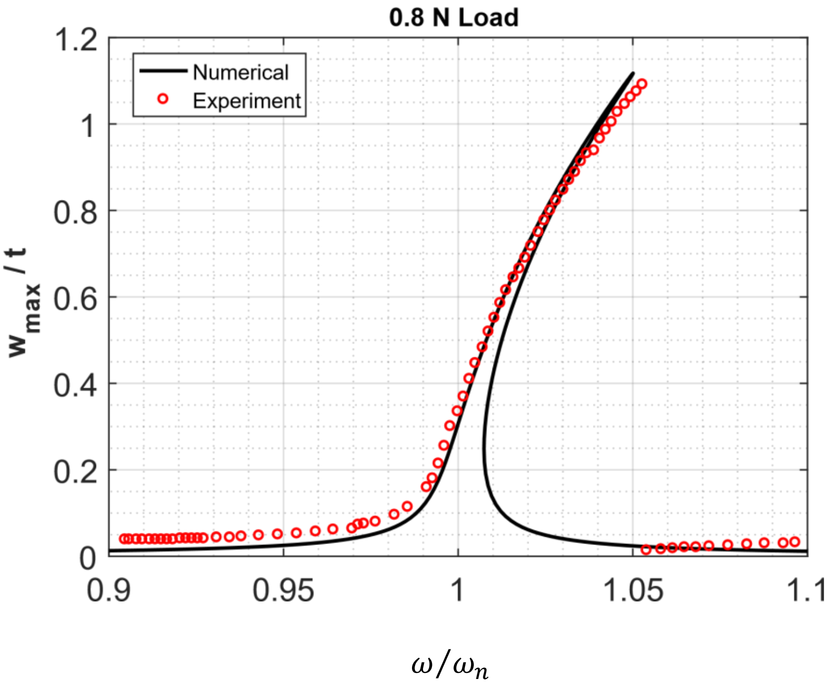

Figure 5.7: *Comparison for ROM and experiments (0.8 N load and damping ratio 0.0011)*

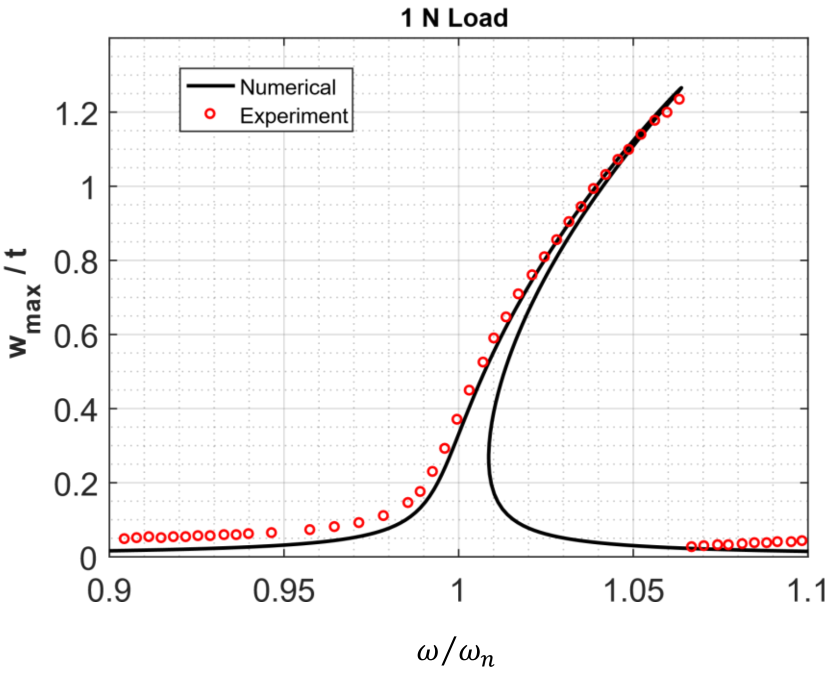

Figure 5.8: *Comparison for ROM and experiments (1 N load and damping ratio 0.0012)*

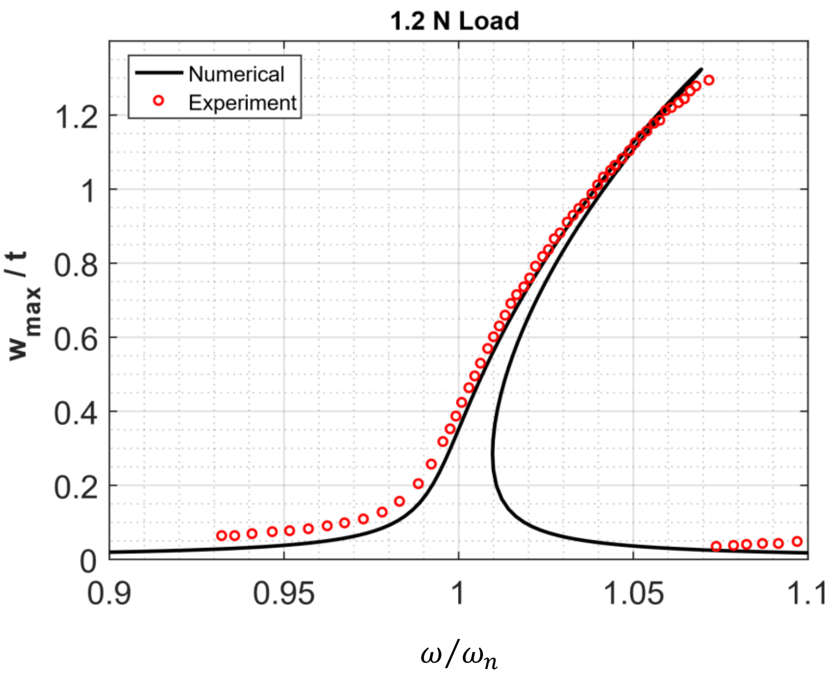

Figure 5.9: *Comparison for ROM and experiments (1.2 N load and damping ratio 0.0014)*

The peak frequency ratios $\omega/\ \omega_n$ for the numerical results, in comparison to the experiments, are found to have deviations 0.2%, -0.19 %, -0.38%, -0.19% and -0.28% in sequential order of the increasing loads. The errors are found to be within an acceptable limit and therefore, the results provide a good validation for the numerical method. A very distinctive shift in the resonant frequency is observable as the applied force and vibration amplitudes are increased. This demonstrates the need of considering geometric nonlinearity in modal analysis for large amplitude vibrations.

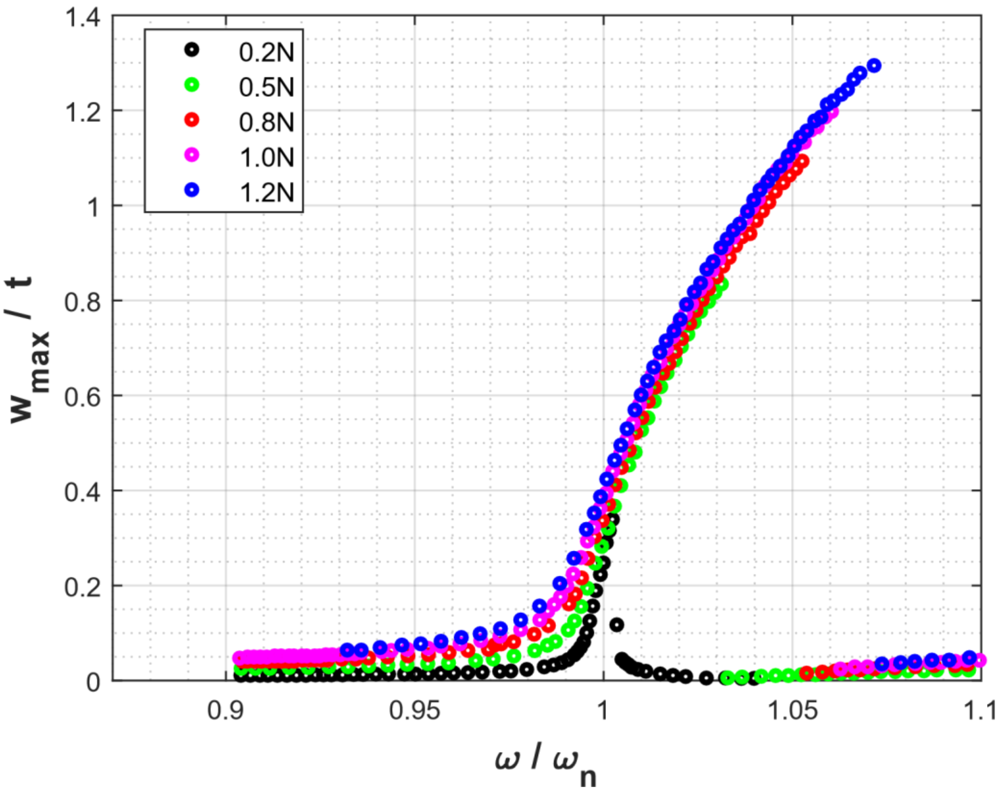

Figure 5. 10 *: Comparison of the peak amplitude / plate thickness vs applied frequency / modal frequency for all load cases in the experiments*

The results show that when the applied load is increased from 0.2 N to 1.2 N, the frequency ratio at the peak vibration amplitude changes from 1.005 to 1.072. In terms of the actual frequency, this change occurs from 35.57 Hz to 37.94 Hz which is an increment of 6.67 %.

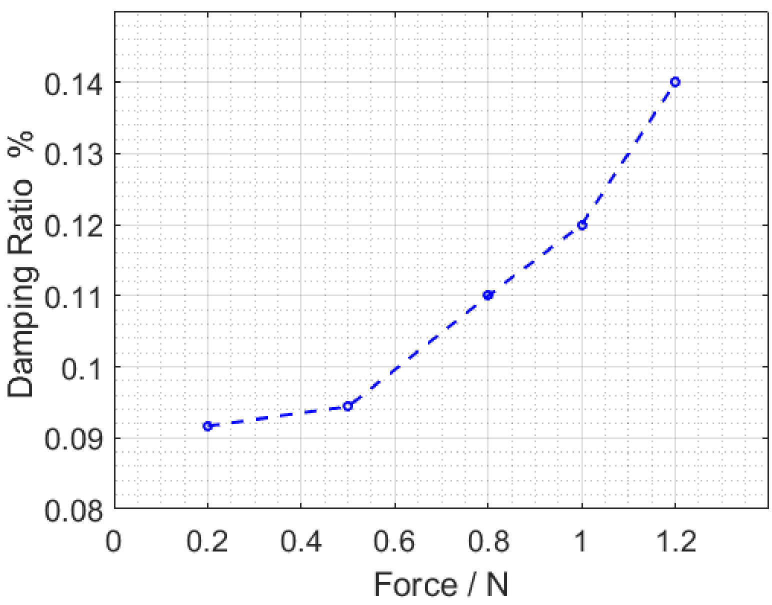

Figure 5. 11 *: Evolution of % damping ratio with force amplitudes*

It is further observed from the numerical analysis that a variable damping ratio is required for different load cases to obtain comparable results with the experimental response. The damping ratios are varied in the neighbourhood of the initial prediction obtained through the linear vibration test. This demonstrates a dependency of the damping on the vibration amplitude and load. The damping ratios are found to increase with increasing vibration amplitude. Figure 5.11 depicts the evolution of damping ratio with increasing force amplitudes. This observation is in agreement with the work of Alijani et al. [39] and Amabili et al. [42] who have demonstrated a similar requirement of nonlinear damping model. Furthermore, the authors have shown through a wide variety of analysis that the damping behaviour is not specific to certain type of structure, material or boundary conditions and therefore, can be generically accepted for all large amplitude vibrations. With the results of the present analysis, it is not possible to conclusively determine the cause of the damping increment. However, it can be theorized that the damping increment could be an effect of the change in the interaction between structure and the surrounding fluid.

As stated previously, all the results have been obtained by using a single mode in the basis matrix of the ROM. By increasing the number of modes in the basis matrix, a comparison is made to check for the possibility of improvement in results. The numerical analysis for 1 N force is repeated for a three-mode basis, five-mode basis and six-mode basis ROM formulations. The peak values of frequency ratio ω/ω_n and displacement ratio w_{max}/t are compared for each of the analyses. The frequency ratio is found to be nearly constant for each of these analysis with a maximum deviation of 0.094 %. The results, therefore, show that the first mode is sufficient to obtain accurate frequency vs amplitude response graphs.

5.5. Comparison of dynamics of stiffened and unstiffened plates

The effect of using a stiffener on the dynamic behaviour of the plate is presented in this section. A comparison is made between the backbone curve approximations of the stiffened and un-stiffened plate. The backbone curves are obtained through several forced vibration analyses of the structures. The dimensions of the stiffened plate are same as defined in Section 4.1. For the second analysis, the stiffener is eliminated keeping the other dimensions constant. Simply supported boundary conditions are used for both plates. The load is applied at the centre of the plates. For the stiffened plate, the load is varied from 5N to 30N in steps of 5N. For the un-stiffened plate, lower load magnitudes are chosen since the deflections are much higher due to lower stiffness. The applied loads are: 1N, 2N, 5N, 7N, 10N, 12N. The loads are applied at a circular frequency of 225 rad /s. A damping ratio of 0.0404 is used for analysis of both the plates.

The fundamental linear modal frequency for the stiffened plate for simply supported boundary conditions is found to be 78.8 Hz. The fundamental linear modal frequency for the un-stiffened plate using simply supported boundary conditions is found to be 50.84 Hz. Both plates show hardening behaviour on load increment. However, comparison of backbone curves for the plates show that the hardening behaviour in the unstiffened plate is much more pronounced. The frequency shift due to nonlinearity in stiffened plate for 10N load is found to be 9.8 % whereas the frequency changes by 70.3 % at 10N load for un-stiffened plate. The comparison of the backbone curves is presented in Figure 5.13.

The results are as expected since the hardening behaviour primarily arises due to quadratic and cubic relationship between higher order stiffness and the vibration amplitudes. The addition of stiffener to the plate reduces the vibration amplitude for the same applied load and therefore, the corresponding hardening effect is less prominent.

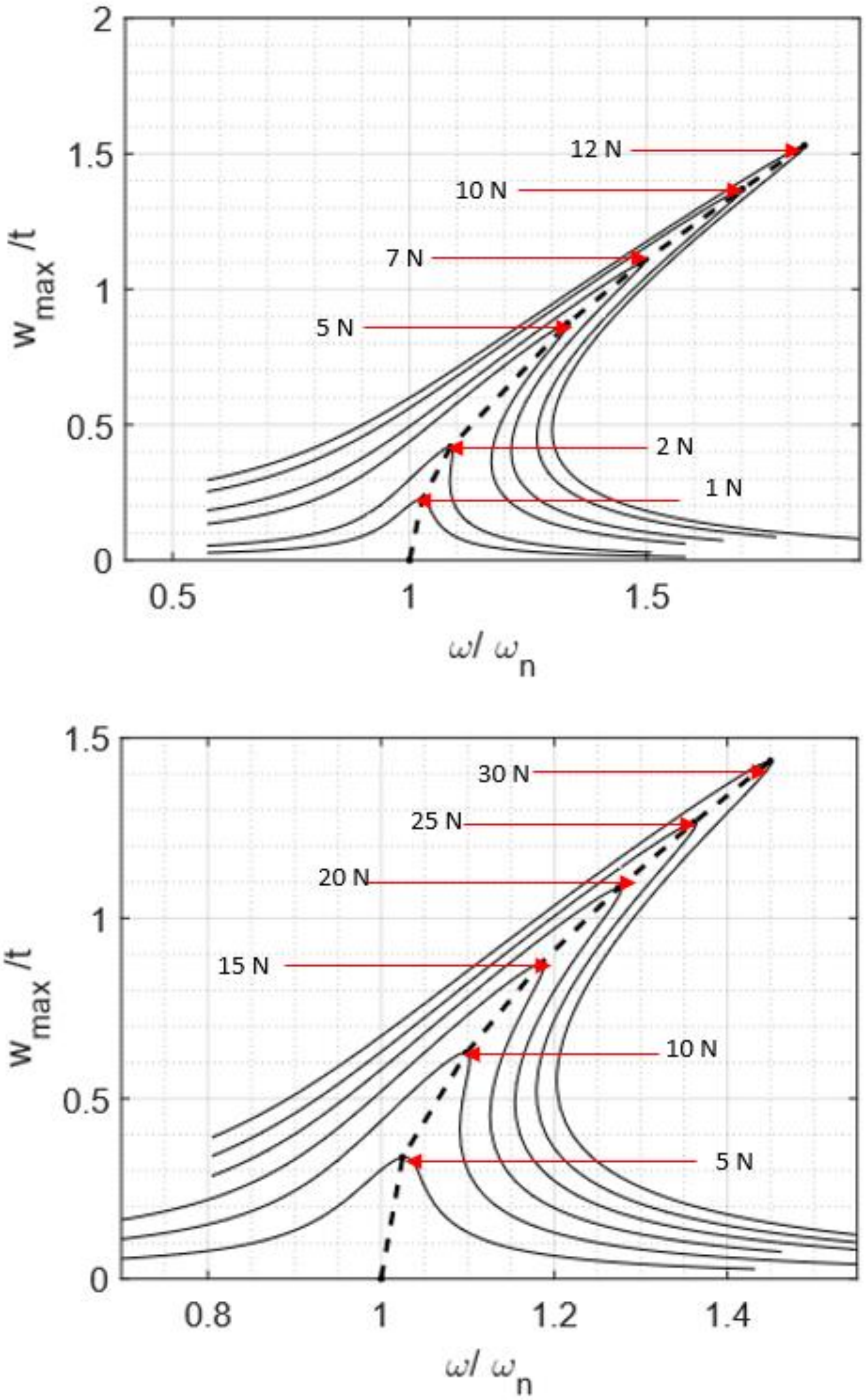

Figure 5. 12 *: Forced vibration response of unstiffened (top) and stiffened plates (bottom)*

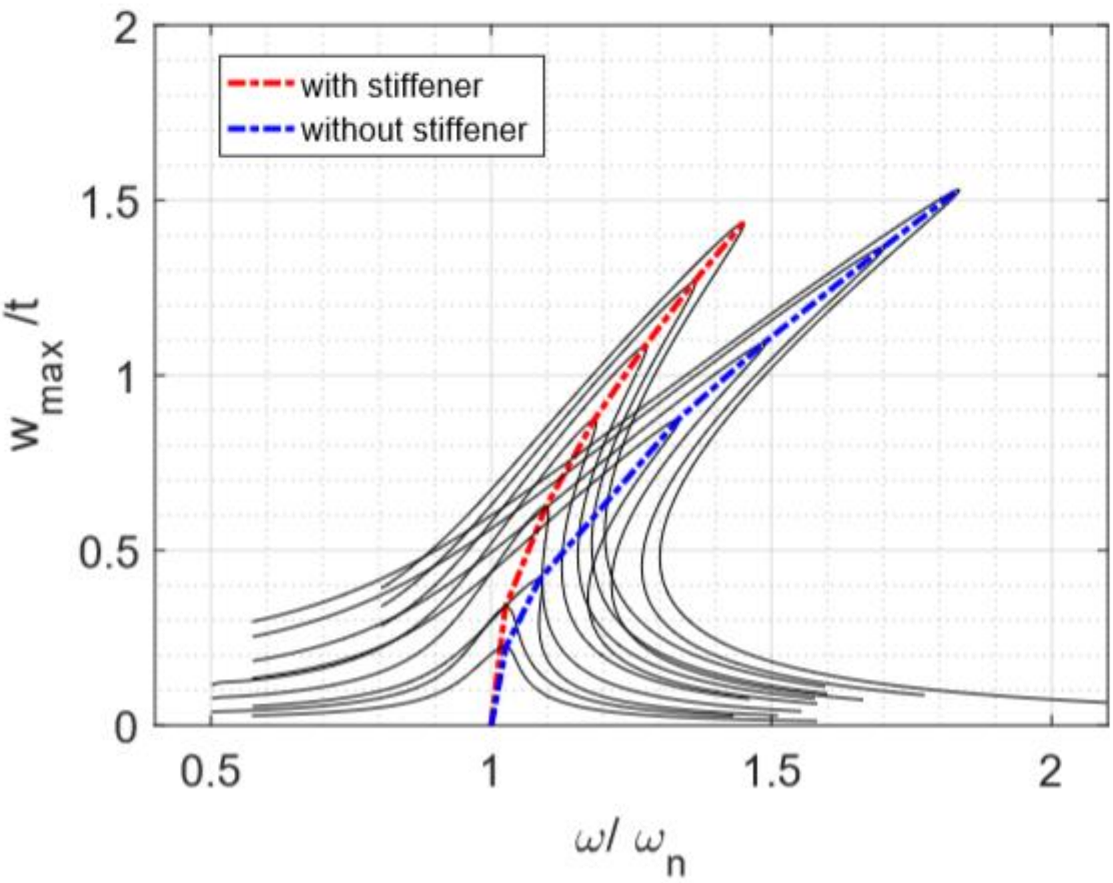

Figure 5. 13 : *Comparison of backbone curves for stiffened and unstiffened plates*

5.6. Conclusion

In this chapter, results generated to meet the objectives of this thesis have been presented. In the first section, the methodology of combining the ROM with the pseudo arc-length algorithm has been used to compute the frequency vs peak amplitude response of a simple rectangular plate. The results have been compared to literature and found to have been in good agreement. This was done for a preliminary validation of the compilation in AUTO. In the second section, a comparison has been made between the numerical model of the stiffened plate and a finite element model created in Patran. The comparison validates the ROM of the stiffened plate. Results from modal analysis and nonlinear dynamic analysis have been presented in the second section. In the third section, the results from a linear vibration test are presented. The frequency response graph depicting the modal peaks is presented. Furthermore, linear modal frequencies and mode shapes obtained from the experiments are compared to the results from the numerical model. The agreement in mode shapes gives confidence in the use of the mode shapes in the ROM formulation. The damping ratios have also been predicted from linear modal analysis and used in the subsequent nonlinear numerical analysis.

The reduced order model has been used for formulation of governing equations of the stiffened plate. The equations have been solved using the pseudo arc-length algorithm in AUTO to generate the frequency vs peak amplitude response graphs. The numerical results are compared to the experimentally obtained results. The results for five load cases are presented in the fourth section of this chapter. The frequency response of the numerical model is in good agreement with the experiments. It is found that only a single mode is sufficient for formulation of the ROM to get the desired accuracy in the results. The use of ROM reduces the problem to a single degree of freedom model which is a very useful reduction from the full-scale model. A distinct frequency shift is observable in the frequency response graph. Furthermore, it is found that the damping ratio must be varied by a small extent to be able to match the experimental results. A higher damping ratio is required in the numerical model for higher load amplitudes to match with the experiments. This behaviour demonstrates the requirement of a nonlinear damping model for accurate prediction of the nonlinear modal frequencies. In the final section of the chapter, a comparison has been made between dynamic behaviour of a stiffened plate and a plate without stiffeners. The response shows that the hardening behaviour due to geometric nonlinearity is less pronounced for the stiffened plate for lower loads. The trend is as per expectations since the stiffener reduces the vibration amplitude and therefore, the corresponding hardening behaviour.

Chapter 6

Conclusions

The thesis presents the work done in the validation study for the Hamiltonian reduced order model for computing nonlinear modal frequencies of thin walled structures. To demonstrate the utility of the numerical formulation, a stiffened plate has been designed with an isotropic material Aluminium 5083. The reduced order model has been derived from a finite element formulation of the stiffened plate. The governing equations of motion of the structure have been derived using the Hamiltonian approach. The system of equations has been solved using the program AUTO which is based on the pseudo-arc length continuation scheme. Numerical analyses on the stiffened plate model have been conducted for five load cases to demonstrate the hardening nonlinearity present in the structure for large amplitude vibrations. Experiments have been conducted to validate the numerical model. Firstly, a linear vibration test has been conducted to validate the mode shapes and linear modal frequencies. The mode shapes are utilized in the formulation of ROM and therefore, a verification gives assurance on the choice of the mode shapes. Furthermore, a prediction of modal damping ratios has been made using the linear vibration test results. These damping ratios are utilized in the numerical analysis for the nonlinear vibrations. Nonlinear vibration tests have been conducted using a combination of the laser scanner of the vibrometer and the PAK MK-II measurement system. Finally, a comparison has been made between the frequency domain vibration response of the stiffened plate and a plate without stiffeners.

The linear modal frequencies and mode shapes have been found to be in excellent agreement with the numerical model. This verifies the finite element formulation for the stiffened plate. To compare the nonlinear behaviour of the structure, frequency–amplitude response graphs have been plotted for all five load cases. Similar graphs are obtained from the nonlinear vibration tests using the PAK analysis software. The numerical and experimental graphs have been superimposed for comparison. The numerical analysis provides a very close prediction of the hardening behaviour with a maximum deviation of 0.38 % from experiments in the peak frequency ratio.

The numerical results with this level of accuracy was achievable using only a single mode in the ROM basis which shows that the use of ROM can significantly reduce the overall analysis time. The full-scale finite element model consisting of one thousand and eighty five (1085) nodes was reduced to a single degree of freedom system for the analysis. The deviations between numerical and experimental results can be attributed to either error in the numerical formulation and / or errors in measurements. The most significant cause of the deviation is possibly the fact that the structure has been assumed to be perfectly flat in the analysis. Even though measures were taken in the design process to ensure that the manufacturing imperfections are minimal, it is visibly present in the structure in the form of a minor curvature. It has already been established through previous research that imperfections can have an impact on the nonlinear behaviour. Furthermore, the mass and stiffness added by the stinger assembly connecting the modal exciter to the structure can have a small influence on the dynamics of the plate. These effects have not been included in the finite element model for simplicity. Nevertheless, the numerical results are within an acceptable limit.

The comparison also highlights the necessity of a nonlinear damping model for large amplitude vibrations. A graph has been presented depicting the evolution of damping ratio with increasing load amplitudes. The general trend is that a higher damping ratio is required in the numerical analysis for higher load amplitudes to obtain a match with the experimental results. Based on the trend, an anomaly is observed that the damping ratio predicted from the linear vibration test is higher than the damping ratio used at lower load amplitudes in the nonlinear numerical analyses. An extreme accuracy in the prediction of damping ratio is inconsequential due to the known variation with vibration amplitude in the nonlinear regime. Therefore, a close estimate was deemed sufficient to progress with the nonlinear numerical analysis. The exact cause of the variation in damping is indeterminate purely based on the results of the present analysis. However, it can be speculated that it is a result of change in the interaction between the structure and surrounding air due to increased vibration amplitudes.

Comparative results between stiffened plates and plates without stiffeners have also been presented. An approximation of backbone curve has been generated for each plate considering several load amplitudes. The backbone curves clearly demonstrate the effect of the presence of stiffener. As expected, the hardening behaviour is much lesser in the stiffened plate for same load levels, since the vibration amplitudes are relatively lower. This gives an indication that a linear analysis would be sufficient for stiffened structures in a larger domain of force amplitudes. The overall results of this thesis provide conclusive evidence on the accuracy and efficiency of the adopted numerical method. The results open a wide range of possibilities to develop and test the numerical method further. In the next chapter, some recommendations are provided for possible areas of improvement in consideration of the limitations of this thesis.

Chapter 7

Recommendations

The validation study for the Hamiltonian reduced order model is a first attempt to gain an insight on the performance of the ROM based numerical model through experimental validation. Undeniably, this leaves a broad scope for further studies and experimentation. A few recommendations are presented in this section for further extension of the approach to industrial scale analyses.

- The present study has been conducted on a structure built of an isotropic material. Composite structures are gaining applicability on a much larger scale and therefore, it is prudent to conduct a similar study on a structure designed with composite materials. The study can also be extended to curved shells which tend to show a softening nonlinearity i.e. a reduction in the modal frequencies with increasing amplitudes.

- The accuracy in the numerical analysis can be improved by considerations of geometrical imperfections in the manufactured structure. The imperfection can be added as an initial condition of the structure in the ROM formulation.

- The numerical analysis using the ROM showed that inclusion of certain modes in the ROM basis induced greater inaccuracies. The comparison to the experimental results with the present geometry and material requires only a single mode for an accurate response. However, it is possible that for more complex geometries greater number of modes are required for accurate analysis. In such a case, there are no pre-determined guidelines on the selection of appropriate modes in the ROM basis to get accurate results. Further studies are required to test the validity of the single degree of freedom model and to develop a concrete method for selection of mode shapes in the ROM basis.

- In this thesis, the analyses have been conducted on a forced and damped vibrations which produces a single frequency–amplitude response. Conducting similar analyses for multiple load amplitudes can be a relatively time-consuming process. Analyses can be conducted on structures undergoing free and undamped vibrations to generate a backbone curve which would provide information on the modal frequency at any amplitude.

The free undamped vibration analysis requires an additional phase constraint on the displacement vector. This is necessary in the continuation scheme to fix the phase of the harmonic motion in every cycle.

- The experiments are conducted using Polytec laser doppler vibrometer. The measurement system used in this thesis did not allow useful measurements beyond 1.2 N load case because of sensitivity limitations. The hardening behaviour should be studied for larger loads and vibration amplitudes to further affirm the utility of the numerical model. Different versions of the LDV are available which allow for higher sensitivity measurements.

- The PAK MK-II system used for nonlinear measurements, does not allow a scan of the structure i.e. measurement at multiple points in the same measurement run. This does not allow the user to study the nonlinear mode shape of the structure. If measurement capabilities are available an interesting comparison can be made between the linear and nonlinear mode shapes.

The Hamiltonian reduced order model is applicable to any engineering structure. The recommendations have been made with the objective of providing further credibility to the presented numerical method, the ultimate goal of the developments being applicability on real-life structural problems.

References

[1] G. Kerschen, M. Peeters, J.C. Golinval, A. F. Vakakis. Nonlinear normal modes part I: A useful framework for the structural dynamicist. *Mechanical Systems and Signal Processing, Vol. 23*, pp.170-194, 2009.

[2] M. Peeters, R. Viguie, G. Serandour, G. Kerschen, J.C. Golinval. Nonlinear normal modes part II: Towards a practical computation using numerical continuation techniques. Mechanical Systems and signal Processing, Vol. 23, pp. 195-216, 2009.

[3] H.R.E. Siller*. Non-linear Modal analysis methods for engineering structures*. Ph.D. dissertation, Imperial College London, 2004.

[4] K. Liang, M. Abdalla, Z. Gürdal. A Koiter- Newton approach for nonlinear structural analysis. *International Journal for Numerical methods in engineering, Vol. 96,* pp. 763-786, 2013.

[5] J. M. Londoño, S. A. Neild, J. E. Cooper. Identification of backbone curves of nonlinear systems from resonance decay responses. *Journal of Sound and Vibration, Vol. 348,* pp. 224-238, 2015.

[6] H.N. Chu, G. Herrmann. Influence of Large Amplitudes on Free Flexural Vibrations of rectangular elastic plates*. Journal of Applied Mechanics, Vol. 23*, pp. 532-540, 1956

[7] N. Yamaki. Influence of large amplitudes on flexural vibrations of elastic plates. ZAMM - *Journal of Applied Mathematics and Mechanics / Zeitschrift für Angewandte Mathematik und Mechanik*, *Vol. 41,* pp. 501–510, 1961.

[8] J. G. Eisley. Nonlinear vibrations of beams and rectangular plates. *Journal of Applied Mathematics and Physics (ZAMP), Vol. 15(2),* pp. 167-175, 1964.

[9] M. Sathyamoorthy. A Study of Nonlinear Vibration of Skew Plates with attention to shear and rotary inertia

[10] N. Yamaki, M. Chiba. Nonlinear Vibrations of a clamped rectangular plate with initial deflection and initial edge displacement - Part I: Theory*. Thin Walled Structures, Vol. 1*. pp. 3-29, 1983.

[11] N. Yamaki, K. Otomo, M. Chiba. Nonlinear Vibrations of a clamped rectangular plate with initial deflection and initial edge displacement - Part II: Experiment. *Thin Walled Structures, Vol. 1*. pp. 101-119, 1983.

[12] A.H. Nayfeh, B. Balachandran. *Applied Nonlinear dynamics: Analytical, Computational and Experimental methods*. Wiley and Sons, 1995.

[13] D. Hui. Soft Spring Nonlinear Vibrations of Anti-Symmetrically Laminated Rectangular Plates*. International Journal of Mechanical Sciences, Vol 27(6*), pp. 397 -408, 1985.

[14] H. Yoshida. Construction of Higher Order Symplectic Integrator. *Physics Letters A, Vol. 150 (5-7),* pp. 262-268, 1990.

[15] W. Han, M. Petyt. Geometrically Nonlinear Vibration Analysis of Thin Rectangular Plates using the Hierarchical Finite element method - I: the fundamental mode of isotropic plates*. Computers and Structures, Vol. 63 (2)*, pp. 295-308, 1997.

[16] W. Han, M. Petyt. Geometrically Nonlinear Vibration Analysis of Thin Rectangular Plates using the Hierarchical Finite element method - II: 1st mode of laminated plates and higher modes of isotropic and laminated plates*. Computers and Structures, Vol. 63 (2)*, pp. 295-308, 1997.

[17] P. Ribeiro, M. Petyt. Nonlinear vibration of plates by the hierarchical finite element and continuation methods. *International Journal of Mechanical Sciences, Vol. 41,* pp. 437-459, 1999.

[18] P. Ribeiro, M. Petyt. Nonlinear vibration of composite laminated plates by the hierarchical finite element. *Composites and Structures, Vol. 46(3),* pp. 197-208, 1999.

[19] P. Ribeiro. Periodic Vibration of Plates with Large Displacements. *American Institute of Aeronautics and Astronautics Journal, Vol. 40(1),* pp. 185-188, 2002.

[20] F. Alijani, M. Amabili. Nonlinear vibrations of laminated and sandwich rectangular plates with free edges. Part 1: Theory and Numerical Simulations*. Composite Structures, Vol. 105,* pp. 422-436, 2013.

[21] M. Amabili, S. Carra. Thermal effects on geometrically nonlinear vibrations of rectangular plates with fixed edges. *Journal of Sound and Vibration, Vol. 321,* pp. 936-954, 2009.

[22] G. Prathap, T.K. Varadan. Large Amplitude Flexural vibrations of stiffened plates*. Journal of Sound and Vibration, Vol. 57(4*), pp. 583-593, 1978.

[23] M. Kolli, K. Chandrashekhara. Nonlinear static and dynamic analysis of Stiffened laminated plates. *International Journal of Nonlinear Mechanics, Vol. 32(1),* pp. 89-101, 1997.

[24] A Mitra, P Sahoo, K Saha. Nonlinear vibration analysis of simply supported stiffened plate by a variational method*. Mechanics of Advanced Materials and Structures, Vol. 20*, pp. 373 - 396, 2013.

[25] N. Ma, R. Wang, P. Li. Nonlinear dynamics of stiffened plate with four edges clamped under primary resonance excitation*. Nonlinear Dynamics, Vol. 70*, pp. 627-648, 2012.

[26] C. Militello, C. A. Felippa. The first andes elements: 9-dof plate bending triangles. *Computer methods in applied mechanics and engineering, Vol. 93(2),* pp. 217-246, 1991.

[27] K. Alvin, M. Horacio, B. Haugen, and C.A. Felippa. Membrane triangles with corner drilling freedoms-I. The EFF element. *Finite Elements in Analysis and Design*, *Vol 12(3),* pp. 163–187, 1992.

[28] E.J. Doedel. Lecture Notes on Numerical Analysis of Nonlinear Equation. In Numerical continuation methods for dynamical systems, Krauskopf et al.(Eds.), Springer, 2007.

[29] E.J. Doedel, H. B. Keller, J.P. Kernévez. Numerical analysis and control of bifurcation problems (II): Bifurcation in infinite dimensions. *International Journal of Bifurcation and Chaos. Applied Science and Engineering,* pp. 745-772. 1991.

[30] N. Singh. *A Hamiltonian Reduction method for Nonlinear Dynamics.* Master thesis, TU Delft, Delft university of Technology, 2015. (uuid:bc6a6d49-8ea4-4aca-ace6-0cd6934070da)

[31] K. Liang. *A Koiter Newton arclength method for buckling sensitive structures.* PhD thesis, TU Delft, Delft University of Technology, 2013.

[32] H. Goldstein, C.P. Poole, and J.L. Safko. Classical Mechanics. Addison-Wesley, 3rd edition, 2002.

[33] W. Greiner. Classical Mechanics: Systems of Particles and Hamiltonian Dynamics. Classical theoretical physics. Springer, 2009.

[34] Man Liu, D.G Gorman. Formulation of Rayleigh Damping and its extensions. *Computers and Structures, Vol. 57,* pp. 277 – 285, 1995.

[35] E. J. Doedel, A. R. Champneys, T. F. Fairgrieve, Y. A. Kuznetsov, B. Sandstede, and X. Wang. Continuation and bifurcation software for ordinary differential equations (with HomCont). *AUTO97, Concordia University, Canada*, 1997.

[36] P. Castellini, M. Martarelli, E.P. Tomasini. Laser Doppler Vibrometry: Development of advanced solutions answering to technology's needs. *Mechanical Systems and Signal Processing, Vol. 20,* pp. 1265-1285, 2006.

[37] P. Sriram, J. I. Craig, and S. Hanagud. A scanning laser Doppler vibrometer for modal testing. *International Journal of Analytical and Experimental Modal Analysis*, *Vol. 5* .1990

[38] H. Tabatabai, D.E. Oliver, J.W. Rohrbaugh, C. Papadopoulos. Novel Applications of Laser Doppler Vibration measurement to medical imaging. *Sensing and Imaging, Vol 14,* pp 13-28, 2013.

[39] F. Alijani, M. Amabili, P. Balasubramanian, S. Carra, G. Ferrari, R. Garziera. Damping for large amplitude vibrations of plates and curved panels, Part 1: Modelling and Experiments. *International Journal of Nonlinear Mechanics, Vol 85,* pp. 23-40, 2016.

[40] M. Amabili. Nonlinear vibrations of rectangular plates with different boundary conditions: theory and experiments. *Computers and Structures, Vol. 82,* pp. 2587-2605, 2004.

[41] A. Y. T. Leung, S. G. Mao. A Symplectic Galerkin method for nonlinear vibrations of beams and plates. *Journal of Sound and Vibration, Vol 183(3),* pp. 475 -491. 1995.

[42] M. Amabili, F. Alijani, J. Delannoy. Damping for large amplitude vibration of plates and curved panels, part 2: Identification and comparisons. *International Journal of Nonlinear Mechanics, Vol. 85,* pp. 226-240, 2016.

[43] R.E. Nickell. Nonlinear Dynamics by Mode Superposition. *Computer Methods in Applied Mechanics and Engineering, Vol. 7,* pp. 107-129. 1976.

[44] M. Amabili, A. Sarkar, M. P. Païdoussis. Reduced order model for nonlinear vibration of cylindrical shells via the proper orthogonal decomposition method*. Journal of Fluids and Structures, Vol. 18*, pp. 227-250, 2003.

[45] F. Boumediene, L. Duigou, E. H. Boutyour, A. Miloudi, J. M. Cadou. Nonlinear forced vibrations of damped plates coupling asymptotic numerical method and reduction models*. Computational Mechanics, Vol. 47*, pp. 359-377, 2011.

[46] E. Pesheck, N. Boivin, C. Pierre, S. Shaw. Nonlinear modal analysis of structures using multi-mode invariant manifold*. Nonlinear dynamics Vol. 25*, pp. 183-205, 2001.

[47] C. Touzé. M. Amabili. Nonlinear normal modes for damped geometrically nonlinear systems: Application to reduced order modelling of harmonically forces structures. *Journal of Sound and Vibration, Vol. 298.* pp. 958 - 961, 2006.

[48] M. Amabili, C. Touzé. Reduced- order models for nonlinear vibrations of fluid filled circular cylindrical shells: Comparison of POD and asymptotic nonlinear normal mode method*. Journal of Fluids and Structures, Vol. 23*, pp. 885-903, 2007.

Appendix

A. Continuation Scheme in AUTO

The numerical computations of the nonlinear periodic solutions in this thesis have been done using the continuation and bifurcation software AUTO which uses the method of orthogonal collocation for solving boundary value problems and parameter based pseudo arclength continuation method for generating the solution branch from a known initial solution. The theoretical background for the continuation scheme used in this analysis is presented in this section.

A.1. Implicit Function Theorem

The Implicit Function Theorem forms the basis for the validity of the continuation method implemented in AUTO. The theorem ensures the existence of a solution branch locally for a given set of conditions. The theorem, in mathematical terms, is based on three conditions and defined as following:

Condition1: Let **G** be a vector valued function with a domain and range defined by **G:** $\boldsymbol{\mathcal{B}} \times \mathbb{R}^m \rightarrow \boldsymbol{\mathcal{B}}$**,** where $\boldsymbol{\mathcal{B}}$ denotes a normed vector space. For a known set of equations given by Equation A.1.

$$\boldsymbol{G}\,(\boldsymbol{u_0}\,, \lambda_0) = \boldsymbol{0} \tag{A. 1}$$

where $\boldsymbol{u}_0 \,\epsilon\, \mathcal{B}$ is a known solution for the system of equations and $\lambda_0 \,\epsilon\, \mathbb{R}^m$ is the known value of the continuation parameter / parameters involved in the computation.

Condition 2: The partial derivative with respect to the state variable $\boldsymbol{G_u}(\boldsymbol{u}_0\,, \lambda_0)$ is non-singular with a bounded inverse such that for a positive real number M it satisfies the condition:

$$\left\|\boldsymbol{G_u}(\boldsymbol{u_0}\,, \lambda_0)^{-\boldsymbol{1}}\right\| \leq M \tag{A. 2}$$

Condition 3: $\boldsymbol{G}$ and $\boldsymbol{G_u}$ satisfy the conditions of Lipschitz continuity i.e. for all $\boldsymbol{u}\,, \boldsymbol{v} \,\epsilon\, \boldsymbol{S_\rho}(u_0)$ and for all $\lambda\,, \mu \,\epsilon\, \boldsymbol{S_\rho}(\lambda_0)$ the following inequalities hold true for some $K_0 > 0$:

$$\|\boldsymbol{G}\,(\boldsymbol{u}\,, \lambda) - \boldsymbol{G}\,(\boldsymbol{v}\,, \mu)\| \leq K_0\,(\|\boldsymbol{u} - \boldsymbol{v}\| + \|\lambda - \mu\|) \tag{A. 3}$$

$$\|\boldsymbol{G_u}\,(\boldsymbol{u}\,, \lambda) - \boldsymbol{G_u}\,(\boldsymbol{v}\,, \mu)\| \leq K_0\,(\|\boldsymbol{u} - \boldsymbol{v}\| + \|\lambda - \mu\|) \tag{A. 4}$$

where $\boldsymbol{S_\rho}(\boldsymbol{u_0})$ and $\boldsymbol{S_\rho}(\lambda_0)$ are spherical regions with radius ρ and centre at $\boldsymbol{u_0}$ and λ_0 respectively.

If all the three conditions given by Equations A.1 – A.4 is satisfied then there exists a sub-region of the sphere $\boldsymbol{S}_{\boldsymbol{\rho}}(\lambda_0)$ given by $\boldsymbol{S}_{\boldsymbol{\delta}}(\lambda_0)$ and a unique function $\boldsymbol{u}(\lambda)$ that is continuous in $\boldsymbol{S}_{\boldsymbol{\delta}}(\lambda_0)$ with $\boldsymbol{u}(\lambda_0) = \boldsymbol{u}_0$, such that for all $\boldsymbol{\lambda} \epsilon S_\delta(\boldsymbol{\lambda}_0)$

$$\boldsymbol{G}(\boldsymbol{u}(\lambda), \lambda) = \boldsymbol{0} \tag{A. 5}$$

The Equation A.5 shows a conditional implicit dependency of the variable $\boldsymbol{u}$ on a parameter or set of parameters involved in the system of equations for a small region in the vicinity of the initially known solution within the normed vector space $\boldsymbol{\mathcal{B}}$**.** This parameter dependency is used to approximate a segment of the solution branch within a small region of validity.

A.2. Keller's Pseudo-Arclength Continuation

Continuation of solutions families in a parameter dependent setting involves the usage of predictor– corrector approach where a predictor step estimates an approximate solution based on a previously known solution point while a corrector step converges the approximation to the true solution. Newtons arclength method is a commonly used corrector step in such continuation schemes. The continuation of periodic solution in AUTO is done using the Keller's pseudo arclength method which has the ability to continue the solution branch over folds or limit points. This ability arises from the choice of the continuation parameter in this approach which is the arclength. For equations of the form of Equation A.1 the solution curve is parameterized using the arclength 's' while the variables '**u**' and λ are computed through variation of 's'. Assuming that an initial solution point $(\boldsymbol{u}_0, \lambda_0)$ is known along with the direction vectors at that point $\dot{\boldsymbol{u}}_0$ and $\dot{\lambda}_0$, the next point on the solution branch is found using the Equation A.6 and Equation A.7 :

$$\boldsymbol{G}(\boldsymbol{u}_{\boldsymbol{1}}, \lambda_1) = \boldsymbol{0} \tag{A. 6}$$

$$(\boldsymbol{u}_{\boldsymbol{1}} - \boldsymbol{u}_{\boldsymbol{0}})^{\boldsymbol{t}} \times \dot{\boldsymbol{u}}_{\boldsymbol{0}} + (\lambda_1 - \lambda_0) \times \dot{\lambda}_0 - \Delta s = 0 \tag{A. 7}$$

The direction derivatives here are taken with respect to the arclength 's' chosen as the continuation parameter. The graphical interpretation of the equation variables in the continuation method can be seen in Figure A.1.

The initial approximation to the next solution point is introduced through Equation A.8 and Equation A.9 with $\Delta\boldsymbol{s}$ as the arclength increment.

$$\boldsymbol{u}_{\boldsymbol{1}}{}^{\boldsymbol{0}} = \boldsymbol{u}_{\boldsymbol{0}} + \dot{\boldsymbol{u}}_{\boldsymbol{0}} \times \Delta s \tag{A. 8}$$

$$\lambda_1{}^0 = \lambda_0 + \dot{\lambda}_0 \times \Delta s \tag{A. 9}$$

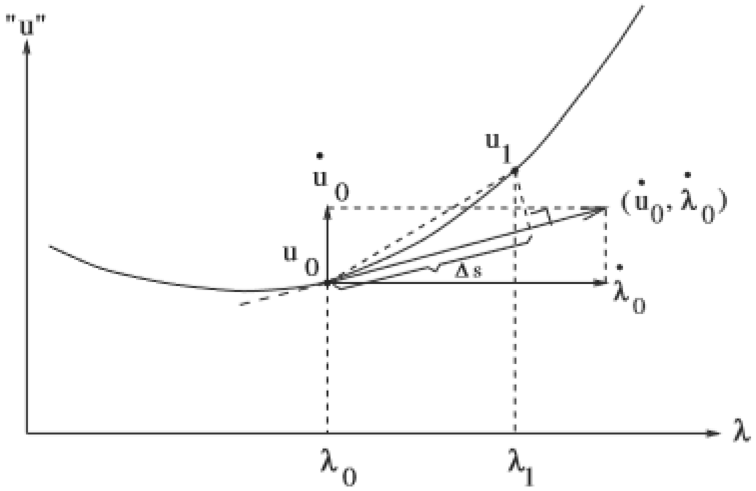

Figure A.1: Graphical interpretation of the pseudo-arclength method (Doedel [28])

A Newton method is used as a corrector step for the initial approximation. The equations to be solved are obtained from a truncated Taylor series expansion in two variables

$$\boldsymbol{u_1}^{\boldsymbol{1}} = \boldsymbol{u_1}^{\boldsymbol{0}} + \boldsymbol{\Delta u} \tag{A. 10}$$

$$\lambda_1{}^1 = \lambda_1{}^0 + \Delta\lambda \tag{A. 11}$$

$$\boldsymbol{G}\left(\boldsymbol{u_1}^{\boldsymbol{1}}, \lambda_1{}^1\right) = \boldsymbol{G}\left(\boldsymbol{u_1}^{\boldsymbol{0}} + \boldsymbol{\Delta u}, \lambda_1{}^0 + \Delta\lambda\right) = 0 \tag{A. 12}$$

Expanding Equation A.12 using the Taylor series truncated at the first order terms the first equation for the corrector step is obtained.

$$\boldsymbol{G}\left(\boldsymbol{u_1}^{\boldsymbol{0}}, \lambda_1{}^0\right) + \boldsymbol{\Delta u} \times \boldsymbol{G_u}\left(\boldsymbol{u_1}^{\boldsymbol{0}}, \lambda_1{}^0\right) + \Delta\lambda \times \boldsymbol{G_\lambda}\left(\boldsymbol{u_1}^{\boldsymbol{0}}, \lambda_1{}^0\right) = \boldsymbol{0} \tag{A. 13}$$

The second equation of the corrector step is obtained by substituting Equation A.10 and Equation A.11 into Equation A.7.

$$\left(\boldsymbol{u_1}^{\boldsymbol{0}} + \boldsymbol{\Delta u} - \boldsymbol{u_0}\right)^{\boldsymbol{t}} \times \dot{\boldsymbol{u}}_{\boldsymbol{0}} + \left(\lambda_1{}^0 + \Delta\lambda - \lambda_0\right) \times \dot{\lambda}_0 - \Delta s = 0 \tag{A. 14}$$

Equation A.13 and Equation A.14 can be further generalized for any iteration step for the convergence procedure.

$$\begin{bmatrix} \boldsymbol{G_u}(\boldsymbol{u_1}^{\boldsymbol{v}}, \lambda_1{}^v) & \boldsymbol{G_\lambda}(\boldsymbol{u_1}^{\boldsymbol{v}}, \lambda_1{}^v) \\ \dot{\boldsymbol{u}}_{\boldsymbol{0}}{}^{\boldsymbol{t}} & \dot{\lambda}_0 \end{bmatrix} \begin{bmatrix} \boldsymbol{\Delta u_1}^{\boldsymbol{v}} \\ \Delta\lambda_1{}^v \end{bmatrix} = -\begin{bmatrix} \boldsymbol{G}(\boldsymbol{u_1}^{\boldsymbol{v}}, \lambda_1{}^v) \\ (\boldsymbol{u_1}^{\boldsymbol{v}} - \boldsymbol{u_0})^{\boldsymbol{t}} \times \dot{\boldsymbol{u}}_{\boldsymbol{0}} + (\lambda_1{}^v - \lambda_0) \times \dot{\lambda}_0 - \Delta s \end{bmatrix} \tag{A. 15}$$

Once a converged solution point is achieved the direction vector for the next computation step is obtained using Equation A.16 which is derived simply by taking a first order derivative of the Equation A.6 and Equation A.7 with respect to the arclength s.

$$\begin{pmatrix} \boldsymbol{G_u}(\boldsymbol{u_1}, \lambda_1) & \boldsymbol{G_\lambda}(\boldsymbol{u_1}, \lambda_1) \\ \dot{\boldsymbol{u}}_{\boldsymbol{0}}{}^{t} & \dot{\lambda}_0 \end{pmatrix} \begin{pmatrix} \dot{\boldsymbol{u}}_{\boldsymbol{1}} \\ \dot{\lambda}_1 \end{pmatrix} = \begin{pmatrix} \boldsymbol{0} \\ 1 \end{pmatrix} \tag{A. 16}$$

The pseudo-arclength continuation can be used for generating a full solution family provided the conditions of the implicit function theorem is satisfied for each region of validity.

A.3. Orthogonal Collocation

In AUTO, the periodic solution to boundary value problems (BVP) is computed using a method called Orthogonal collocation with piecewise polynomials (Doedel [28]). Consider a system of equations defined by the set of first order differential equations given in Equation A.17.

$$\mathbf{u}'(\mathrm{t}) = \boldsymbol{f}(\mathbf{u}(\mathrm{t}), \lambda) \tag{A. 17}$$

The normalized time period is discretized into N distinct steps such that:

$$0 < t_1 < t_2 \ldots < t_j \ldots < 1 \quad \text{where j = 1: N}$$

$$h_j = t_j - t_{j-1} \tag{A. 18}$$

Further, each time interval is subdivided into intermediate computation points which are called collocation points.

$$t_{j-1} < z_{j,1} < z_{\boldsymbol{j},\boldsymbol{2}} < \cdots < z_{j,i} < \cdots < t_{\boldsymbol{j}} \quad \text{where i=1:m}$$

AUTO has the capability of adaptive time step discretization which means that depending on the convergence rate of the solution the time steps are automatically adjusted to make it optimal for the analysis.

The periodic solution curve for one cycle is assumed to be a piecewise polynomial function i.e. for each interval of time period an independent assumption for the solution curve is chosen in the form of a polynomial function. The Lagrange basis polynomials are used as the polynomial function in AUTO (Doedel and Keller [29]).

$$l_{j,i}(t) = \prod_{k=0,k\neq i}^{m} \frac{t - t_{j-\frac{k}{m}}}{t_{j-\frac{i}{m}} - t_{j-\frac{k}{m}}} \;, \quad t_{j-\frac{i}{m}} = t_j - \frac{i}{m} h_j \tag{A. 19}$$

$$\boldsymbol{p_j}(t) = \sum_{i=0}^{m} l_{j,i}(t)\ \boldsymbol{u}_{j-\frac{i}{m}} \tag{A. 20}$$

The Equation A.19 and Equation A.20 define the piecewise polynomial function assumption. The solution to the unknown $u_{j-\frac{i}{m}}$ is obtained by using the collocation Equation A.21.

$$\mathbf{p'}_{\mathbf{j}}(\mathrm{z_{j,i}}) = \boldsymbol{f}(\mathbf{p_j}(\mathrm{z_{j,i}}), \lambda) \tag{A. 21}$$

The orthogonal collocation method is used to obtain the periodic solution for the first step in the continuation scheme. Once the initial solution is obtained, the solution can be further extended by varying the parameter in sufficiently small steps. Therefore, a combination of orthogonal collocation and pseudo- arclength continuation approach is used to generate solution families of periodic solutions.

B. Derivation of the ROM equations

To compute the stiffness terms in the reduced system, three sets of equations are to be solved. Substituting Equation 2.17 and Equation 2.13 into Equation 2.12 and solving for the coefficient of ξ, the following equations are obtained:

$$\boldsymbol{\mathcal{L}}(\mathbf{u}_{\alpha}) = \mathbf{F}\,\bar{\mathbf{L}}_{\alpha} \tag{B. 1}$$

$$\boldsymbol{\mathcal{L}}(\mathbf{u}_{\alpha\beta}) + \boldsymbol{Q}(\mathbf{u}_{\alpha\beta}) = \mathbf{F}\,\bar{\mathbf{Q}}_{\alpha\beta} \tag{B. 2}$$

$$\boldsymbol{\mathcal{L}}(\mathbf{u}_{\alpha\beta\gamma}) + \frac{2}{3}\left[\boldsymbol{Q}(\mathbf{u}_{\alpha\beta}, \mathbf{u}_{\gamma}) + \boldsymbol{Q}(\mathbf{u}_{\beta\gamma}, \mathbf{u}_{\alpha}) + \boldsymbol{Q}(\mathbf{u}_{\gamma\alpha}, \mathbf{u}_{\beta})\right] + \boldsymbol{C}(\mathbf{u}_{\alpha}, \mathbf{u}_{\beta}, \mathbf{u}_{\gamma}) = \mathbf{F}\bar{\mathbf{C}}_{\alpha\beta\gamma} \tag{B. 3}$$

The terms related to first order displacement fields are combined from Equation B.1 and Equation 2.16a to form the equation set for computing the linear stiffness matrix of reduced system.

$$\begin{bmatrix} \mathbf{K}_t & -\mathbf{F} \\ -\mathbf{F}^{\mathrm{t}} & \mathbf{0} \end{bmatrix} \begin{Bmatrix} \mathbf{u}_{\alpha} \\ \bar{\mathbf{L}}_{\alpha} \end{Bmatrix} = \begin{Bmatrix} \mathbf{0} \\ -\mathbf{E}_{\alpha} \end{Bmatrix} \tag{B. 2}$$

In the above equation $\mathbf{K}_t = \mathbf{L}$ is the tangential stiffness matrix in the finite element model.

The second set of equations is obtained by combining Equation B.2 and the constraint Equation 2.16b. These equations combined gives us the second order stiffness term.

$$\begin{bmatrix} \mathbf{K}_t & -\mathbf{F} \\ -\mathbf{F}^{\mathbf{t}} & \mathbf{0} \end{bmatrix} \begin{Bmatrix} \mathbf{u}_{\alpha\beta} \\ \bar{\mathbf{Q}}_{\alpha\beta} \end{Bmatrix} = \begin{Bmatrix} -\boldsymbol{Q}(\boldsymbol{u}_\alpha, \boldsymbol{u}_\beta) \\ \mathbf{0} \end{Bmatrix} \tag{B. 3}$$

The linear and quadratic stiffness terms $\bar{\mathbf{L}}$ and $\bar{\mathbf{Q}}$ can be also computed through an alternate simplified form given by Equations 2.20 - 2.21. The constraint equations are utilized to obtain the simplified forms. Multiplying the Equation B.1 with $\boldsymbol{u_\beta}^t$, the right hand side of the equation can be transformed to $\bar{L}_{\alpha\beta}$ by using the constraint Equation 2.16a. This results in the simplified form of the first equation given by:

$$\bar{\mathrm{L}}_{\beta\alpha} = \mathbf{u_\beta}^{\mathbf{t}}\, \boldsymbol{\mathcal{L}}(\mathbf{u}_\alpha) \tag{B. 4}$$

A similar approach is adopted to obtain the quadratic stiffness tensor. Equation B.2 is multiplied by $\boldsymbol{u_\gamma}^t$. Since the stiffness matrix is symmetric for conservative systems, the following condition can be derived by taking a transpose:

$$\mathbf{u_\gamma}^{\mathbf{t}}\, \boldsymbol{\mathcal{L}}\big(\mathbf{u}_{\alpha\beta}\big) = \mathbf{u_{\alpha\beta}}^{\mathbf{t}}\, \boldsymbol{\mathcal{L}}(\mathbf{u}_\gamma) \tag{B. 5}$$

The left hand side of the Equation B.2 is transformed to $\mathrm{u_{\alpha\beta}}^{\mathrm{t}}\, \mathcal{L}\big(\mathrm{u}_\gamma\big) + \mathrm{u_\gamma}^{\mathrm{t}}\, Q\big(\mathrm{u}_{\alpha\beta}\big)$ which can be further transformed to $\big(\mathrm{F}^t \mathrm{u}_{\alpha\beta}\big)^t\, \bar{\mathrm{L}}_\alpha + \mathrm{u_\gamma}^{\mathrm{t}}\, Q\big(\mathrm{u}_{\alpha\beta}\big)$ by using Equation B.1. The second constraint Equation 2.16b nullifies the first terms of the equation. The right hand side of the equation is also transformed to $\bar{Q}_{\alpha\beta\gamma}$ by using the first constrain Equation 2.16a. The resultant simplified form of the equation is:

$$\bar{\mathrm{Q}}_{\alpha\beta\gamma} = \mathbf{u_\gamma}^{\mathbf{t}}\, \boldsymbol{Q}\big(\mathbf{u}_{\alpha\beta}\big) \tag{B. 6}$$

To derive the cubic stiffness tensor, the Equation B.3 is multiplied by $\mathrm{u_\delta}^{\mathrm{t}}$. Using the symmetricity in the matrices, the first term is $\mathrm{u_\delta}^{\mathrm{t}} \mathcal{L}\big(\mathrm{u}_{\alpha\beta\gamma}\big) = \mathrm{u_{\alpha\beta\gamma}}^{\mathrm{t}} \mathcal{L}(\mathrm{u}_\delta)$. Using Equation B.1 this can be further transformed to $(\mathrm{u_{\alpha\beta\gamma}}^{\mathrm{t}}\, \mathbf{F}\, \bar{\mathrm{L}}_\delta)$. The third constraint Equation 2.16c makes this term zero. Equation B.2 is multiplied by $\mathrm{u_\delta}^{\mathrm{t}}$ and $\mathrm{u_\gamma}^{\mathrm{t}}$ and utilized in modifying the second term.

$$\mathbf{u_\delta}^{\mathbf{t}}\, \mathbf{u_\gamma}^{\mathbf{t}}\, \boldsymbol{\mathcal{L}}\big(\mathbf{u}_{\alpha\beta}\big) + \mathbf{u_\delta}^{\mathbf{t}}\, \mathbf{u_\gamma}^{\mathbf{t}}\, \boldsymbol{Q}\big(\mathbf{u}_{\alpha\beta}\big) = \mathbf{u_\delta}^{\mathbf{t}}\, \mathbf{u_\gamma}^{\mathbf{t}}\, \mathbf{F}\, \bar{\mathbf{Q}}_{\alpha\beta} = \big(\mathbf{F}^t\, \mathbf{u}_{\delta\gamma}\big)^t\, \bar{\mathbf{Q}}_{\alpha\beta} = \mathbf{0} \tag{B. 7}$$

Simplifying the above equation,

$$\mathbf{u_{\gamma\delta}}^{\mathbf{t}}\, \boldsymbol{\mathcal{L}}\big(\mathbf{u}_{\alpha\beta}\big) = -\mathbf{u_\delta}^{\mathbf{t}}\, \boldsymbol{Q}\big(\mathbf{u}_{\alpha\beta}, \mathbf{u}_\gamma\big) \tag{B. 8}$$

The right hand side can be simplified to $\bar{C}_{\alpha\beta\gamma\delta}$ using the orthogonal constraint relations. The final form of the Equation B.3 is:

$$\bar{\mathrm{C}}_{\alpha\beta\gamma\delta} = \boldsymbol{C}\big(\mathbf{u}_\alpha, \mathbf{u}_\beta, \mathbf{u}_\gamma, \mathbf{u}_\delta\big) - \frac{2}{3}\left[\mathbf{u_{\alpha\beta}}^{\mathbf{t}}\, \boldsymbol{\mathcal{L}}\big(\mathbf{u}_{\delta\gamma}\big) + \mathbf{u_{\beta\gamma}}^{\mathbf{t}}\, \boldsymbol{\mathcal{L}}(\mathbf{u}_{\delta\alpha}) + \mathbf{u_{\gamma\alpha}}^{\mathbf{t}}\, \boldsymbol{\mathcal{L}}\big(\mathbf{u}_{\delta\beta}\big)\right] \tag{B. 9}$$

C. Reduced Damping Matrix

The damping matrix for the reduced order model is derived from considering the dissipation energy.

$$D = \frac{1}{2}\ \dot{\mathbf{u}}^{t}\ \mathbb{C}\ \dot{\mathbf{u}}$$

$$= \frac{1}{2}\ \mathbf{p}^{\mathbf{t}}\ (\mathbf{M}^{-\boldsymbol{t}}\ \mathbb{C}\ \ \mathbf{M}^{-\mathbf{1}})\ \mathbf{p}$$

$$= \frac{1}{2}\ \boldsymbol{\pi}^{t}\ \left(\mathbf{P}^{\mathrm{t}}\ \mathbf{M}^{-\boldsymbol{t}}\ \mathbb{C}\ \ \mathbf{M}^{-\mathbf{1}}\ \mathbf{P}\ \right)\boldsymbol{\pi}$$

$$= \frac{1}{2}\ \dot{\boldsymbol{\xi}}^{t}\ \overline{\mathbf{M}}\ \left(\mathbf{P}^{\mathrm{t}}\ \mathbf{M}^{-\boldsymbol{t}}\ \mathbb{C}\ \ \mathbf{M}^{-\mathbf{1}}\ \mathbf{P}\ \right)\overline{\mathbf{M}}\ \dot{\boldsymbol{\xi}}$$

From the above equation, the damping matrix can be derived to be:

$$\bar{\mathbb{C}} = \ \overline{\mathbf{M}}\left(\mathbf{P}^{\mathrm{t}}\ \mathbf{M}^{-\boldsymbol{t}}\ \mathbb{C}\ \ \mathbf{M}^{-\mathbf{1}}\ \mathbf{P}\ \right)\overline{\mathbf{M}}$$

D. Fortran Module for reading the ROM as input

The following code section is written in Fortran programming language to read the output of the ROM generation code and utilize it in the continuation analysis.

```
module romdata
implicit none

integer :: ndof
double precision :: omega
double precision, dimension(:), allocatable :: From
double precision, dimension(:,:), allocatable :: Lrom, Drom
double precision, dimension(:,:,:), allocatable :: Qrom
double precision, dimension(:,:,:,:), allocatable :: Crom

contains

subroutine initrom()

integer :: i1, i2, i3, i4

open (unit = 10, file = "fort.10", status='old', action = 'read')

!  dummy lines are added to skip the metadata in ROM output file

do i1 = 1, 5
      read(10,*)
end do

read(10,*) ndof

read(10,*) omega

allocate(From(ndof))

allocate(Lrom(ndof, ndof))

allocate(Drom(ndof, ndof))

allocate(Qrom(ndof, ndof, ndof))

allocate(Crom(ndof, ndof, ndof, ndof))

! reading the linear stiffness of the ROM

do i1 = 1, ndof

    do i2 = 1, ndof

        read(10,*) Lrom(i2,i1)

    end do

end do
```

```
! reading the quadratic stiffness of the ROM
do i1 = 1, ndof
    do i2 = 1, ndof
        do i3 = 1, ndof
            read(10,*)  Qrom(i3,i2,i1)
        end do
    end do
end do

! reading the cubic stiffness of the ROM
do i1 = 1, ndof
    do i2 = 1, ndof
        do i3 = 1, ndof
            do i4 = 1, ndof
                read(10,*)  Crom(i4,i3,i2,i1)
            end do
        end do
    end do
end do

! reading the reduced damping matrix
do i1 = 1, ndof
    do i2 = 1, ndof
        read(10,*)  Drom(i2,i1)
    end do
end do
! reading the load vector
do i1 = 1, ndof
        read(10,*) From(i1)
end do

close(10)
end subroutine
end module
```